

3-6-2026 2:00 PM

Production and properties of hexahistidine-tagged recombinant human galectin-12

Aranya Nagar

Supervisor: Timoshenko, Alexander V., *The University of Western Ontario*

A thesis submitted in partial fulfillment of the requirements for the Master of Science degree in Biology

© Aranya Nagar 2026

Abstract

Galectin-12 is a tissue-specific galectin that participates in the regulation of cellular differentiation, cell cycle progression, and lipid metabolism. Despite these important roles, the mechanisms underlying its function and regulation remain a growing area of research. To provide insight into these mechanisms, I expressed and purified hexahistidine-tagged human recombinant galectin-12 (hrGal-12) in BL21(DE3) *E. coli* cells using a variety of biochemical approaches. In addition, I characterized its activity by showing that: (1) hrGal-12 induces hemagglutination of rabbit red blood cells, (2) hrGal-12 promotes aggregation and adhesion of HL-60 cells, (3) hrGal-12 reduces HL-60 cell growth without reducing viability over six days, and (4) hrGal-12 treatment was associated with changes in selected cell differentiation-related markers. While hrGal-12 was successfully purified and shown to exhibit measurable cell-interacting properties, further investigation is required to address challenges with solubility, stability, and refolding.

Keywords

Galectin-12, recombinant protein expression, protein purification, myeloid cell model, hemagglutination, cell-based assays, size exclusion chromatography

Summary for Lay Audience

Galectins are a family of proteins that generally bind to sugars and are key in many cell responses including cell differentiation. Galectin-12 is abundant in fat tissue and white blood cells and is downregulated in several types of cancer. Even though significant progress has been made, scientists still do not fully understand how galectin-12 works at the molecular level. Inside cells, galectin-12 is found in lipid droplets, which are structures that store fats and help control how fats are used. Galectin-12 can also be found outside cells where its functions remain unexplored. My project aimed to make human recombinant galectin-12 (hrGal-12) in *E. coli* and study its biological properties. First, I produced hrGal-12 in *E. coli* using common molecular techniques. hrGal-12 was then purified using affinity and size-based methods and the protein made soluble in a complex buffer. The folding, heat stability, and storage stability of hrGal-12 were tested using different lab tools. Next, I showed that hrGal-12 caused clumping of rabbit red blood cells. It also induced HL-60 cell aggregation in a dose-dependent manner. hrGal-12 also helped HL-60 cells stick to surfaces coated with the protein. This shows the protein is active even without the buffer used to prepare it. HL-60 cells likely have surface structures that galectin-12 can attach to. These structures probably include some sugar molecules that are not fully identified yet. hrGal-12 boosted the activity of genes related to cell differentiation, like *NCF1* and *NCF2*, and slowed the growth of HL-60 cells. This study shows a new way to prepare recombinant galectin-12. It also highlights the protein's roles in basic cell responses and cancer biology.

Acknowledgments

First, I would like to acknowledge my supervisor Dr. Alexander Timoshenko, you have helped me become a better critical thinker for which I am grateful. It has been a pleasure working with you from taking the cell biology lab as an undergraduate, to teaching it these past years, and working in your lab.

Secondly, I want to thank Dr. Peter Stathopoulos, you are an amazing mentor and got me started in the world of recombinant proteins. I appreciate all our conversations about science, and your unwavering support throughout. I am deeply grateful for the opportunity to learn from you both, not only in science, but through your leadership and teaching styles.

Thanks to my advisors Dr. Jim Karagiannis and Dr. Robert Cumming, your feedback and experimental advice have been quite helpful and appreciated. Further, I want to thank Chunhui Liu, the Cell Biology Lab technician, for all the interesting chats and help over past two years. Another major thanks to the BioCORE facility in Biochemistry Department, especially Victoria Clark and Heidi (Yinyin) Lao. Another big thanks to Taylor Lake, the technician in Stathopoulos lab, I appreciate all your help over last two years a lot.

A major thanks goes to all the members of both the Timoshenko and Stathopoulos labs. You all have been so supportive and amazing people to learn and work with. I have great memories of our time in the lab and will miss working with you all!

Another major thanks go to my mom. You have helped me believe in myself and have played a major part in making me who I am. I gain so much strength as I know how hard you have worked and the adversities you have faced as a single parent. You have always taught me to think critically, work hard, and be kind, which have been essential skills as a developing scientist. Thanks to my aunt as you have supported me so much, believed in me, and sparked my love for science from a young age. I could not have done this without my family and friends.

I acknowledge the use of AI-based tools solely for editing and proofreading of thesis text that I originally wrote.

Table of Contents

Abstract.....	ii
Summary for Lay Audience.....	iv
Acknowledgments.....	v
Table of Contents.....	vi
List of Tables.....	x
List of Figures.....	xi
List of Appendices.....	xiii
List of abbreviations.....	xiv
Chapter 1.....	1
1 Introduction.....	1
1.1 Galectins.....	1
1.1.1 Galectin-1 and galectin-3.....	4
1.1.2 Tandem-repeat galectins.....	4
1.2 Galectin-12.....	6
1.2.1 Galectin-12 properties.....	8
1.2.2 Galectin-12 in adipocytes.....	8
1.2.3 Intracellular galectin-12: function and localization.....	10
1.2.4 Galectin-12 in sebocytes.....	11
1.2.5 Lipid droplets, lipogenesis, and lipolysis.....	12
1.2.6 Galectin-12 in myeloid differentiation and macrophage polarization.....	13
1.2.7 Galectin-12 in colorectal cancer and pancreatic cancer.....	15
1.2.8 Extracellular and secreted galectin-12.....	16
1.2.9 Porcine galectin-12: expression and function.....	17
1.3 Recombinant protein production.....	18

1.3.1	Overview of recombinant proteins.....	18
1.3.2	Cloning and expression in bacterial systems	20
1.3.3	Purification of recombinant proteins expressed in <i>E. coli</i>	22
1.3.4	Other common recombinant expression systems.....	25
1.3.5	Recombinant galectins and galectin-12	26
1.4	HL-60 cell line as a model system to study galectins.....	30
1.4.1	HL-60 cell line and acute myeloid leukemia	30
1.4.2	HL-60 cells and galectins.....	33
1.4.3	Neutrophil phenotypes and myeloid differentiation	34
1.5	Objectives and Hypothesis.....	37
Chapter 2.....		38
2	Materials and Methods.....	38
2.1	Chemicals and reagents.....	38
2.2	Cloning and expression of hrGal-12	39
2.2.1	Preparation of <i>LGALS12</i> cDNA plasmid.....	39
2.2.2	Cloning of <i>LGALS12</i> into pET-28a plasmid	40
2.2.3	Colony PCR and Sanger sequencing	42
2.2.4	Expression of hrGal-12 in BL21(DE3) <i>E. coli</i>	42
2.3	Purification of hrGal-12	43
2.4	Western Blotting and Protein Measurement.....	46
2.4.1	Antibodies.....	46
2.4.2	Protein quantification.....	46
2.4.3	SDS-PAGE and Western Blotting	47
2.5	Chemical denaturation and dynamic light scattering.....	48
2.5.1	Intrinsic fluorescence spectroscopy	48
2.5.2	Dynamic Light Scattering.....	48

2.6	<i>In Silico</i> analysis	48
2.7	Cell culture.....	49
2.7.1	HL-60 Cell Culture	49
2.7.2	Cell treatments	49
2.8	Brightfield and fluorescence microscopy	49
2.8.1	DAPI nuclear staining.....	50
2.9	RNA isolation, cDNA synthesis, and RT-PCR	50
2.10	Cell aggregation and adhesion assays	51
2.10.1	Cell aggregation assay	51
2.10.2	Adhesion assay and hrGal-12 immobilization.....	52
2.11	Hemagglutination assay	52
2.12	Cell viability and proliferation assays.....	53
2.13	Statistical analysis	54
	Chapter 3.....	55
3	Results	55
3.1	Cloning, expression, and purification of hrGal-12	55
3.1.1	<i>In silico</i> analysis of human galectin-12 sequence.....	55
3.1.2	Cloning of <i>LGALS12</i> cDNA into pET-28a vector and expression in BL21(DE3) cells	58
3.1.3	hrGal-12 purification with Ni-NTA and Size Exclusion Chromatography	61
3.1.4	Assessment of hrGal-12 stability, precipitation, and folding state	70
3.2	Biological activity of hexahistidine-tagged hrGal-12.....	74
3.2.1	hrGal-12 induced hemagglutination of rabbit RBCs	74
3.2.2	hrGal-12 induced aggregation and adhesion of HL-60 cells	76
3.3	Effects of hrGal-12 on growth and differentiation of HL-60 cells	80
3.3.1	hrGal-12 lowers growth rate of HL-60 cells.....	80

3.3.2	hrGal-12 increases cell differentiation markers <i>NCF1</i> and <i>NCF2</i> in HL-60 cells	80
Chapter 4	84
4	Discussion	84
4.1	Interpretation.....	85
4.1.1	Challenges and optimization of hrGal-12 production.....	85
4.1.2	hrGal-12 induced aggregation and adhesion of HL-60 cells confirms compatible cell-surface galectin-12 ligands.....	88
4.1.3	hrGal-12 lowers growth rate of HL-60 cells and upregulates cell differentiation markers.....	92
4.1.4	Galectin-12 in lipid metabolism.....	95
4.2	Conclusions and applications.....	96
4.3	Study limitations and future directions	100
References	103
Appendices	118
Curriculum Vitae	122

List of Tables

Table 1. AKTA GO™ columns & buffer conditions assessed with hrGal-12 in UAG.....	45
Table 2. List of antibodies.	46
Table 3. List of RT-PCR primers.....	51
Table 4. Summary of refolding and dialysis buffers assessed with hrGal-12.	67

List of Figures

Figure 1. Overview of human galectins and galectin structure.	3
Figure 2. Overview of galectin-12 functions, subcellular localization, and expression in various conditions.	7
Figure 3. Overview of recombinant protein production.	19
Figure 4. Proposed model of HL-60 neutrophil like differentiation.	32
Figure 5. Myeloid cell differentiation from bone marrow.	36
Figure 6. Cloning, expression, purification, and refolding of hrGal-12 in BL21(DE3) <i>E. coli</i>	41
Figure 7. Sequence and structure of human galectin-12.	56
Figure 8. <i>In silico</i> prediction of human galectin-12 solubility and hydropathy.	57
Figure 9. Digestion of <i>LGALS12</i> cDNA insert and ligation in pET-28a plasmid.	59
Figure 10. BL21(DE3) expression of hrGal-12 analyzed with SDS-PAGE and western blotting.	60
Figure 11. SDS-PAGE of pooled hrGal-12 fractions purified following lysis with detergents and subsequent Ni-NTA purification.	64
Figure 12. SDS-PAGE of recombinant hrGal-12 Ni-NTA purification.	65
Figure 13. SDS-PAGE of hrGal-12 following dialysis and refolding in UAG buffer.	66
Figure 14. Size Exclusion Chromatography of hrGal-12 and immunodetection.	68
Figure 15. Additional western blots and SDS-PAGE analysis of hrGal-12 expressed at three different temperatures.	69
Figure 16. Stability of hrGal-12 at varying temperatures.	71

Figure 17. hrGal-12 precipitation and aggregation <i>in vitro</i>	72
Figure 18. Chemical denaturation of hrGal-12 with Gdn-HCl.	73
Figure 19. hrGal-12 induced hemagglutination of Rabbit Red Blood Cells.....	75
Figure 20. hrGal-12-induced aggregation of HL-60 cells.	77
Figure 21. Visualization of hrGal-12 induced HL-60 aggregates.....	78
Figure 22. Adhesion of HL-60 cells to immobilized hrGal-12.....	79
Figure 23. hrGal-12 reduces HL-60 cell growth at 10 µg/mL without affecting cell viability.	81
Figure 24. hrGal-12 increases cell differentiation markers <i>NCF1</i> and <i>NCF2</i>	82
Figure 25. Nuclear morphology of HL-60 cells following treatment with hrGal-12, ATRA, and DMSO.	83
Figure 26. Biological effects of human recombinant galectin-12 on HL-60 cells and rabbit red blood cells.	98

List of Appendices

Figure S1. SDS-PAGE of hrGal-12 BL21(DE3) lysates purified under non-denaturing conditions with Ni-NTA beads.	118
Figure S2. hrGal-12 purification attempt using protocol from (Maller et al., 2020) developed for mrGal-12 and Cagnoni et al., 2024 for hrGal-12 in Rosetta DE3 <i>E. coli</i>	119
Figure S3. hrGal-12 has no effect on <i>DGATI</i> expression..	120
Figure S4. Western blots of hrGal-12 purified using various buffers on carboxymethyl fast flow ion exchange Cytiva column on AKTA GO chromatography system.	121

List of abbreviations

3T3-L1	Mouse pre-adipocyte cell line
AML	Acute myeloid leukemia
APL	Acute promyelocytic leukemia
ATRA	All-trans retinoic acid
BME	2-mercaptoethanol
BP	Base Pairs
BSA	Bovine Serum Albumin
CD	Cluster of differentiation molecules
CDK	Cyclin dependent kinase
CM FF	Carboxymethyl sepharose fast flow
CRD	Carbohydrate-recognition domain
DAPI	4',6-diamidino-2-phenylindole
DGAT1	Diacylglycerol O-acyltransferase 1
DLS	Dynamic light scattering
DMSO	Dimethyl Sulfoxide
DPBS	Dulbecco's phosphate buffered saline
EMT	Epithelial to mesenchymal transition
Erk	Extracellular signal-regulated kinase
FPLC	Fast protein liquid chromatography
GSH	Glutathione Reduced
GSSH	Glutathione Oxidized
HBSS	Hank's Balanced Salt Solution
HEPES	4-(2-Hydroxyethyl)-1-piperazineethanesulfonic acid
HIC	Hydrophobic interaction chromatography
HL-60	Human myeloid leukemia cell line
hrGal-12	Human recombinant galectin-12
HRP	Horseradish peroxidase
IMEM	Iscove's Modified Eagle Medium

IEX	Ion exchange chromatography
IMAC	Immobilized metal affinity chromatography
IPTG	Isopropyl β -D-1-thiogalactopyranoside
kDa	Kilodalton
LB	Luria-Bertani broth
MAPK	Mitogen activated protein kinase
MW	Molecular weight
NADPH	Nicotinamide adenine dinucleotide phosphate
NAFLD	Non-alcoholic fatty liver disease
NB4	Acute promyelocytic leukemia cell line (M3 subtype)
NCF	Neutrophil cytosolic factor
NET	Neutrophil extracellular traps
Ni-NTA	Nickel-Nitrilotriacetic
PDT	Population doubling time
Phox	NADPH oxidase complex
PMA	Phorbol 12-myristate 13-acetate
PPAR γ	Peroxisome proliferator-activated receptor γ
RAR	Retinoic acid receptor
RBC	Red blood cell
RCA	<i>Ricinus communis</i> agglutinin
RIPA	Radioimmunoprecipitation
ROS	Reactive oxygen Species
RPM	Revolutions per minute
RXR	Retinoid X receptor
SDS	sodium dodecyl sulfate
SEC	Size exclusion chromatography
SLC1A5	Neutral amino acid transporter B (0)
TBST	Tris Buffered Saline with Tween-20
UAG	Urea, Arginine, Glutathione Buffer
VPS13C	Vacuole protein sorting 13 homolog C

Chapter 1

1 Introduction

1.1 Galectins

Galectins are a family of β -galactoside binding proteins involved in cell differentiation, proliferation, and apoptosis (Liu & Rabinovich, 2005; Liu & Stowell, 2023). Of 16 identified galectins, 12 are found in humans, including the prototype galectins (1, 2, 7, 10, 13, 14, 16), the chimeric type galectin-3, and the tandem-repeat galectins (4, 8, 9, 12) (**Figure 1**) (Liu & Rabinovich, 2005). Prototype galectins have one carbohydrate-recognition domain (CRD), while tandem repeat galectins have two CRDs separated by a linker sequence. Chimeric galectins have one CRD and a non-lectin domain. Prototype galectins can form homodimers, while tandem-repeat galectins form heterodimers and chimeric galectins can oligomerize via their N- or C-terminal regions. Galectins are soluble and can function both intra- and extracellularly (Liu & Stowell, 2023).

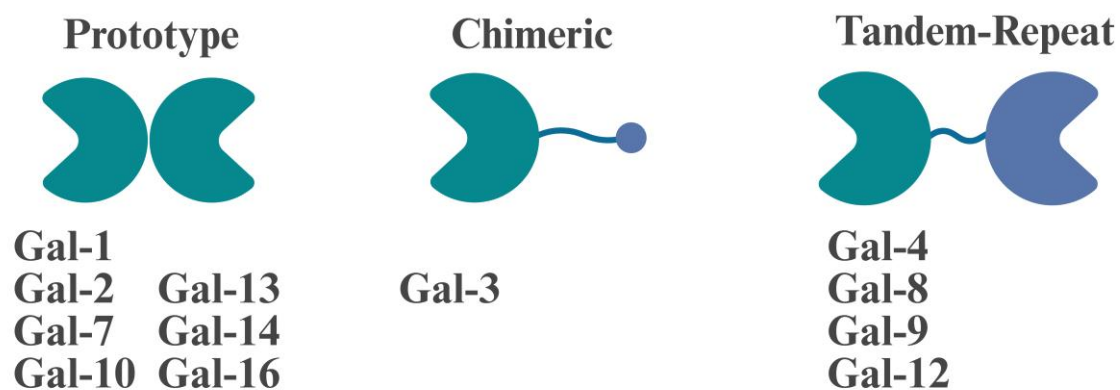
Extracellular galectins can bind to cell surface glycolipids and glycoproteins.

Intracellularly, galectins can regulate gene expression and protein function through glycan-independent mechanisms (Jacob & Gorek, 2024). Although mammals have more galectins, all vertebrates express galectins to some degree. Galectin-like proteins can also be found in less developmentally complex life forms (Günther & Galuska, 2023). The first galectin identified was in the electric eel and named ‘electrolectin,’ with tissue extracts displaying hemagglutination (HA) activity and inhibition by both lactose and thiogalactoside (Teichberg et al., 1975; Leffler, 2018). This first electrolectin is now known as the eel homolog of human galectin-1. This electrolectin was successfully

purified in 1975 using lactosyl-agarose affinity chromatography, which is now a standard tool in the purification of galectins.

Galectins vary greatly in their glycan recognition, and even small changes in CRD sequence can shift their binding to specific modifications like sulfation or fucosylation. For example, galectin-4 shows enhanced binding to β -galactosides modified with 3'-sulfation (Cao & Guo, 2016). Galectin CRDs are approximately 130 amino acids in length and fold into a conserved antiparallel β -sheet sandwich (Liu & Stowell, 2023). Although this β -sandwich structure is shared across the family, the specific CRD sequences vary considerably, with only a handful of key residues conserved to support glycan binding (Modenutti et al., 2019). These subtle sequence differences underlie the diverse binding preferences observed across galectins and are particularly relevant for understanding galectin-12, which is known to prefer fucosylated glycans (Maller et al., 2020; Cagnoni et al., 2024).

Altered galectin expression is associated with a wide range of pathological conditions, including cancer, diabetes, inflammatory disorders, cardiovascular disease, neurodegeneration, and skin disease (Almkvist & Karlsson, 2002; Liu & Rabinovich, 2005; Liu & Stowell, 2023). Reflecting their broad immunomodulatory roles, several galectins are actively being explored as targets for cancer immunotherapy (Nehmé & St-Pierre, 2023). Galectins, including galectin-12, may be involved in immune cell polarization and differentiation.



Galectin β -Sheet Structure

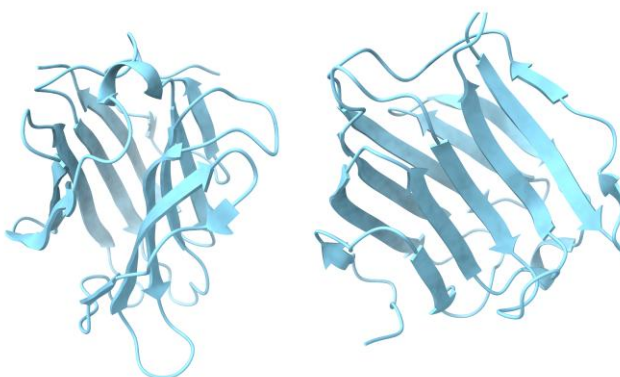


Figure 1. Overview of human galectins and galectin structure. Human galectins are categorized into their structural groups: prototype, chimeric, and tandem repeat. Figure made in BioRender. Sample galectin-7 crystal structure rendered in PyMOL. Adapted from Liu & Stowell, 2023.

1.1.1 Galectin-1 and galectin-3

Galectin-1 and galectin-3 are two extensively studied members of the galectin family, providing insight into glycan-binding, oligomerization, and cellular functions (Hermenean et al., 2022; Liu & Stowell, 2023). Galectin-1 is a 14 kDa homodimer involved in immune regulation, cell adhesion, and apoptosis, while galectin-3 is a 31 kDa chimeric galectin that exists as a monomer or oligomer and is found in both intracellular and extracellular compartments (Farhad et al., 2018). Both proteins have been successfully produced recombinantly in bacterial systems, enabling detailed biochemical and functional studies (Nishi, 2020; Prato et al., 2020).

Galectin-1 and galectin-3 are involved in immune cell fate and inflammation. Galectin-1 regulates T-cell apoptosis and macrophage polarization, contributing to tissue repair and immune responses (Perillo et al., 1995; Hermenean et al., 2022), whereas galectin-3 promotes cell survival, fibrosis, and inflammatory signaling and has been implicated in cancer, metabolic disease, and cardiovascular pathology (Yang et al., 1996; Thijssen et al., 2006; Huang et al., 2021). In addition, galectin-1 regulates metabolic and vascular pathways, and pharmacologic inhibition of galectin-1 with OTX008 reduces fibrosis and lipogenesis in mouse models (Mukherjee et al., 2015; Kathiriya et al., 2017; Fryk et al., 2022), highlighting the therapeutic potential of modulating galectin levels.

Together, these studies demonstrate that galectins can regulate immune cell behavior, metabolism, and disease progression, and that recombinant expression and small-molecule inhibition are viable experimental strategies. These properties provide important context for investigating galectin-12, a less-characterized galectin that may be involved in metabolic and immune signaling in myeloid cells.

1.1.2 Tandem-repeat galectins

Understanding the behavior of other tandem-repeat galectins provides a basis for interpreting the biological activity of galectin-12. The two CRDs that distinguish tandem repeat galectins allow them to simultaneously bind different ligands, enabling them to crosslink cell surface glycans and trigger signaling. A particularly relevant example is

galectin-8, which regulates cell adhesion through protein-glycan interactions with integrins in the extracellular matrix (Zick et al., 2002).

Like galectin-8, galectin-12's tandem-repeat structure suggests it may crosslink cell-surface glycoproteins, yet whether it similarly influences cell adhesion and aggregation remains untested. Determining if galectin-12, hrGal-12, and other galectins can similarly influence cell adhesion is of interest. Galectin-8 can operate both intracellularly and extracellularly to target damaged vesicles for autophagy which parallels emerging views that galectin-12 may be secreted via secretory autophagy (Thurston et al., 2012; Tazhitdinova et al., 2024). Galectin-4 demonstrates the crosslinking capacity typical of tandem-repeat galectins, allowing it to aggregate cells and influence cell adhesion (Cao & Guo, 2016). This ability to bridge glycoproteins on separate cell surfaces makes galectin-4 a useful comparison for testing whether galectin-12 can similarly agglutinate red blood cells or promote cell-cell adhesion. Galectin binding and crosslinking at the cell surface can trigger downstream signaling events that may contribute to the regulation of cell differentiation.

In the context of cancer, both galectin-8 and galectin-9 are increased in various human cancers (Yang et al., 2021). For instance, galectin-9 interacts with immune checkpoint proteins PD-1 and TIM-3 to modulate T-cell responses, which has made it an appealing cancer immunotherapy target (Yang et al., 2021). As galectin-12 levels are lowered in Acute Myeloid Leukemia (AML) and breast cancer, it may function differently as a tumor suppressor gene (El Leithy et al., 2015; Assem et al., 2023).

The outlined examples have important considerations in testing the biological properties of hrGal-12. Can hrGal-12 promote cell adhesion and aggregation of human cells? Can galectin-12 interact with cell surface glycans to induce hemagglutination and/or differentiation? Addressing these questions will allow for clarification as to galectin-12's role in differentiation and tumor suppression separate from other tandem-repeat galectins.

1.2 Galectin-12

Galectin-12 is a tandem-repeat galectin that is highly expressed in adipocytes, leukocytes, sebocytes, and breast tissue. Galectin-12 is a 37.5 kDa protein originally identified in the Jurkat T-cell line and adipose tissue (Hotta et al., 2001; Yang et al., 2001). The *LGALS12* gene is located on the 11q13 human chromosome, which is a region commonly associated with genetic aberrations in cancer (El Leithy et al., 2015). *LGALS12* mRNA was also found at lower levels in skeletal muscle, kidney, reproductive organs, heart, thymus, pancreas, and spleen (Yang et al., 2001). *LGALS12* levels increased upon activation of the G1/S checkpoint and this increased expression is associated with cell cycle arrest and reduced proliferation (Yang et al., 2001). Cell differentiation is often associated with cell cycle exit and lowered proliferation, and it will be important to check if the hrGal-12 produced in this study can influence cell differentiation. Overall, galectin-12 is a multi-faceted protein involved in cellular differentiation, apoptosis, cell-cycle regulation, cell proliferation, and lipogenesis (**Figure 2**).

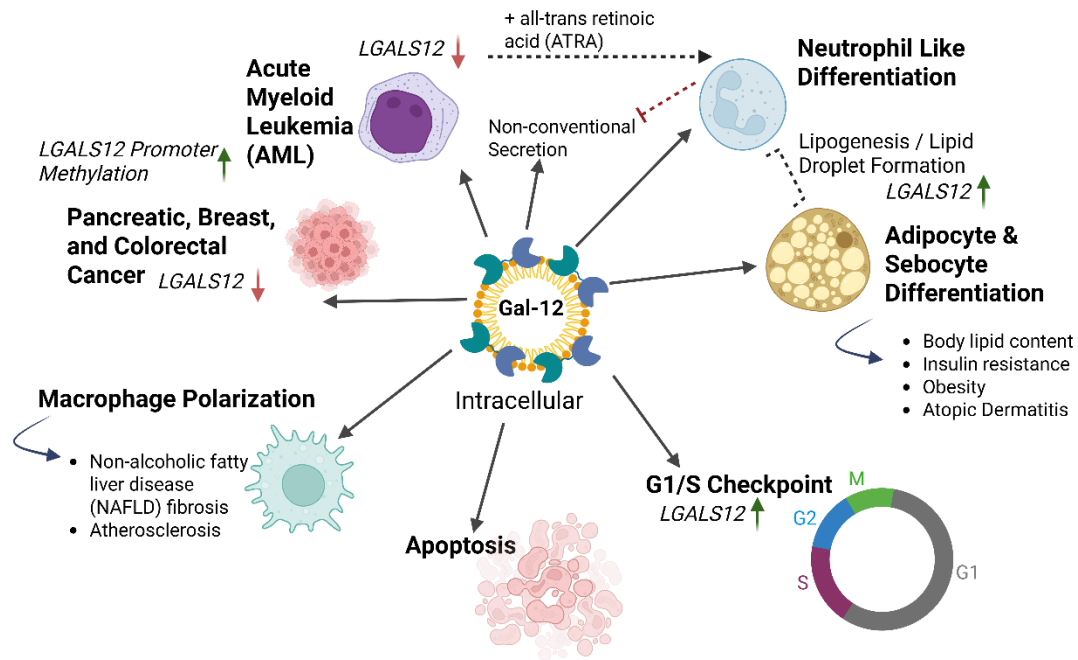


Figure 2. Overview of galectin-12 functions, subcellular localization, and expression in various conditions. Galectin-12 is involved in differentiation of neutrophils and adipocytes, and polarization of macrophages. Galectin-12 is upregulated at the G1/S cell cycle checkpoint. Galectin-12 levels are lowered in various cancers and the *LGALS12* promoter is known to be hypermethylated. Red arrows show lowered *LGALS12* expression and green arrows show increased *LGALS12* expression. Dotted red line indicates inhibition. Blue arrows link galectin-12 associated cellular processes to diseases and metabolic states. Figure prepared in BioRender.

1.2.1 Galectin-12 properties

Although galectin-12 has proven difficult to produce recombinantly, both the human and mouse forms have been purified and shown to prefer fucosylated glycans (Maller et al., 2020; Cagnoni et al., 2024). Galectin-12's C-terminal domain is the most divergent compared to other galectins, sharing less than 20% sequence identity. This divergence in C-terminal domain may explain why galectin-12 is challenging to produce recombinantly and prefers fucosylated glycans. The N-terminal domain of galectin-12 has many of the key residues as other galectins supporting its capacity for glycan binding. Early data showed galectin-12 binding lactose, but newer studies shows that its affinity to lactose is extremely low. Recombinant mouse galectin-12 could not be purified using lactosyl-sepharose beads (Yang et al., 2001; Maller et al., 2020). In a contradictory study in colorectal cancer cells, lactose completely blocked the SLC1A5-galectin-12 interaction (Katzenmaier et al., 2019). This raises further questions about which ligands galectin-12 binds to. Galectin-12 is closest in homology to galectin-8 but displays a more selective affinity for fucosylated glycans (Maller et al., 2020; Cagnoni et al., 2024). Galectin-12 is also predicted to oligomerize, which would enhance its cross-linking ability, and could explain its hemagglutination activity. (Baum, 2011). Overall, questions remain about galectin-12's biochemical properties and structure, highlighting the need for detailed recombinant expression and functional characterization in human cell-based systems.

1.2.2 Galectin-12 in adipocytes

Galectin-12 is required for adipocyte differentiation, with *LGALS12* expression increasing after three days of differentiation in 3T3-L1 mouse adipocytes and continuing to rise throughout the differentiation process (Hotta et al., 2001; Yang et al., 2004; Tazhitdinova et al., 2024). siRNA-mediated knockdown of *LGALS12* in mouse adipocytes results in reduced expression of key adipogenic transcription factors, including peroxisome proliferator-activated receptor γ (PPARG) and CCAAT enhancer-binding protein, accompanied by impaired adipogenic signaling and differentiation. Galectin-12 is also upregulated at both the mRNA and protein levels during cell cycle arrest, a state that is tightly coupled to terminal differentiation in adipocytes.

Beyond its role in differentiation, galectin-12 has been linked to metabolic state and apoptosis in adipose tissue. *LGALS12* mRNA levels were significantly elevated in monkeys subjected to caloric restriction, although no differences were observed between obese and lean monkeys or in insulin-resistant rat models (Hotta et al., 2001). Galectin-12 has also been implicated in adipocyte apoptosis, a process that adipocytes partially resist due to high basal expression of anti-apoptotic proteins such as B-cell lymphoma 2 (Hotta et al., 2001). Consistent with a metabolic regulatory role, hormones known to induce insulin resistance, including insulin, tumor necrotic factor α , and dexamethasone (steroid hormone), reduced *LGALS12* mRNA expression in mouse adipocytes, suggesting that decreased galectin-12 expression may contribute to the pathogenesis of insulin resistance (Fasshauer et al., 2002).

Galectin-12 plays a central role in adipocyte lipid metabolism by localizing to lipid droplets and regulating lipogenic signaling. Yang et al. (2011) were the first to identify galectin-12 localization to lipid droplets and demonstrated that galectin-12 deficient mice exhibit increased lipolysis and improved insulin sensitivity. Mechanistically, galectin-12 acts upstream of protein kinase A to regulate cyclic adenosine monophosphate levels and control fatty acid release from lipid droplets. Mice lacking galectin-12 showed reduced visceral and subcutaneous adipose tissue, lower leptin levels, and approximately 40% lower whole-body lipid content. Galectin-12 secretion from adipocytes was minimal, and its association with lipid droplets appeared to be glycan-independent, likely mediated by hydrophobic interactions. Consistent with enhanced lipolysis, phosphorylated protein kinase A levels were increased in galectin-12 deficient mice, enabling hormone-sensitive lipase to associate with lipid droplets and interact with adipocyte triglyceride lipase to promote lipid hydrolysis. Together, these findings establish galectin-12 as a lipid droplet-associated regulator of lipolytic signaling in adipocytes.

If inhibition of galectin-12 can enhance lipolysis while preserving overall adiposity *in vivo*, galectin-12 could be a potential therapeutic target for obesity and type II diabetes (Baum, 2011). 3T3-L1 adipocytes have previously been treated with corn silk extract and β -sitosterol to explore their effects on galectin-12 levels. These adipocytes exhibited reduced *LGALS12* expression, accompanied by decreased lipid droplet accumulation and

down-regulation of key adipogenic markers, including C/EBP β , C/EBP α , PPAR γ , Ap2, and adipsin, effects attributed to inhibition of protein kinase B and ERK1/2 signaling (Hsu et al., 2018). Consistent with galectin-12's involvement in adipocyte, sebocyte, and leukocyte differentiation, therapeutic strategies based on siRNA-mediated inhibition of *LGALS12* have been patented (Yang et al., 2005). These approaches propose reducing adipogenesis and modulating wound healing through altered white blood cell production (Yang et al., 2005).

Together, these findings show galectin-12 regulates differentiation, cell cycle arrest, apoptosis, and metabolic signaling in adipocytes. As myeloid differentiation similarly involves changes in proliferation and metabolic state, these adipocyte studies provide important context for investigating the role of galectin-12 during myeloid differentiation.

1.2.3 Intracellular galectin-12: function and localization

Galectin-12 localizes intracellularly to lipid droplets, where it colocalizes with key lipid-droplet associated proteins, including vacuolar protein sorting-associated protein VPS13C and Perilipin-1 (Yang et al., 2011, 2016; Wan et al., 2018). The role of intracellular galectin-12 in myeloid differentiation, and whether galectin-12 interacts with the same proteins in neutrophils is unknown. Galectin-12's association to the lipid droplet complicates its isolation from native tissue, and it behaves like a membrane protein *in vitro*, making recombinant purification difficult. Functional studies in mouse adipocytes demonstrate that both *LGALS12* and *VPS13C* are required for proper adipogenic differentiation. Notably, *VPS13C* knockdown results in a more pronounced reduction in galectin-12 levels than *LGALS12* knockdown alone, indicating that *VPS13C* is necessary for galectin-12 stability. Loss of *VPS13C* leads to lysosomal degradation of galectin-12 without affecting Perilipin-1, suggesting a specific stabilizing role rather than a general disruption of lipid-droplet structure (Yang et al., 2016).

Proteomic analyses have further identified additional galectin-12-interacting proteins, including molecular chaperones such as TriC/CCT subunits and HSC70, as well as proteins involved in cytoskeletal organization, transport, and cell-cycle regulation, including cluster of differentiation molecule 44 (CD44), tubulin beta isoforms 2A/4A,

neutral amino acid transporter B(0) (SLC1A5), and cyclin-dependent kinase 1 (CDK1) (Yang et al., 2016; Katzenmaier et al., 2019). These interactions suggest that galectin-12 participates in many protein interactions linked to its stability, trafficking, and function. From a biochemical perspective, these findings also raise the possibility that galectin-12 folding or stability may depend on interacting partners, an important consideration for recombinant expression and functional studies.

1.2.4 Galectin-12 in sebocytes

Galectin-12 is also highly expressed in sebocytes, which like adipocytes, undergo significant lipid accumulation and differentiation. Expression of galectin-12 was first confirmed in human sebocytes using the SZ95 cell line and whole human skin, where it was detected at both the gene and protein levels and linked to skin barrier function and immune responses (Harrison et al., 2007; Tsao et al., 2023, 2025). In sebocytes, galectin-12 localizes to both the nucleus and cytoplasm, consistent with its intracellular distribution in other cell types. The conserved involvement of galectin-12 in differentiation and cell-cycle regulation across adipocytes and sebocytes supports the hypothesis that galectin-12 may play a similar regulatory role in myeloid cells.

Functional studies further demonstrate a role for galectin-12 in regulating cell cycle progression and differentiation. Knockdown of *LGALS12* in SZ95 sebocytes increased cell cycle progression and reduced expression of key cell-cycle regulators, including cyclin A1 and cyclin-dependent kinase 2 (CDK2) (Tsao et al., 2022). *In vivo*, *LGALS12*-deficient mice exhibited smaller sebaceous glands, and testosterone-induced gland enlargement was abolished in these animals, indicating that galectin-12 is required for normal sebocyte differentiation and hormone response (Tsao et al., 2022).

Galectin-12 deficiency consistently lowers *PPAR* γ signaling and lipogenesis. In galectin-12 knockdown mice and *LGALS12*-deficient mouse skin, both *PPAR* γ expression and lipogenic activity were significantly reduced (Tsao et al., 2022). Conversely, overexpression of *LGALS12* in SZ95 sebocytes increased *PPAR* γ transcriptional activity, as measured using a firefly luciferase reporter assay (Tsao et al., 2022, 2023). These findings support the proposal that galectin-12 functions as a transcriptional co-factor for

PPARG and its partner, the retinoid X receptor (RXR). Knockdown of *LGALS12* in SZ95 sebocytes results in reduced expression of PPAR γ target genes, including diacylglycerol O-acyltransferase 1 (DGAT1) and acetyl-CoA synthetase 2, and is accompanied by a marked reduction in neutral lipid production (Tsao et al., 2023). Similar decreases in lipogenesis were observed in SEB-1 sebocytes and in galectin-12 knockout mice, indicating a conserved role for galectin-12 in regulating lipid accumulation across sebocyte models. Beyond metabolism, emerging evidence suggests that galectin-12 also contributes to immune regulation in the skin. Altered galectin-12 expression has been linked to Th2-mediated inflammatory responses, and galectin-12 knockout mice display attenuated atopic dermatitis severity, which may be attributed to lower PPAR γ signaling (Lin et al., 2023). Increases in *PPARG* and changes in lipid metabolism are features of adipocyte and hematopoietic cell differentiation, and work with galectin-12 in sebocytes, which provides a rationale to see whether hrGal-12 may be involved in cell differentiation.

1.2.5 Lipid droplets, lipogenesis, and lipolysis

Lipid droplets are dynamic organelles that store neutral lipids and triglycerides (TGs) and are made of a phospholipid monolayer studded with regulatory proteins (Jiang et al., 2022). Among these proteins, perilipin-1 has been shown to colocalize with galectin-12 on lipid droplets (Yang et al., 2011; Wan et al., 2018; Jiang et al., 2022). Recent work further highlights that lipid droplet size and function are regulated through interactions with other cellular organelles, emphasizing their dynamic functions beyond being passive lipid stores (Jiang et al., 2022).

Lipid storage and release are governed by the balance between lipogenesis and lipolysis, two tightly coordinated metabolic processes that shift in response to cellular state.

Lipolysis is the enzymatic breakdown of stored TGs into free fatty acids, which can then be utilized for energy production through β -oxidation or other metabolic pathways (Grabner et al., 2021). In contrast, lipogenesis involves the synthesis of new TGs from metabolic precursors such as glucose-derived acetyl-CoA or glycerol released from existing lipid stores. The balance between these processes is altered during metabolic stress, obesity, cancer, and cellular differentiation (Grabner et al., 2021).

Since galectin-12 localizes to lipid droplets and has been shown to regulate lipogenic and lipolytic signaling in adipocytes, understanding lipid droplet biology provides essential context for interpreting galectin-12 function. Importantly, metabolic reprogramming is a known aspect of hematopoietic and myeloid cell differentiation. Thus, lipid droplet-associated pathways that are regulated by galectin-12 in adipocytes may also be relevant in leukocytes.

1.2.6 Galectin-12 in myeloid differentiation and macrophage polarization

Increasing similarities between adipocytes and white blood cells have been reported, despite their distinct functions, including shared metabolic and differentiation pathways originating from bone marrow progenitors (Majka et al., 2010; Yang et al., 2012). Consistent with this overlap, galectin-12 has been implicated in both lipid metabolism and myeloid differentiation, although its role appears to be context-dependent.

In acute myeloid leukemia, galectin-12 expression varies by subtype and differentiation state. In the NB4 cell line, which is derived from acute promyelocytic leukemia (APL), galectin-12 levels are elevated, whereas expression is lower in HL-60 promyelocytic leukemia cells (Xue et al., 2016). Functional studies have explored varying galectin-12, and *LGALS12* knockdown in NB4 cells enhances all-trans retinoic acid (ATRA)-induced differentiation, accompanied by reduced lipid droplets and decreased PPAR γ expression, indicating that lipogenic signaling and myeloid differentiation can be uncoupled (Xue et al., 2016). Notably, galectin-12 knockdown in NB4 cells also increases p47^{phox} expression and reactive oxygen species (ROS) production, a hallmark of neutrophil maturation.

In contrast, HL-60 cells display increased *LGALS12* expression following neutrophil-like differentiation induced by ATRA and decreased *LGALS12* with DMSO (Vinnai et al., 2017; Tazhitdinova et al., 2024). Unlike NB4 cells, HL-60 cells lack the promyelocytic leukemia-retinoic acid receptor alpha (PML-RAR α) fusion protein, which may underlie these opposing expression patterns. Together, these findings indicate that galectin-12 plays a dynamic and cell-context-specific role during myeloid differentiation. This complexity underscores the need to directly assess how galectin-12 influences

differentiation programs in leukocytes, providing a rationale for studying the functional effects of recombinant human galectin-12 in this model.

Galectin-12 is also expressed in cells of the monocyte and macrophage lineages, further supporting its role in myeloid cell biology. Bone marrow–derived macrophages and macrophages isolated from mice exhibit substantial galectin-12 expression (Wan et al., 2016). Loss of galectin-12 biases macrophage polarization toward an M2, anti-inflammatory phenotype, whereas pro-inflammatory M1 polarization induced by lipopolysaccharide and tumor necrotic factor α is associated with increased *LGALS12* expression (Wan et al., 2016; Yunna et al., 2020). Mechanistically, elevated galectin-12 levels in macrophages enhance inflammatory cytokine production through activation of AKT, ERK, and NF- κ B signaling pathways (Wan et al., 2016).

M2 macrophages secrete transforming growth factor- β 1, a cytokine associated with tissue repair and fibrosis during chronic inflammation (Lee et al., 2023). In the liver, Kupffer cells, which are tissue-resident macrophages located in the hepatic sinusoids, play a central role in innate immunity by clearing cellular debris and endotoxins (Basit et al., 2025). In metabolic disorders such as non-alcoholic fatty liver disease (NAFLD), which is strongly linked to obesity, lipid metabolism is dysregulated and galectin-12 protein expression is increased in hepatic tissue, particularly at early disease stages (Lee et al., 2023). Functional studies show that galectin-12 knockout mice exhibit increased M2 macrophage polarization, hepatosteatosis, elevated hepatic lipid droplet accumulation, and accelerated NAFLD progression. These mice also display increased hepatic macrophage numbers when fed a high-fat diet, suggesting enhanced inflammatory recruitment or altered macrophage survival (Lee et al., 2023). Consistent with these findings, inducible knockdown of galectin-12 in THP-1 human monocytic leukemia cells increased expression of the M2-associated transcription factor STAT6 following interleukin-4 stimulation, a key driver of M2 polarization. Beyond NAFLD, galectin-12 also regulates macrophage lipid metabolism in other inflammatory contexts: galectin-12 knockout mice exhibit reduced atherosclerosis, adiposity, and hepatic lipid accumulation, together with fewer foam cells, which are lipid-laden macrophages formed by uptake of oxidized low-density lipoprotein during early atherogenesis (Lin et al., 2020). Consistent

with these *in vivo* findings, galectin-12 knockdown in THP-1 human macrophages reduces lipid droplet formation following oleic acid stimulation and increases expression of M2 macrophage markers, indicating that galectin-12 promotes lipid storage while modulating macrophage polarization.

1.2.7 Galectin-12 in colorectal cancer and pancreatic cancer

Several studies show that galectin-12 expression is lowered in multiple malignancies, including colorectal cancer and acute myeloid leukemia (Katzenmaier et al., 2017; Assem et al., 2023). In both cancers, reduced galectin-12 expression is linked to promoter hypermethylation, indicating epigenetic silencing as a shared mechanism of galectin-12 loss. Increasing promoter methylation using 5-aza-2'-deoxycytidine increased galectin-12 expression in colorectal cancer cells, highlighting the potential plasticity of galectin-12 regulation in cancer.

Consistent with its predicted tumor-suppressive role, galectin-12 levels are significantly reduced in colorectal cancer cell lines and patient-derived colon mucosa, while galectin-3 levels remain elevated, suggesting an inverse relationship between these two galectins in cancer metabolism and progression (Gopalan et al., 2016; Katzenmaier et al., 2017). Galectin-12 was shown to bind the glutamine transporter SLC1A5 in HCT116 cells, resulting in reduced glutamine uptake and suppression of glutamine anaplerosis, a key metabolic pathway supporting cancer cell growth (Katzenmaier et al., 2019). Cancer cells rely on altered metabolic pathways like the Warburg effect (elevated glucose consumption) and glutamine anaplerosis for cell growth (Yoo et al., 2020). Galectin-12 may reduce cancer cell growth and promote differentiation by decreasing glutamine anaplerosis.

Importantly, increased galectin-12 expression correlates with less invasive disease and improved survival in a subset of colorectal cancer patients (Gopalan et al., 2016). Induction of differentiation in colorectal cancer cells using sodium butyrate also resulted in elevated galectin-12 levels, further supporting an association between galectin-12 expression, reduced proliferation, and cellular differentiation (Katzenmaier et al., 2014).

Together, these findings suggest that galectin-12 may act at the intersection of metabolism and differentiation in cancer.

These cancer-associated functions of galectin-12 provide important context for the present study. Given that myeloid and leukocyte populations undergo metabolic and phenotypic changes during differentiation, and that galectin-12 expression is epigenetically suppressed in AML, these cells provide a relevant system in which to evaluate the properties of recombinant galectin-12. Accordingly, this study uses a myeloid leukocyte model to assess whether the purified hrGal-12 preparation exhibits biological effects consistent with previously reported galectin-12 functions.

1.2.8 Extracellular and secreted galectin-12

Galectin secretion generally occurs through unconventional mechanisms apart from the endoplasmic reticulum/Golgi pathway, and there is evidence for galectin-3 secretion in extracellular vesicles (Popa et al., 2018). It is unknown whether this secretion happens via microvesicles or exosomes, and galectin-1 can be secreted via direct translocation. Stress has also been shown to promote unconventional galectin secretion. In a key finding, Tazhitdinova et al. (2024) show that HL-60 cells can secrete galectin-12 into media under standard culture conditions while 3T3-L1 cells failed to do so. Further, this galectin-12 secretion was inhibited upon neutrophil-like differentiation with both ATRA and DMSO. Galectin-12 secretion appears to be tissue-specific, but the mechanism of its unconventional secretion remains unknown (Tazhitdinova et al., 2024). AML patients with lower *LGALS12* expression had worse survival outcomes, and the varying levels of *LGALS12* expression between AML patients is likely due to varying levels of promoter methylation (El Leithy et al., 2015; Assem et al., 2023). *LGALS12* upregulation is associated with higher AML remission rates.

1.2.9 Porcine galectin-12: expression and function

Human galectin-12 is predicted to regulate lipogenesis, and porcine models provide a relevant basis for understanding its function in lipid metabolism. In pigs, galectin-12 has been studied extensively in the context of fat deposition, where the goal is to reduce subcutaneous fat while increasing intramuscular adipose tissue to improve meat quality, such as marbling (Jiang et al., 2022). These studies indicate that galectin-12 integrates metabolic signaling pathways that influence adipocyte differentiation, and because lipid metabolism also changes during myeloid differentiation, these findings suggest that similar mechanisms may operate in human leukocytes (Jiang et al., 2022).

Mechanistic insight into galectin-12 function has been obtained through siRNA-mediated knockdown and CRISPR/Cas9 knockout of *LGALS12* in porcine adipocytes, where loss of galectin-12 reduces lipid droplet formation and overall lipid accumulation (Wu et al., 2018; Wu et al., 2024). *LGALS12* depletion leads to decreased expression of lipogenic markers including *PPARG*, fatty acid binding protein 4, and fatty acid synthase, along with increased expression of lipolytic enzymes such as adipose triglyceride lipase, lipoprotein lipase, and hormone sensitive lipase, effects that are conserved across porcine fetal fibroblasts, subcutaneous adipocytes, and intramuscular adipocytes (Wu et al., 2018; Wu et al., 2024). In parallel, cloning and characterization of the porcine *LGALS12* promoter demonstrated adipocyte-specific expression, providing a starting point for generating genetically modified pigs to investigate galectin-12 function (Zhang et al., 2022).

Together, these findings support a conserved role for galectin-12 as a positive regulator of lipogenesis and a suppressor of lipolysis. Since metabolic remodeling is a feature of myeloid cell biology, these findings provide important context for evaluating the biochemical properties of recombinant human galectin-12 *in vitro*.

1.3 Recombinant protein production

1.3.1 Overview of recombinant proteins

Recombinant proteins serve as an invaluable resource for the investigation of protein structure and function. Bacterial expression systems are extensively employed for the synthesis of recombinant proteins, including galectins, which do not have intricate post-translational modifications (Rosano & Ceccarelli, 2014; Prato et al., 2020). While it is feasible to purify proteins from native tissues, such methods frequently prove to be laborious, costly, and yield suboptimal amounts. An example of this is human insulin, which was initially extracted by pharmaceutical companies from pancreatic β -cells. Nonetheless, the exceedingly low yields rendered native purification impractical for extensive production, thereby propelling the advancement of recombinant insulin expression utilizing *E. coli* (Johnson, 1983).

This principle applies to galectin-12 as its low abundance and intracellular localization to lipid droplets make native purification inefficient. Therefore, recombinant expression provides a feasible route to obtain enough hrGal-12 for downstream studies.

Recombinant protein production is a multistep process which includes upstream cloning and expression, followed by purification, activity testing, and quality control (**Figure 3**).

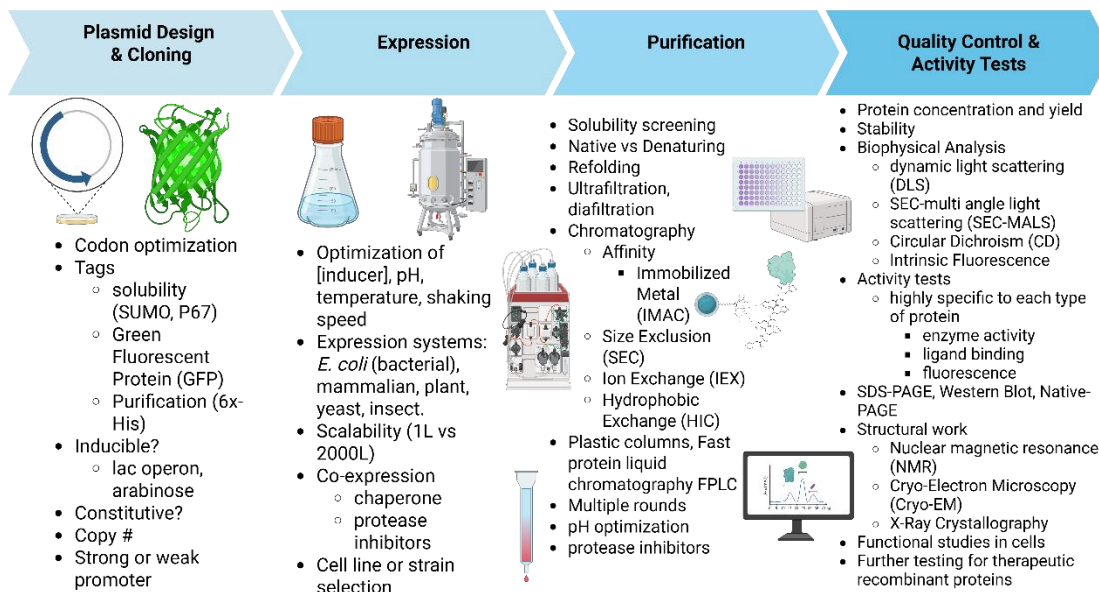


Figure 3. Overview of recombinant protein production. Upstream bioprocessing includes plasmid design and cloning, along with expression of recombinant protein in each host. Host species are carefully chosen based on complexity of each protein. Downstream bioprocessing includes purification of the recombinant protein, activity testing, biophysical analysis, quality control, structural determination, and *in vitro* or *in vivo* experimentation. Figure prepared in BioRender.

1.3.2 Cloning and expression in bacterial systems

The first stage of recombinant protein development is to clone the gene of interest into an expression vector. Conventional cloning techniques based on restriction enzymes, Golden Gate assemblies, and ligation-independent cloning work for most proteins (Celie et al., 2016). In the case of human proteins, it is often necessary to perform codon optimization to enhance translational efficiency within *Escherichia coli*. The selection of an appropriate vector is also of paramount importance; inducible systems such as T7-based IPTG induction or arabinose-inducible promoters provide a means for controlled expression while concurrently mitigating basal toxicity (Rosano & Ceccarelli, 2014; Riggs, 2018).

Factors in vector design and host selection influence whether a mammalian protein can be expressed and purified in an active form. These were key factors for developing a vector for a low-solubility protein like galectin-12. An N-terminal hexahistidine (His) tag was chosen for hrGal-12 in this study to slightly improve solubility and enable immobilized metal-affinity purification. Although hexahistidine tags are the standard, the number of histidine molecules can be modified (Rosano & Ceccarelli, 2014). Larger expression tags such as green fluorescent protein, glutathione s-transferase, or small ubiquitin-like modifiers were avoided because their size and structural complexity can interfere with the folding and activity of some recombinant galectins (Nishi, 2020).

Plasmid copy number and promoter strength were also considered in designing the hrGal-12 plasmid. High-copy plasmids can increase recombinant production but increase metabolic stress on *E. coli*, which can lead to protein aggregation (Rosano & Ceccarelli, 2014). As galectin-12 is an aggregation prone protein, an inducible T7-based system was selected to control expression and reduce metabolic stress to *E. coli* cells. Inducible expression proves to be especially advantageous for proteins that exhibit a propensity for misfolding or aggregation, as it facilitates the modulation of expression at reduced temperatures or elevated concentrations when deemed necessary.

Linker regions of recombinant proteins such as the linker region of tandem-repeat galectins can be targeted by native bacterial proteases, making bacterial strain selection

an important decision. *E. coli* BL21(DE3) cells were chosen for this study as they lack common bacterial proteases, including OmpT, and are the most common strain of *E. coli* used for recombinant production (Rosano & Ceccarelli, 2014). These combined vector and host considerations were critical for the successful expression and downstream purification of hrGal-12. While mouse recombinant galectin-12 and N-terminal tagged variants have been successfully purified, production of high-quality full length hrGal-12 needs further work (Maller et al., 2020; Cagnoni et al., 2024; Tsao et al., 2025). Understanding why previous attempts failed, and how to overcome these challenges, guided the design of this study's expression strategy.

Previous work with recombinant galectins and galectin-12 has utilized bacterial expression as they are low cost, easy to scale up, and compatible with established pET plasmids. Membrane proteins and hydrophobic proteins like galectin-12 are more likely to misfold in bacteria and be expressed in inclusion bodies. Inclusion bodies are insoluble protein aggregates that form during expression and complicate the purification process (Roufarshbaf & Akbari, 2023). Although purification of therapeutic proteins from inclusion bodies has become more common, this process utilizes strong denaturants like guanidine hydrochloride (Gdn-HCl) or urea, followed by refolding and dialysis (Buscajoni et al., 2022). *In vitro* refolding can be challenging and often requires extensive optimization.

To address the low solubility of galectin-12 in bacteria, many strategies can be employed. Co-expression with a molecular chaperone or a solubility tag can prevent aggregation. Various expression temperatures need to be tested, as lower temperatures can slow protein synthesis and allow for more soluble expression. Alternatively, directing expression to the periplasm using an N-terminal secretion sequence can bypass inclusion body formation entirely (Wingfield, 2015).

As galectin-12 is known to have low solubility, the cell lysis methodology also required careful consideration. Given galectin-12's hydrophobic nature, lysing the cells and denaturing hrGal-12 with guanidine was a logical choice. This allows solubilization of the inclusion bodies and hrGal-12 can be refolded following purification. Guanidine-

based denaturation offered several advantages over attempting to maintain the native state. Mechanical lysis methods like sonication or French press are designed to release soluble proteins but cannot solubilize inclusion body proteins, even with strong detergents. Following purification under denaturing conditions, hrGal-12 could then be gradually refolded through dialysis or dilution into physiological buffer. While refolding introduces the risk of producing inactive protein, it remained the most viable strategy for a protein that has consistently resisted soluble expression. The addition of reducing agents like 2-mercaptoethanol (BME) or dithiothreitol during cell lysis can prevent aberrant disulfide bond formation during the controlled refolding process.

1.3.3 Purification of recombinant proteins expressed in *E. coli*.

After cell lysis, recombinant proteins must be purified from host-cell contaminants using chromatographic methods selected according to the protein's physicochemical properties. Common purification strategies for protein expressed in *E. coli* include immobilized metal affinity chromatography (IMAC), ion-exchange chromatography, and size-exclusion chromatography (SEC) (Labrou, 2021). In this study, IMAC was particularly suitable because hrGal-12 was expressed with an N-terminal hexahistidine tag, allowing selective binding to Ni-NTA resin and elution with imidazole.

Affinity purification is frequently followed by additional chromatographic steps to improve purity and remove aggregates or misfolded species. Fast protein liquid chromatography (FPLC) systems enable reproducible implementation of these purification steps while monitoring protein elution by ultraviolet absorbance and conductivity, facilitating optimization and scalability (Morimoto & Walinda, 2024).

During cell lysis, endogenous bacterial proteases and phosphatases can degrade or modify recombinant proteins, reducing yield and functional integrity (Ryan & Henehan, 2017). This is a particular concern for proteins that require refolding or extended purification workflows, such as galectin-12. To minimize proteolysis, purification is typically performed at low temperatures with the inclusion of protease inhibitors appropriate for bacterial lysates. Protease inhibitors can be irreversible or reversible, which bind proteases transiently and therefore must be replenished throughout the

purification process (Ryan & Hennehan, 2017). The use of appropriate inhibitor combinations is critical for maintaining protein stability during multi-step purification procedures.

Ion exchange chromatography is another widely used purification strategy in which proteins bind to charged resins based on their net surface charge at a given pH (Labrou, 2021). Binding typically occurs at low ionic strength, with elution achieved by increasing salt concentration through either gradient or stepwise approaches. Both cation- and anion-exchange resins are commonly used within FPLC workflows (Labrou, 2021). However, for proteins that are expressed with affinity tags or require purification under denaturing or refolding conditions, ion exchange is often used as a secondary or polishing step rather than as the primary capture method. In the case of galectin-12, affinity-based purification followed by size-exclusion chromatography provided greater selectivity and compatibility with refolding requirements.

Another common method used with challenging proteins is, hydrophobic interaction chromatography (HIC), which separates proteins based on exposed hydrophobic surfaces. HIC operates under conditions opposite to ion-exchange chromatography, with proteins binding at high salt concentrations and eluting as salt concentration is reduced (McCue, 2009). High salt environments, commonly achieved using ammonium sulfate, promote hydrophobic interactions by reducing the solvation of nonpolar protein regions, thereby increasing their affinity for hydrophobic ligands on the resin (McCue, 2009). While HIC can be effective for purifying proteins with moderate surface hydrophobicity, excessively hydrophobic proteins like galectin-12 may bind too tightly to the column, limiting recovery and elution efficiency. In such cases, resins with lower hydrophobicity should be considered. (McCue, 2009).

SEC, also known as gel filtration, separates proteins based on their hydrodynamic radius (Fekete et al., 2014). Larger proteins elute earlier because they are excluded from the internal pores of the resin, whereas smaller proteins diffuse into the pores and elute later. Size-exclusion chromatography is especially useful for galectins, as their tendency to oligomerize or aggregate can complicate downstream functional assays. Accordingly,

SEC was employed as a secondary purification step to isolate hrGal-12 suitable for biochemical and cell-based experiments. SEC resins are commonly composed of neutral polymers such as Sepharose; however, this can be problematic for lactose-binding proteins, including many galectins, because Sepharose is derived from agarose, a galactose-containing polysaccharide that can be recognized by the carbohydrate-recognition domains of galectins, leading to nonspecific binding and reduced recovery. (Prato et al., 2020). This consideration is particularly relevant for galectin-12, as nonspecific binding during SEC could compromise recovery and obscure downstream functional assays. For effective resolution, SEC is most suitable when the proteins being separated differ in size by at least ~10 kDa (Fekete et al., 2014). In addition to purification, SEC can be coupled with multi-angle light scattering to assess molecular weight, oligomerization state, and aggregation, properties that are relevant for lectins such as galectin-12.

Following chromatographic purification, recombinant proteins typically undergo buffer exchange and dialysis, which can also serve as a critical refolding step when denaturants such as guanidine or urea are used during cell lysis (Popot, 2014). For proteins like galectin-12, which exhibit limited solubility and a strong tendency to aggregate, refolding represents a major bottleneck in recombinant production. Protein aggregation and precipitation during dialysis can substantially reduce yield and functional recovery, necessitating careful optimization of refolding conditions.

To address these challenges, refolding is often performed at small scale using solubility screening approaches, where buffer composition and additives are systematically varied prior to scale-up (Buscajoni et al., 2022). Additives such as urea, arginine, Triton X-100, sodium dodecyl sulfate (SDS), and polyethylene glycol are commonly included to suppress aggregation and stabilize partially folded proteins (Buchanan, 1999; Roufarshbaf & Akbari, 2023). While these strategies have traditionally relied on empirical trial-and-error methods, recent advances have incorporated design-of-experiments frameworks and automated screening platforms to improve reproducibility and efficiency (Vincentelli et al., 2004; Buscajoni et al., 2022; Sharma et al., 2022).

For proteins intended for therapeutic use, additional downstream steps such as endotoxin removal and validation are required. Endotoxin contamination is commonly assessed using the Limulus Amebocyte Lysate assay, which exploits the sensitivity of horseshoe crab amebocytes to bacterial lipopolysaccharides (Tindall et al., 2021). While endotoxin removal was not a primary objective of this work, such considerations are essential for translating recombinant galectins toward clinical applications.

After purification, recombinant proteins are evaluated for purity, quality, and functional activity. The specific activity assays employed depend on the biochemical properties of the protein of interest. For lectins such as galectins, hemagglutination assays are commonly used to assess carbohydrate-binding activity and confirm lectin activity. Because multiple purification routes can yield comparable outcomes, optimization of individual steps is often required. However, extensive high-throughput process development can be limited by time and resource constraints. In addition, batch-to-batch variability is a common challenge in recombinant protein production, emphasizing the importance of monitoring key parameters such as purity, yield, and activity throughout both upstream expression and downstream purification. These principles guided the selection and optimization of chromatographic and refolding approaches used to purify hrGal-12 in this work.

1.3.4 Other common recombinant expression systems

Although *E. coli* was selected to produce recombinant human galectin-12 in this study, several alternative expression systems are commonly used depending on the structural and functional requirements of a given protein. These systems are particularly relevant for proteins requiring complex post-translational modifications (PTMs), secretion, or specialized folding environments.

Mammalian expression systems, most notably Chinese hamster ovary CHO-K1 and HEK293 cells, are widely used for producing proteins with complex PTMs such as glycosylation, including monoclonal antibodies, hormones, and vaccines (Tihanyi & Nyitray, 2020). CHO-K1 cells are popular for industrial biotherapeutic production due to their capacity for human-like PTMs and scalability, especially with suspension-adapted

lines such as CHO-S (Tihanyi & Nyitray, 2020). However, mammalian systems generally produce lower protein yields, require longer culture times, and incur substantially higher costs than bacterial expression. In addition, the generation and maintenance of stable mammalian cell lines is time- and resource-intensive. Given that galectin-12 does not require complex glycosylation for activity and is predominantly intracellular, mammalian expression was not pursued in this work.

Insect cell expression systems, particularly *Spodoptera frugiperda* (Sf9 and Sf21) cells, are frequently used for toxic or multi-domain proteins and for viral protein production (Kwiatkowska et al., 2025). These systems provide more advanced folding machinery than bacteria and can support limited PTMs. Engineered derivatives, such as SfSWT-1 cells expressing mammalian glycosyltransferases, further expand their utility (Kwiatkowska et al., 2025).

Plant-based expression platforms represent another alternative, offering low production costs and scalability through transient expression systems such as *Nicotiana benthamiana* (Burnett & Burnett, 2019). Plant systems can perform certain complex glycosylation reactions and have been used to produce clinically relevant proteins, including virus-like particle vaccines (Benvenuto et al., 2023). Despite these advantages, plant expression systems require specialized steps and are not considered optimal for expressing galectins.

While multiple expression systems are available for recombinant protein production, *E. coli* expression provided the most practical balance of yield, cost, speed, and experimental flexibility for producing hrGal-12. This choice enabled optimization of purification and refolding strategies necessary to support functional studies *in vitro*.

1.3.5 Recombinant galectins and galectin-12

Past work with recombinant galectins has been critical for establishing effective production strategies, identifying functional assays, and revealing insights into galectin biology. Many human galectins have been successfully expressed in *E. coli* BL21 strains, which remain the standard host system because galectins generally lack complex post-translational modifications (Prato et al., 2020). Although lactose–Sepharose affinity

chromatography is commonly used for galectin purification, galectin-12 exhibits weak lactose binding, making His-tag-based affinity purification a more reliable strategy for recombinant hrGal-12 (Prato et al., 2020).

Functionally, recombinant galectins are frequently assessed using hemagglutination assays, as they can induce agglutination of erythrocytes from multiple species, including mouse, chicken, rabbit, and turkey (Nishi, 2020). The hemagglutination inhibition assay is an additional test that can be done to assess the glycan binding specificity of a recombinant galectin, and the IC₅₀ value for inhibition. Recombinant galectins typically lose hemagglutination activity within weeks when stored at 4°C, whereas recombinant mouse galectin-12 has been reported to remain active for up to four months under similar conditions (Maller et al., 2020).

Expression conditions also influence galectin stability and activity. Temperatures ranging from 20°C to 37°C have been reported for optimal expression of different galectins using either glutathione s-transferase or hexahistidine tags, highlighting the need to empirically optimize expression parameters for each galectin (Nishi, 2020). Importantly, galectins often require substantially higher concentrations to elicit cellular responses than to induce hemagglutination, an observation that has direct implications for dosing strategies in HL-60 differentiation assays and hemagglutination experiments performed in this study.

There is a growing body of literature demonstrating that recombinant galectins can directly influence immune cell growth, survival, and polarization. For example, recombinant galectin-1 induces apoptosis in activated human T-cells but not in resting T-cells (Perillo et al., 1995). Human galectin-1 has been successfully expressed in *E. coli* BL21(DE3) and purified under native conditions using β -lactosyl-sepharose, producing biologically active protein suitable for T-cell assays (Pace et al., 2003).

In contrast to galectin-12, galectin-1 and galectin-3 exhibit higher solubility *in vitro*, likely due to their single carbohydrate recognition domains and lower hydrophobic residue content. Galectin-9, another tandem-repeat galectin, has been expressed in a wide range of systems including *E. coli*, yeast, insect, mammalian, and moss cells; however, *E. coli*-based expression consistently yielded the highest purity and recovery (Nishi, 2020).

Functionally, recombinant galectins have been shown to modulate innate immune responses. Affinity-purified recombinant galectin-8 induces superoxide production in neutrophils at levels comparable to stimulation with fMLP (Nishi et al., 2003). Given these findings, exploring whether recombinant human galectin-12 can similarly influence reactive oxygen species production and myeloid differentiation in HL-60 cells represents a logical extension of prior work.

Previous work has demonstrated that active mouse recombinant galectin-12 (mrGal-12) can be expressed and purified, providing important insight into galectin-12 biochemistry (Maller et al., 2020). mrGal-12 was soluble in a simple 4-(2-Hydroxyethyl)-1-piperazineethanesulfonic acid (HEPES) buffer containing 8 mM BME and exhibited low affinity for lactose while preferentially binding fucosylated glycans (Maller et al., 2020; Cagnoni et al., 2024). While these findings establish proof-of-principle for galectin-12 activity, results obtained with the mouse protein do not necessarily translate to the human ortholog. Species-specific differences in glycan recognition have been documented even among closely related tandem-repeat galectins. For example, mouse and human galectin-9, despite both being successfully purified and crystallized, display markedly different carbohydrate-binding specificities, with mouse galectin-9 exhibiting approximately 100-fold lower affinity for the Forssman pentasaccharide compared to the human protein (Nagae et al., 2008). Such observations highlight that differences in CRD sequence can profoundly influence glycan-binding specificity of galectins. Additional complexity arises from structural divergence between the two CRDs present in tandem-repeat galectins. In galectin-8, for instance, the N-terminal CRD binds lactose with high affinity, whereas the C-terminal CRD does not, demonstrating the potential binding variability within a single galectin. Galectin-12 has a divergent C-terminal CRD, which is hypothesized to contribute to its atypical glycan-binding properties, hydrophobic character, and low solubility.

A major challenge in galectin-12 research is the lack of an experimentally resolved structure, largely due to difficulties in obtaining high-quality recombinant protein. Galectin-12 is highly hydrophobic and prone to aggregation *in vitro*, which has also limited the availability of specific and reliable antibodies (Tsao et al., 2025). Consistent

with these properties, attempts to purify soluble recombinant human galectin-12 using pGEX vectors with either N- or C-terminal glutathione s-transferase fusions were reported to be “practically impossible,” due to severe aggregation and poor solubility of the tagged protein (Nishi, 2020). The large size of the glutathione s-transferase tag likely amplified these issues. Collectively, these findings support the use of smaller affinity tags and alternative purification strategies, such as denaturing purification followed by controlled refolding, as a rational approach for producing active recombinant human galectin-12.

Recently, the N-terminal domain of human galectin-12 was purified and refolded using a P67 fusion tag composed of eight anti-parallel β -sheets. The isolated N-terminal domain was sufficient to induce hemagglutination of chicken red blood cells, whereas the full-length P67-tagged galectin-12 was inactive, suggesting that the divergent C-terminal domain may interfere with proper folding or lectin activity (Zhang et al., 2025). In a separate study, full-length human recombinant galectin-12 was produced using the same protocol previously established for mouse galectin-12, allowing characterization of its glycan-binding properties in solid-phase affinity assays (Cagnoni et al., 2024). This preparation confirmed that human galectin-12, like its murine counterpart, preferentially binds 3'-fucosylated glycans. However, functional assays such as hemagglutination or differentiation studies were not performed with the full-length human protein, in contrast to prior work with mrGal-12.

Notably, both studies relied on expression in Rosetta (DE3) *E. coli*, which differs from the more commonly used BL21(DE3) strain and may influence protein solubility and folding. Together with prior work on other tandem-repeat galectins, these studies highlight persistent challenges associated with producing soluble, functionally active hrGal-12 and demonstrate that tag choice, expression strain, and plasmid design strongly influence activity *in vitro*. Developing effective strategies to solubilize and purify hrGal-12 is essential for enabling reliable assessment of hrGal-12 properties, which is a central aim of this study.

1.4 HL-60 cell line as a model system to study galectins

1.4.1 HL-60 cell line and acute myeloid leukemia

Acute myeloid leukemia is a malignancy of myeloid progenitor cells characterized by a block in cellular differentiation. Differentiation therapy using all-trans retinoic acid, in combination with chemotherapy, is among the most effective treatment strategies for specific AML subtypes (Tallman et al., 1997). Acute promyelocytic leukemia (APL), a distinct form of AML, is defined by a t(15;17) chromosomal translocation involving the *PML* and *RAR α* genes. This translocation produces a chimeric PML–RAR α protein that disrupts transcriptional regulation and prevents normal leukocyte differentiation. ATRA functions by binding RAR α , thereby overcoming the dominant-negative effects of the fusion protein and restoring expression of genes required for terminal differentiation (Kamili & Stowell, 2016).

Previous work from this laboratory has shown that *LGALS12* expression increases in HL-60 promyelocytic leukemia cells and MDA-MB-231 breast cancer cells following treatment with ATRA. ATRA is a well-established inducer of cellular differentiation and cell-cycle arrest, particularly in myeloid leukemia models such as HL-60. The observed upregulation of *LGALS12* under these conditions suggests that galectin-12 expression may be linked to differentiation-associated transcriptional programs rather than proliferation, providing a rationale for examining the functional role of recombinant galectin-12 during HL-60 differentiation. (**Figure 4**) (Tazhitdinova, 2023; Tazhitdinova et al., 2024).

The AML HL-60 cell line originates from a middle-aged female patient, grows in suspension, and can be readily differentiated into multiple myeloid lineages using defined chemical stimuli (Collins, 1987; Bhakta et al., 2024). HL-60 cells represent the M2 subtype of AML in the French–American–British classification system and therefore lack the canonical t(15;17) PML–RAR α translocation, yet they remain highly responsive to differentiation-inducing agents. These characteristics make HL-60 cells a widely used model for studying immune responses, myeloid differentiation, and differentiation-based therapeutic strategies.

Previous work in this laboratory has established a role for *LGALS12* in HL-60 neutrophil-like differentiation (Vinnai et al., 2017; Tazhitdinova et al., 2024). Specifically, *LGALS12* expression was found to decrease following DMSO-induced differentiation, while remaining largely unchanged after menadione treatment. Further analysis revealed that DMSO-treated HL-60 cells exhibited reduced *LGALS12* expression; this decrease is hypothesized to be consistent with a shift toward an N2-like, pro-tumorigenic neutrophil phenotype. Although both ATRA and DMSO treatment induced characteristic lobulated nuclear morphology associated with neutrophilic differentiation, ATRA produced more pronounced morphological changes and had minimal effects on cell viability, in contrast to DMSO, which significantly reduced viability (Tazhitdinova et al., 2024). These differences reflect the distinct signaling pathways engaged by each differentiation stimulus (**Figure 4**).

Following ATRA-induced differentiation of HL-60 cells, subsequent treatment with *Porphyromonas gingivalis* lipopolysaccharide increased both lipid droplet size and number (Nose et al., 2013). This observation aligns with findings from this laboratory showing that ATRA treatment alone increases lipid droplet abundance in HL-60 cells. Because *LGALS12* expression also increases following ATRA-induced differentiation, these data raise the question of whether galectin-12 directly contributes to lipid droplet formation during myeloid differentiation. Addressing whether recombinant human galectin-12 (hrGal-12) can independently modulate lipid droplet formation or differentiation-associated phenotypes in HL-60 cells is of interest.

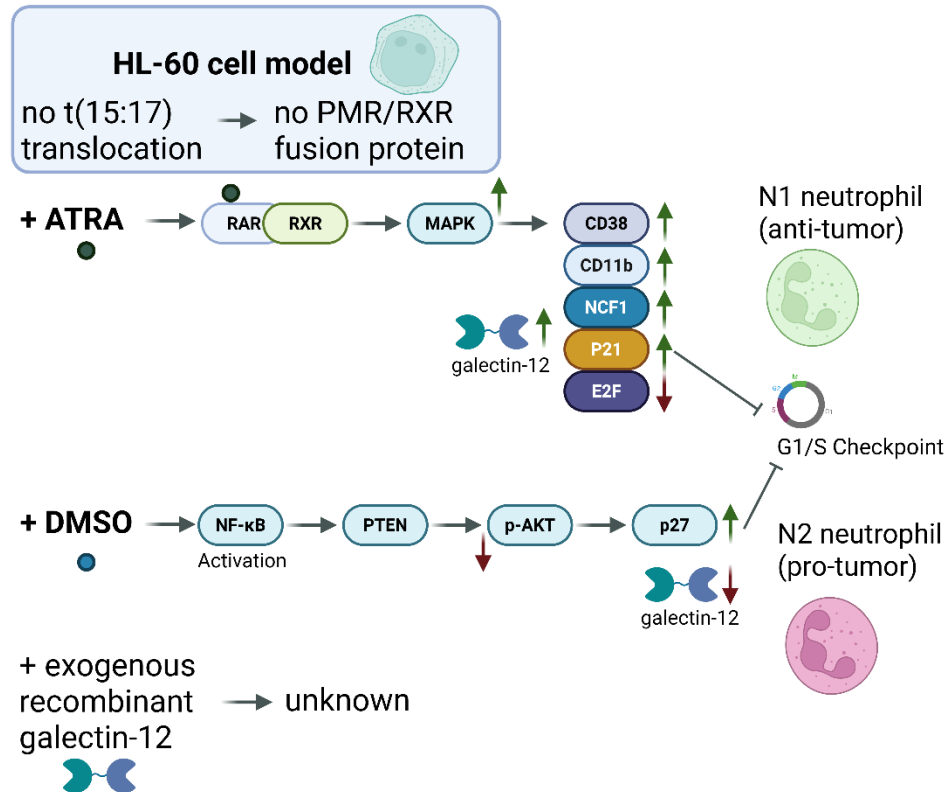


Figure 4. Proposed model of HL-60 neutrophil like differentiation. ATRA induces differentiation by binding to RAR and RXR directly stimulating MAPK and may promote an N1 anti-tumor phenotype. DMSO also inhibits G1/S checkpoints by modulating p27 levels resulting in a pro-tumor phenotype and lowered cell viability. ATRA treatment increases *LGALS12* levels while DMSO treatment lowers *LGALS12* levels. Adapted from Lee et al., 2005; Tasseff et al., 2017; Tazhitdinova et al., 2024; Wang et al., 1996. Figure made in BioRender

1.4.2 HL-60 cells and galectins

Galectins are master regulators of neutrophil function, contributing to neutrophil extravasation, chemotaxis, reactive oxygen species (ROS) production, and turnover (Robinson et al., 2019). Studies in the Timoshenko laboratory have established HL-60 and related cancer cell line models to explore galectin-mediated regulation of neutrophil phenotypes. Treatment of HL-60 cells with DMSO upregulates galectins-1, -3, and -10, while downregulating galectins-9 and -12 (Vinnai et al., 2017; Tazhitdinova et al., 2024). HL-60 cells treated with either ATRA or DMSO show increased expression of the cell differentiation marker *NCF1* (Figure 4). Both differentiation stimuli also increased lipid droplet numbers in HL-60 cells; however, how lipid droplet formation intersects with galectin-12 regulation and neutrophil differentiation remains unclear, providing a rationale for examining the effects of recombinant galectin-12 in this model (Tazhitdinova et al., 2024). Although the role of galectins in myeloid differentiation is still being elucidated, HL-60 cells provide a well-established model in which distinct lineage programs can be selectively induced. Treatment with sodium butyrate, phorbol 12-myristate 13-acetate (PMA), or DMSO drives HL-60 differentiation toward eosinophilic, monocytic, and neutrophilic phenotypes, respectively (Abedin et al., 2003). In this system, galectin-10 is upregulated during neutrophilic differentiation, whereas galectin-9 is downregulated during monocytic and eosinophilic differentiation, indicating that individual galectins are differentially regulated in a lineage-dependent manner.

Treatment of HL-60 cells with the O-linked N-acetylglucosamine inhibitor Thiamet G led to an increase in *LGALS12* expression while other galectins remained unchanged (Sherazi et al., 2018). It has been proposed that cellular differentiation is associated with reduced O-linked N-acetylglucosamine signaling and increased galectin secretion, whereas elevated intracellular galectins are linked to cell stemness (Tazhitdinova & Timoshenko, 2020), supporting a role for galectin-12 in myeloid cell differentiation.

Given that galectin expression in general, and specifically in HL-60 cells, is dynamically regulated by differentiation stimuli, defining how individual galectins such as galectin-12 influence this process is critical for understanding their functional roles in myeloid differentiation.

1.4.3 Neutrophil phenotypes and myeloid differentiation

Cellular differentiation is a tightly regulated process in which stem and progenitor cells become specialized cell types through tightly controlled transcriptional programs. In acute myeloid leukemia, this process is disrupted by a differentiation block that prevents malignant cells from progressing to mature myeloid lineages (Kamili & Stowell, 2016). As a result, understanding the molecular regulators of myeloid differentiation is central to elucidating AML pathophysiology and to developing differentiation-based therapeutic strategies.

Hematopoietic differentiation begins with bone marrow–derived hematopoietic stem cells, which give rise to both lymphoid and myeloid lineages (Mahalingaiah et al., 2018). While lymphoid progenitors differentiate into B and T lymphocytes involved in adaptive immunity, common myeloid progenitors generate megakaryocytes, erythrocytes, and myeloblasts. Myeloblasts subsequently mature through promyelocytic stages into granulocytes, including neutrophils, basophils, and eosinophils, or into monocytes that further differentiate into macrophages and dendritic cells (**Figure 5**). Importantly, AML subtypes defined by the French–American–British classification correspond to distinct stages of myeloid differentiation, providing a framework for studying problems in differentiation in model systems such as HL-60 cells.

Neutrophils are a type of white blood cell (leukocyte) derived from hematopoietic stem cells in the bone marrow and are key effectors of the innate immune response (Jiang et al., 2022). Their functional maturation is characterized by the acquisition of antimicrobial mechanisms including phagocytosis, degranulation, neutrophil extracellular trap (NET) formation, and a robust respiratory burst. Mature neutrophils isolated from human blood typically contain a low number of lipid droplets, often reported as approximately one droplet per cell (Weller et al., 1989), indicating that lipid metabolism is tightly regulated during terminal differentiation.

A hallmark of neutrophil differentiation is activation of the NADPH oxidase (Phox) complex, which drives reactive oxygen species (ROS) production during the respiratory burst. This multicomponent enzyme complex consists of the membrane-bound subunits

gp91^{phox} (NOX2) and p22^{phox} (CYBA), as well as cytosolic regulatory proteins p47^{phox} (NCF1), p67^{phox} (NCF2), and p40^{phox} (NCF4) (Zeng et al., 2019). Expression of *NCF1* and *NCF2* is commonly used as a biomarker of neutrophil differentiation in HL-60 cells and related myeloid models (Vinnai et al., 2017; Tazhitdinova et al., 2024), providing a reliable way to assess differentiation status.

Various immune cell phenotypes are increasingly classified along pro- and anti-inflammatory axes. Neutrophils can adopt functionally distinct N1 (anti-tumor) and N2 (pro-tumor) phenotypes (Wang et al., 2018). N1 neutrophils promote tumor cell cytotoxicity through the production of nitric oxide, hydrogen peroxide (H₂O₂), and tumor necrosis factor- α , and support adaptive immunity by enhancing T-cell activation via CD86 and CD54 expression. In contrast, N2 neutrophils contribute to tumor progression by promoting reactive oxygen species (ROS) production, angiogenesis, and cancer cell growth and metastasis (Wang et al., 2018). Together, these established markers and features of neutrophil differentiation provide a basis for testing the effects of recombinant galectin-12 on HL-60 cell differentiation.

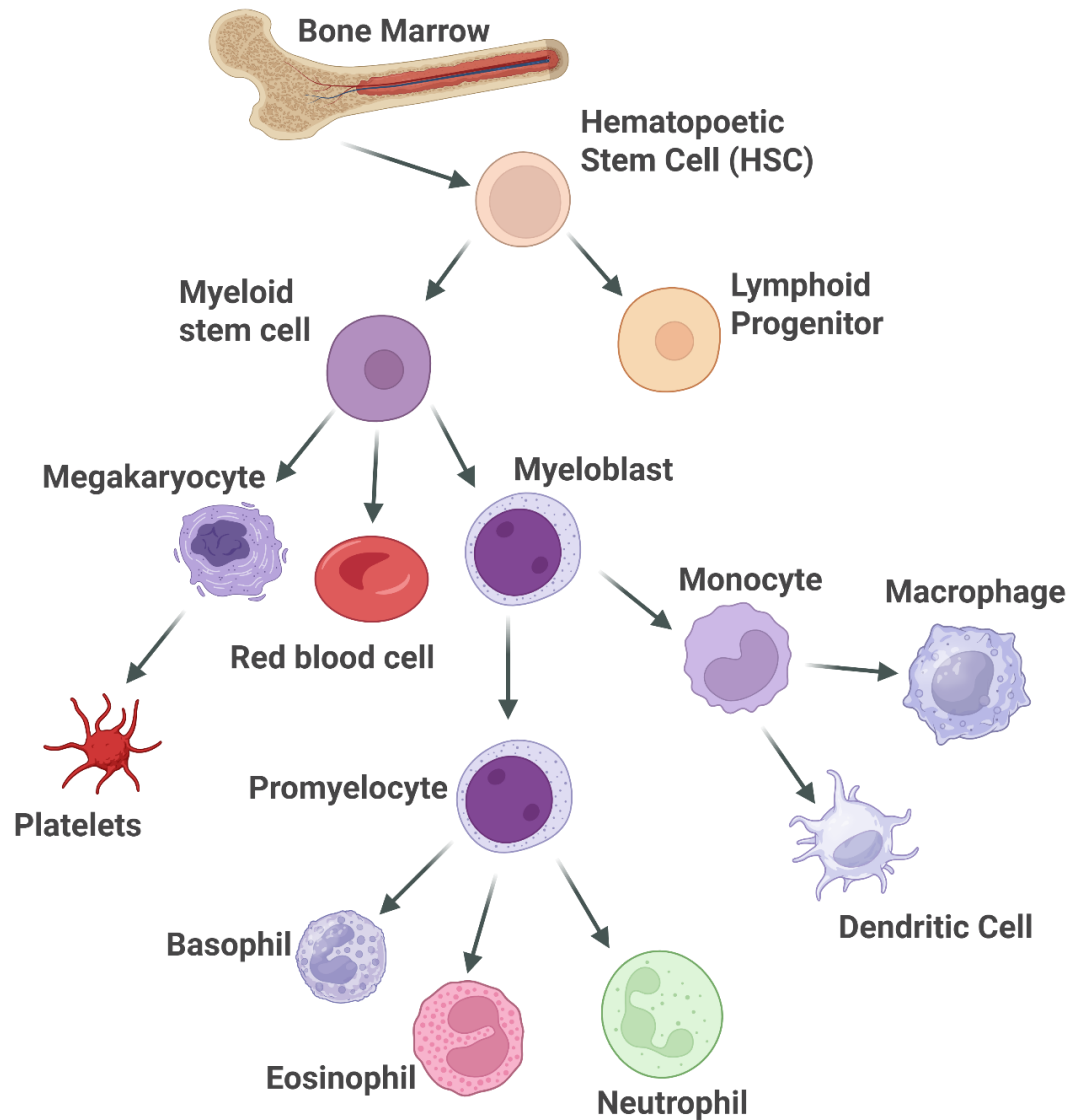


Figure 5. Myeloid cell differentiation from bone marrow. Hematopoietic stem cells from bone marrow respond to various signals to become either lymphoid or myeloid progenitor cells. Myeloblasts become promyelocytes which are represented by the HL-60 cell model. Promyelocytes further differentiate into basophils, eosinophils, and neutrophils. Different subtypes of AML represent different cell types in myeloid differentiation. Figure made in BioRender.

1.5 Objectives and Hypothesis

Although mouse and human recombinant galectin-12 have been produced, purification of full-length hrGal-12 remains technically challenging due to its hydrophobic nature, and no high-resolution human galectin-12 structure is currently available (Maller et al., 2020; Cagnoni et al., 2024; Tsao et al., 2025). Furthermore, it remains unknown whether hrGal-12 can influence myeloid differentiation, which is particularly important because agents that restore myeloid differentiation form the basis of differentiation therapy in AML. AML and breast cancer patients have lowered levels of galectin-12, which supports its role as a tumor suppressor gene (El Leithy et al., 2015; Assem et al., 2023; Tazhitdinova, 2023; Tazhitdinova et al., 2024). Galectin-12 levels have been shown to increase with ATRA treatment in HL-60 cells and decreased with DMSO, while both induced neutrophilic differentiation (Vinnai et al., 2017; Tazhitdinova et al., 2024).

I hypothesize that functionally active hexahistidine-tagged recombinant human galectin-12 expressed in *E. coli* interacts with cell surface ligands on HL-60 cells and, independently, promotes cell differentiation.

Objective 1: Hexahistidine-tagged recombinant human galectin-12 (hrGal-12) will be cloned, expressed in BL21(DE3) *E. coli*, purified and biochemically and biophysically characterized, with its galectin activity evaluated by a rabbit-blood hemagglutination assay.

Objective 2: To examine dose- and time-dependent effects of hrGal-12 on multiple responses of HL-60 cells as a model system including cell aggregation, adhesion, proliferation, and differentiation.

Chapter 2

2 Materials and Methods

2.1 Chemicals and reagents

GeneJET plasmid miniprep kit (K0502), HisPur Ni-NTA beads (88832), 3.5K molecular weight cut-off Snakeskin dialysis tubing (88244), TRIzol™ (15596018), and NaCl (S271) were acquired from Thermo Fisher Scientific (Mississauga, ON). *Ricinus communis agglutinin* (RCA) (L-1080-2) was purchased from Vector Laboratories (Toronto, ON). Ca²⁺ and Mg²⁺ free D-PBS (311-425-CL) and PBS (311-010-CL), Iscove's Modified Eagle Medium (IMEM) (319-105-CL), advanced cDNA synthesis kit (801-100-XR), heat deactivated fetal bovine serum (080-450), Hank's balanced salt solution (HBSS), 100x Penicillin/Streptomycin, and Glycine (800-045-CG) were bought from Wisent Bio Products (Saint-Jean-Baptiste, QC). *LGALS12* cDNA VersaClone plasmid was bought from R&D Systems (AAG40864) (Oakville, ON). pET28a-STIM1 plasmid was kindly provided by Dr. Peter Stathopoulos at the University of Western Ontario. Primers and SYBR Safe DNA gel stain (S33102) were purchased from Invitrogen (Burlington, ON).

Immobilon classico western blot HRP substrate (ABLUC500), citrus pectin (P9135), D-lactose monohydrate (L254), 2-propanol (I9516), sodium azide (S2002), polyvinylidene fluoride (PVDF) Membrane (3010040001), N,N,N',N'-Tetramethylethylenediamine (T9281), all-trans retinoic acid (ATRA) (R2625), dimethyl sulfoxide (DMSO) (D26500) and Trizma Base (T6066) were purchased from Sigma Aldrich (Oakville, ON). 10% washed and pooled rabbit red blood cells (R403-0050) were obtained from Rockland Immunochemicals (Pottstown, PA). Trypan blue 0.4% (15250061) was purchased from Gibco (Mississauga, ON). Methanol (101158.FDL) was obtained from Pharmco (Brampton, ON). 2x Frogga Taq Mix (FBTAQM) and Froggarose LE molecular grade agarose (A87) was bought from FroggaBio (Concord, ON). Glycerol was purchased from Caledon Chemicals (5350-01) (Caledon, ON)

Acryl/Bis 29:1 40% (ACR004), Ampicillin, sodium salt (AMP201), arginine (ARG006), glutathione oxidized (GTH002), glutathione reduced (GTH001), guanidine HCl (GUA003), imidazole (IMD508), kanamycin monosulfate (KAN201), tryptone (TRP402.205), and urea (URE002) were purchased from BioShop (Burlington, ON).

Mammalian Protease Inhibitor Cocktail, 100x Strength Solution (BS386), ammonium persulfate (APS) (AB0072), 2-mercaptoethanol (BME) (MB0338), 2x radioimmunoprecipitation (RIPA) Buffer with EDTA and EGTA (pH 7.4) 2x concentrate (RB4477), and glutaraldehyde 50% solution (G0875) were bought from Bio Basic (Markham, ON). Non-fat dry milk blotting-grade blocker (1706464) and 10% Tween-20 Solution (1610781) were purchased from Bio-Rad (Mississauga, ON). DAPI fluor shield mounting medium (ab104139) and Coomassie InstantBlue[®] (ab119211) were purchased from Abcam (Cambridge, UK).

2.2 Cloning and expression of hrGal-12

2.2.1 Preparation of *LGALS12* cDNA plasmid

DH5 α *E. coli* cells were transformed with 0.2 μ g/mL human *LGALS12* VersaClone cDNA plasmid (AAG40864; R&D Systems, Inc.) by incubation on ice for 30 min, followed by heat shock at 42°C for 1 min. The culture was placed in a shaking incubator for 1 hour at 37°C in 15 mL culture tubes with 1 mL of sterile Luria-Bertani Broth (LB). Transformed bacteria were diluted and a small volume (~150 μ L) was plated onto an LB agar dish with ampicillin. Plates were then placed into an incubator overnight at 37°C. Individual colonies were picked using pipette tips and placed into tubes with 5 mL LB and 50 μ L ampicillin (100 μ g/mL). Colonies were cultured overnight in a shaking incubator at 37°C at 200 RPM. Plasmid DNA was isolated using a GeneJET Plasmid Miniprep Kit (Thermo Fisher Scientific) according to the manufacturer instructions. DNA concentration was determined using a Nanodrop spectrophotometer (ThermoFisher Scientific).

LB media was prepared by mixing 10g Tryptone (BioShop), 10g NaCl (Fisher Chemical), and 5g Yeast extract (BioShop) with 1L ddH₂O. This LB was placed in 4L Erlenmeyer flask covered with tinfoil or 1L Schott bottle and autoclaved for 20 minutes.

2.2.2 Cloning of *LGALS12* into pET-28a plasmid

Both *LGALS12* cDNA plasmid (1 µg) and pET-28a plasmid (1 µg) with STIM-1 were digested with NheI (1 U/µg) and XhoI (1 U/µg) restriction enzymes overnight at 37°C in a water bath. To verify successful restriction digestion, restriction fragments were run on a 1% agarose gel for 45 minutes at 120 Volts in 1x TAE buffer. The gel was stained with ethidium bromide and visualized using a UV transilluminator.

LGALS12 insert and pET28a plasmid were excised using a sterile razor blade from the agarose gel and plasmid DNA purified using a gel/PCR DNA Purification Kit (Geneaid) according to the manufacturer's instructions. Purified DNA was resuspended in autoclaved ddH₂O. *LGALS12* insert was then ligated into a pET-28 plasmid at a 3:1 insert-to-vector molar ratio using T4 DNA ligase (**Figure 6**). The insert, plasmid, and ligase were combined in a tube and heated at 40°C followed by 2 minutes on ice. The tube was briefly centrifuged to collect the contents and incubated overnight in a 16°C water bath.

The *LGALS12*-pET28a plasmid was collected and transformed into DH5α cells using 7.5 µL plasmid and 100 µL of competent DH5α cells and plated onto a LB-agar kanamycin plate (60 µg/mL). Individual colonies were picked and transferred to 5 mL LB medium containing kanamycin (60 µg/mL) and grown at 200 RPM at 37°C overnight. Plasmid DNA was purified using the GeneJET Plasmid Miniprep Kit (Thermo Fisher Scientific), and plasmid DNA concentration was measured with a Nanodrop spectrophotometer.

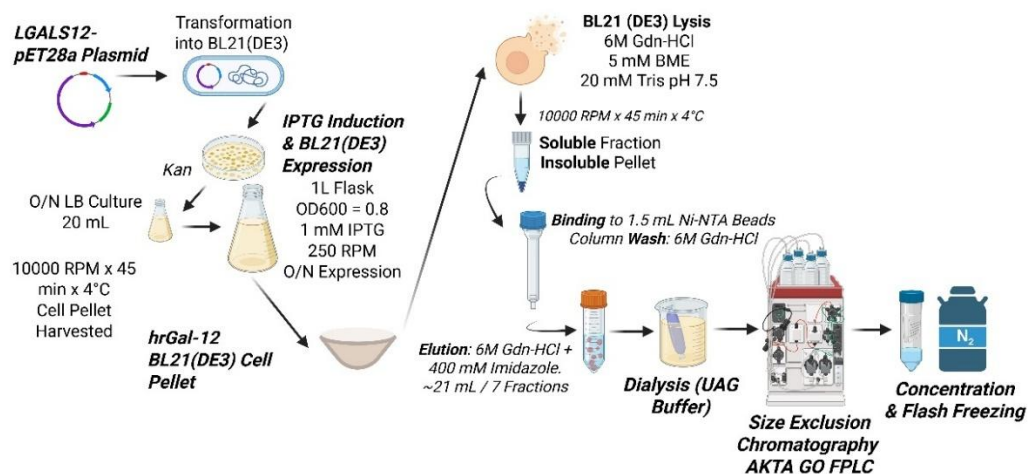


Figure 6. Cloning, expression, purification, and refolding of hrGal-12 in BL21(DE3) *E. coli*. Overview of hrGal-12 production from cloning, expression, purification strategy, and stock solution storage. Figure made in BioRender.

2.2.3 Colony PCR and Sanger sequencing

Purified *LGALS12*-pET28a plasmid was confirmed using colony PCR. At least 10 random DH5 α or BL21(DE3) colonies from ampicillin plates were picked and mixed with ddH₂O. PCR reactions were prepared using 10 μ L of 2 \times FrogaMix, 0.25 μ L of T7 forward primer (5'-TAATACGACTCACTATAGGG-3'; 0.5 μ M final concentration), 0.25 μ L of T7 reverse primer (AT56.1; 5'-GCTAGTTATTGCTCAGCGG-3'; 0.5 μ M final concentration), and 2 μ L of nuclease-free water. Finally, 7.5 μ L of a colony suspension in ddH₂O was added to each reaction. Conventional PCR was performed and bands visualized on 1% agarose gel stained with an ethidium bromide. 5 μ L of the Gene ruler 1 kB ladder (ThermoFisher Scientific) was loaded to determine amplicon size. Randomly selected colonies were sequenced by Sanger sequencing at Robarts Research Institute to confirm *LGALS12* insertion into pET28-a vector. 20 μ L T7 forward (0.5 μ M) and reverse (0.5 μ M) primers per reaction.

2.2.4 Expression of hrGal-12 in BL21(DE3) *E. coli*

Competent BL21(DE3) *E. coli* cells were transformed with 1 μ L of hrGal-12 plasmid (~200 ng/ μ L) and left on ice for 30 minutes. They were then heat shocked for 1 minute at 42°C and then placed back on ice for 2 minutes. 1 mL of LB was added and cells were placed in a shaking incubator for 1 hour at 37°C at 195 RPM. 150 μ L was then plated on LB-agar kanamycin plate (60 μ g/mL). This was wrapped in tinfoil and left to grow at room temperature. Single BL21 colonies with hrGal-12 plasmid were picked and inoculated into a small Erlenmeyer flask with 20 mL LB and 20 μ L kanamycin (60 μ g/mL). Bacterial cells were left to grow overnight in shaking incubator at 37°C at 200 RPM.

Overnight culture was poured into 1L LB media with kanamycin (60 μ g/mL) and left in a large shaking incubator for 1 hour at 37°C at 200 RPM. A 1 mL sample was taken from flask to measure the optical density at 600 nm in a plastic cuvette. OD measurements were continued until the bacterial culture reached an optical density at 600 nm of 0.6 – 0.8. At this point, 1 mM isopropyl β -D-1-thiogalactopyranoside (IPTG) was added and the incubation temperature decreased to 25°C and the culture left to grow overnight.

Overnight culture from 4L flasks was collected in 500 mL tubes and balanced using a scale. These were then loaded into J2-21M centrifuge (Beckman) with compatible rotor. Bacterial cells were then centrifuged at 7250 RPM at 4°C. The LB supernatant was then discarded and the pellet collected in a 50 mL conical tube using a spatula. Bacterial pellets were stored at -80°C until further use.

Samples of bacteria were taken before and after IPTG induction for further SDS-PAGE and Western Blot analysis.

2.3 Purification of hrGal-12

Bacterial cell pellets were thawed and resuspended in lysis buffer containing 45 mL of 6M Guanidine Hydrochloride (Gdn-HCl) (BioShop), 20 mM Tris pH 7.5-, and 5-mM β -mercaptoethanol (BME). The pellet was mechanically disrupted and homogenized in lysis buffer using a serological pipette and manual force. The lysed pellet was then rotated slowly at room temperature for an hour. The bacterial lysate containing hrGal-12 was placed into ultracentrifuge tubes and balanced using a scale. The soluble and insoluble fractions were separated using a J2-21 centrifuge (Beckman) and JA-20 rotor at 10,000 RPM for 45 minutes at 4°C. 1.5 mL of regenerated Ni-NTA beads (HisPur, Thermo Scientific) were added to the soluble fraction and the tube was rotated in a cold room for 90 minutes. The insoluble fraction was collected for SDS-PAGE analysis. Bacterial cell lysis by sonication was also tested.

The bead and soluble fraction mixture was centrifuged for 5 minutes at 2000 g at 4°C and the majority of supernatant poured out. Beads were resuspended in the soluble fraction and all transferred to a plastic gravity-flow chromatography column (BioRad).

Flowthrough was collected. This was followed by 3 washes (10 mL each) with wash buffer containing 20 mM Tris pH 7.5, 5 mM BME, and 30 mL of 6 M guanidine hydrochloride. The wash sample was collected for SDS-PAGE analysis. A plastic tube was attached to the column and a clamp added to restrict flow before elution. The elution buffer contained 400 mM Imidazole (BioShop), 20 mM Tris pH 7.5, 5 mM BME, and 30 mL 6 M guanidine hydrochloride. 3 mL elution buffer was added to the clamped column for 2 minutes, followed by elution into glass tubes (**Figure 6**). The tubes were stored on

ice. Seven elution fractions were collected and sampled individually before pooling together for further use.

The pooled hrGal-12 fractions were loaded into 3.5 kDa molecular weight cut off Snakeskin dialysis tubing (Thermo Scientific) and clipped on both ends. 5 mL elution fractions were dialyzed overnight in 500 mL refolding buffer at 4°C with gentle stirring in a beaker. Dialyzed and refolded hrGal-12 was collected, flash frozen in liquid nitrogen, and stored at -80°C.

Following Ni-NTA purification, hrGal-12 was further purified by SEC with using an AKTA GO™ system. The AKTA GO™ was controlled and monitored using the Unicorn™ V 7.0 (Cytiva) software. A Cytiva S75 16/600 HiLoad column was utilized and various other Cytiva columns were also tested (**Table 3**). UAG buffer was sterile filtered and degassed before use in purification. The column was equilibrated with UAG buffer at 4°C with 1 column volume (140 mL). UV280 and conductivity were monitored continuously on the Unicorn software. The hrGal-12 Ni-NTA sample (1-5 mL) was injected into the AKTA and set to run through column with UAG for 1 column volume and collected in a discard tube until an increase in UV280 was observed. Subsequent fractions were collected using a F9-R fraction collector (Cytiva) in 2 mL fractions in glass tubes. Fractions corresponding to the major peak were analyzed individually by SDS-PAGE to identify those containing hrGal-12. Positive fractions were then pooled and tested using Western blotting. Chromatograms were extracted from Unicorn software and plotted in GraphPad Prism (**Figure 6**).

SEC hrGal-12 was then concentrated to 2 mg/mL using 10 kDa cut off concentrator (Amicon) at 1400g for 2 hours at 4°C. The concentrator was first equilibrated with water and UAG buffer multiple times. Samples were flash frozen, aliquoted, and stored at -80°C. This stock of hrGal-12 was used for all subsequent work. hrGal-12 protein concentration was determined using the Bradford and Nanodrop, and purity with SDS-PAGE and Western blot.

Table 1. AKTA GO™ columns & buffer conditions assessed with hrGal-12 in UAG.

Column Type	Resin	Buffer A	Buffer B	Gradient / Elution Method
S75 16/600 HiLoad	Size Exclusion (SEC)	UAG buffer pH 7.5	N/Ap	1 column volume (135 mL) in 2 mL fractions with F9-R collector
HiTrap SP	Cation (IEX)	UAG buffer no arginine pH 7.5 (low salt)	UAG buffer (0.5M arginine) (high salt)	Gradient Elution 0-100% B
		UAG buffer no arginine pH 7.5	UAG buffer (1M NaCl no arginine)	Gradient Elution 0-100% B
		UAG buffer no arginine pH 7.5	UAG buffer (1M NaCl + 0.25M Arginine)	Gradient Elution 0-100% B
HiTrap SP XL	Cation (IEX)	UAG buffer no arginine pH 7.5 (low salt)	UAG buffer (0.5M arginine) (high salt)	Gradient Elution 0-100% B
CM FF	Cation (IEX)	UAG buffer no arginine pH 7.5	UAG Buffer	Gradient Elution 0-100% B
Octyl FF	Hydrophobic Interaction (HIC)	(high salt) UAG + 1.75M Ammonium Sulfate	(low salt) UAG + no arginine/ammonium sulfate	Gradient Elution 0-100% B

2.4 Western Blotting and Protein Measurement

2.4.1 Antibodies

The antibodies used in this study are listed in **Table 4**. Primary antibodies were diluted in Tris-Buffered Saline with Tween-20 (TBST) with 5% Bovine Serum Albumin (BSA) and 0.01% sodium azide. Secondary antibodies were diluted in TBST with 5% non-fat dry milk powder (BioRad). Goat anti-rabbit HRP (1:5000, ThermoFisher Scientific A16096) and goat anti-mouse HRP (1:5000, ThermoFisher Scientific A16066) were used as secondary antibodies.

Table 2. List of antibodies.

Antibody Specificity	Host	Dilution	Brand/Cat #	Conjugate	Type
α-6His	Mouse	1:1000-1:2000	Invitrogen HIS.H8	N/A	Monoclonal
Galectin-12	Rabbit	1:500-1:1000	Invitrogen PA5-113236	N/A	Polyclonal
Galectin-12	Rabbit	1:1000	Santa Cruz SC-67294	N/A	Polyclonal
Mouse IgG	Goat	1:10000	ThermoFisher Scientific A16066	HRP	Polyclonal
Rabbit IgG	Goat	1:10000	ThermoFisher Scientific A16066	HRP	Polyclonal
β-actin (C4)	Mouse	1:200	Invitrogen SC-47778	N/A	Polyclonal

2.4.2 Protein quantification

hrGal-12 at various stages of purification and BL21(DE3) lysates were quantified, along with HL-60 lysates. Bradford assays were performed using a 1 mL cuvette and Nanodrop Spectrophotometer and Bradford reagent (BioRad). BSA standard curves were performed each day with a range of 50 µg/mL to 1500 µg/mL, and only those with an R^2 above 0.85 were used. Nanodrop microvolume measurement was also performed for recombinant protein with UV280. UAG buffer was also used as a blank for hrGal-12 samples. BSA standards used for hrGal-12 quantification were diluted in UAG buffer to match the buffer composition of the hrGal-12 samples. Bio-Rad BCA assays were performed in 96-well plates according to the manufacturer's instructions. Absorbance was measured using

an 800 TS Absorbance Reader (BioTek®). BSA was diluted in RIPA buffer for HL-60 lysate standard curve generation. For Bradford assays, 5 μ L of buffer or protein was added to 1 mL Bradford reagent and left to incubate for 15 minutes and measured at 595 nm using a NanoDrop spectrophotometer loaded with a plastic cuvette. Different protein quantification methods were used for hrGal-12 to ensure accurate and reliable determination of protein concentration across different sample types. As BL21(DE3) hrGal-12 lysates were highly viscous and contained interfering components, the Bradford assay was used as it was less sensitive to viscosity and detergents.

2.4.3 SDS-PAGE and Western Blotting

The Bio-Rad Mini-PROTEAN system was used to cast 12.5% SDS-PAGE gels of 1.0- and 1.5-mm thickness. Polyacrylamide gels were prepared using Tris-HCl (pH 8.8) resolving buffer. Gels were run in 1x Tris-Glycine SDS running buffer (pH 8.3). Samples were mixed with 5x SDS-Loading buffer containing BME as a reducing agent. hrGal-12 was diluted in a 1x SDS loading buffer. All samples were boiled for 5 minutes prior to loading. Gels for Coomassie InstantBlue (Thermo Scientific) staining were run at 200 V for 45 mins, while gels for western blotting were run at 100 V for 90 mins. Proteins from gels were then transferred onto a PVDF membrane (Sigma Aldrich) for 1 hour at 100 V with ice cold transfer buffer containing methanol. The membrane post-transfer was washed three times for 5 minutes each in TBST at 80 RPM and then blocked for 1 hour with TBST containing 5% BSA and 1% non-fat dry milk powder (BioRad). Membranes were then incubated overnight at 4°C with primary antibody in a small plastic container with gentle shaking. The primary antibody was then decanted, and the membrane washed three times for 5 minutes each at 80 RPM in TBST. The membrane was then incubated with a secondary antibody for 1 hour at room temperature with gentle shaking. The secondary antibody was decanted, followed by three TBST washes for 5 minutes each at 80 RPM. After discarding secondary antibody, Immobilon horseradish peroxidase (HRP) Classico Substrate was added to membrane for 2 minutes and poured off. The membrane was quickly placed in a plastic sheet with no bubbles, followed by chemiluminescent imaging with ChemiDoc XRS system. Western blot images were analyzed in ImageLab (BioRad) software.

The same protocol was used to blot BL21(DE3) *E. coli* cell lysates with an anti-6xHis tag primary antibody. For BL21(DE3) lysates, 500 ng lysates were loaded per lane, while purified recombinant proteins were loaded at 100-500 ng per lane.

2.5 Chemical denaturation and dynamic light scattering

2.5.1 Intrinsic fluorescence spectroscopy

A Cary Eclipse spectrofluorometer (Varian) was used for all measurements along with a quartz cuvette with a 1cm path length. hrGal-12 stock was diluted in UAG, along with varying concentrations of Gdn-HCl (denaturant) from 0-6 M. Each reaction had a 500 μ L volume. Buffer controls with Gdn-HCl and no protein were also created to account for any autofluorescence of Gdn-HCl or UAG buffer. Samples were incubated overnight in water bath at 22.5°C. Samples were measured using an excitation of 280 nm and scanning from 290-450 nm with slow scan control. The excitation and emission slit widths were set to 5 nm. Buffer controls were subtracted from data and smoothed using a 3-point moving average calculated in Excel. The fluorescence intensity (mAU) was plotted across all measured wavelengths, and the shifts in peak wavelength with increasing concentration of Gdn-HCl were analyzed.

2.5.2 Dynamic Light Scattering

The DynaPro NanoStar (Wyatt) Dynamic Light Scattering (DLS) system was used with an angle of scattering at 90°. A JC-501 microcuvette was cleaned thoroughly with water and Contrad 70 detergent. hrGal-12 was diluted to 1 mg/mL in UAG and PBS and loaded into a microcuvette to quantify the formation of hrGal-12 aggregate. All data were collected at 22.5°C with 10 acquisition scans in a row. Autocorrelation functions and regularization fits were extracted from Dynamics software (Wyatt) and plotted in GraphPad Prism.

2.6 *In Silico* analysis

A 3-D galectin-12 visualization was created in PyMol 3.1.6.1 (educational license) using AlphaFold predicted structure for human galectin-12. Sequence alignments between galectin-12 from different species and hrGal-12 in this study were performed and

visualized in AliView. The Protein Sol web server was used to predict protein solubility in *E. coli*. ExPASy ProtScale was used for automated Kyte & Doolittle hydropathy scoring of galectin protein sequences. Kyte & Doolittle hydropathy scale is based on the change in free energy for each amino acid when placed in water (Kyte & Doolittle, 1982).

Hydrophilic residues have a positive change in free energy and a more negative hydropathy index. The opposite is true for hydrophobic residues. First, a window size is chosen from ~7-9 residues. The residue being scored is in the middle of the window.

Hydropathy is calculated by adding all hydropathy indices in the window and dividing by the window size. This is repeated for each residue to generate the hydropathy plot.

2.7 Cell culture

2.7.1 HL-60 Cell Culture

HL-60 cells were originally obtained from American Type Culture Collection and grown at 37°C and 5% CO₂ in IMEM (Wisent) with 10% fetal bovine serum (Wisent) and 1% Penicillin/Streptomycin (Wisent). HL-60 cells were passaged at 1.0 x 10⁶ cells/mL until passage 40. T25, T75, 35 mm, 60 mm, and 100 mm suspension dishes were used to grow cells (Sarstedt).

2.7.2 Cell treatments

HL-60 cells were treated with 1 μM ATRA or 1.3% DMSO for 72 hours with a starting concentration of 0.4 x 10⁶ cells/mL. Control cells were seeded at 0.2 x 10⁶ cells/mL. hrGal-12 was added along with corresponding buffer controls at 10 μg/mL, 1 μg/mL, and 0.1 μg/mL.

2.8 Brightfield and fluorescence microscopy

A brightfield inverted LEICA DM IL LED microscope with EC3 camera was used to take all cell images using 20x-40x objectives. Leica LAS software was used for acquisition. All fluorescence images for data analysis were taken with Zeiss AxioImager A1 fluorescence microscope with an XCD-X700 CCD camera (Sony). Images acquired using the Norther Eclipse 8.0 software (Empix Imaging). A DAPI filter cube was used to image nuclei.

2.8.1 DAPI nuclear staining

After washing cells twice with Dulbecco's phosphate buffered saline (DPBS), cell viability and concentration were determined, and cells diluted to 0.75×10^6 cells/mL. HL-60 suspension cells were attached to glass slides using a Shandon Cytospin 2 centrifuge. Cytofunnels with slides were loaded into the Cytospin with 200 μ L HL-60 cells and centrifuged at 700 RPM for 5 mins. After drying, cells were fixed with ice cold methanol, followed by a gentle PBS rinse to remove excess methanol and unfixed cells. Mounting media with DAPI (Abcam) was applied to each slide, coverslips added, and slides left to dry in a dark environment. Nuclei of control HL-60 cells were predominantly near-circular, with minimal variation in nuclear morphology. Following treatment with ATRA, DMSO, hrGal-12, and UAG, nuclear morphology was quantified using a nuclear lobulation index. Lobulated nuclei were defined as those exhibiting two or more distinct nuclear lobes, segmented nuclei, indented, or elongated oval nuclear structures (Olins & Olins, 2004; Baxter et al., 2009). The lobulation index was calculated as the ratio of the total number of nuclei counted to the number of lobulated nuclei. A minimum of 10 cells per replicate were screened in a blind manner, and nuclei from dead or apoptotic cells were not counted.

2.9 RNA isolation, cDNA synthesis, and RT-PCR

HL-60 cells were washed with PBS and pelleted before RNA isolation was performed using TRIzol (ThermoFisher Scientific). Cells were grown in T25 or 35 mm dishes and seeded at 0.2×10^6 cells/mL. RNA quantification was performed using Nanodrop 200c spectrophotometer (Thermo Scientific) with a quality requirement of $A_{260/280} > 1.8$. cDNA was prepared with 500-1000ng of RNA using the Advanced cDNA Synthesis Kit (Wisent). PCR reactions (20 μ L) were created with 10 μ L 2x FroggaMix (FroggaBio), 8 μ L sterile H₂O, 1 μ L cDNA, and 1 μ L forward/reverse primers (0.5 μ M), and run using T100 Thermocycler (BioRad). The PCR regime included an initial denaturation at 94°C for 3 mins, followed by 30 cycles of denaturation at 94°C for 30 seconds, annealing at 60°C for 30 seconds, and extension at 72°C. All primers were kept as 10 μ M stocks and diluted to 0.5 μ M for use in PCR. Multiplex PCR was also performed for semi-quantification of gene expression relative to *ACTB*, a housekeeping gene. These primers

were verified by nucleotide BLAST and then synthesized by ThermoFisher Scientific (Table 1). PCR products were run on 2% agarose gel with SYBR Safe® for 55 minutes at 90V in 1x TAE buffer. Gels visualized using GelDoc X+ (BioRad) and analyzed using ImageLab software (Bio-Rad).

Table 3. List of RT-PCR primers

Gene Name	REF Seq ID	Primer Seq 5'-3'	Amplicon Size (bp)	Notes
ACTB	NM_001101.3	F: TCAGCAAGCAGGAGTATGACGAG R: ACATTGTGAACTTTGGGGGATG	265	Transcript Variant 3
NCF1	NM_000265.7	F: ACCCCAGCCAGCACTATGTGT R: AGTAGCCTGTGACGTCGTCT	767	Transcript Variants 1, 2
P47phox				
DGAT1	NM_012079.6	F: CGGATCCTTGAGATGCTGTT R: CCATCCACTGCTGGATCA	61	Transcript Variants 1-4
NCF2	NM_001190794.2	F: CGAGGGAACCAGCTGATAGA R: CATGGGAACACTGAGCTTCA	746	Transcript Variants 1-5
P67phox				

2.10 Cell aggregation and adhesion assays

2.10.1 Cell aggregation assay

HL-60 cultures were grown to a maximum concentration of 1.2×10^6 cells/mL while maintaining viability above 90% before being used for the aggregation assay. The cells were spun down for 5 minutes at 300 g, washed once in Hank's Balanced Salt Solution (HBSS), and finally resuspended in HBSS at a concentration of 2.0×10^6 cells/mL. Various cell concentrations were tested to optimize response. UAG buffer controls were performed using 1-6% (v/v) UAG in the 500 μ L cuvette. HL-60 cell aggregation was measured using a platelet aggregometer AP2110 (SOLAR) as previously described for human neutrophils (Gorudko et al., 2008). A cuvette filled with HBSS was used to blank the aggregometer before measurements. A cuvette with a small magnetic stirrer was

placed in the aggregometer containing 500 μL cell suspension and left to heat for 5 minutes. RCA was added at 15 $\mu\text{g}/\text{mL}$ quickly into the cuvette. hrGal-12 stock was further diluted in UAG before use in the aggregation assay. An hrGal-12 dose response curve was generated using concentrations ranging from 5 $\mu\text{g}/\text{mL}$ to 30 $\mu\text{g}/\text{mL}$. HL-60 cell aggregates were transferred from cuvette to 35 mm dishes for imaging.

2.10.2 Adhesion assay and hrGal-12 immobilization

hrGal-12 and RCA were immobilized overnight to COSTAR™ 96 well plates. hrGal-12 was diluted in UAG to 50-800 $\mu\text{g}/\text{mL}$ from the stock solution. RCA was diluted in PBS to 50 $\mu\text{g}/\text{mL}$. UAG and BSA were also added as negative controls. After immobilization for 12 hours, the supernatant was aspirated followed by a blocking step with 100 μL BSA (10 mg/mL) for 30 minutes at room temperature (Timoshenko et al., 2016). HL-60 cells were counted using a hemocytometer and diluted to 0.5×10^6 cells/mL in adhesion media consisting of 1:1 of PBS with Ca^{2+} / Mg^{2+} and serum free IMEM. The BSA was aspirated and each well was washed with PBS. Next, 100 μL of HL-60 cells were added to each well and the plate was placed in the incubator for 1 hour. After aspirating media from the wells, cells were fixed with 50% methanol for 2 minutes, and then 100% methanol for 10 minutes. The methanol was chilled on ice prior to use and aspirated after fixation. Fixed HL-60 cells were stained for 1 hour with 0.1% (w/v) Crystal Violet and imaged using inverted LEICA microscope. The Crystal Violet was aspirated, and each well was filled with 100 μL of 10% (v/v) acetic acid to dissociate Crystal Violet stain from cells. The adhesion index was measured at 570 nm absorbance and read with an 800 TS Absorbance Reader (BioTek®).

2.11 Hemagglutination assay

Hemagglutination (HA) assays were performed with 2% rabbit red blood cells (RBCs) and rabbit RBCs which were Trypsinized and fixed with glutaraldehyde (Nishi, 2020; Prato et al., 2020). Rabbit RBCs (Rockland Immunochemical) were stored at 4°C as a 10% solution in PBS. 5 mL of rabbit RBCs at 10% were Trypsinized with a 1:1 volume of TrypLE Express (ThermoFisher Scientific) for 15 minutes at 37°C in a CO₂ incubator. Next, 40 mL of Ca^{2+} Mg^{2+} free DPBS (Wisent) was added, and cells were centrifuged at

500 g for 5 mins. The PBS was decanted, and the RBC pellet was resuspended in 1% (v/v) glutaraldehyde in DPBS. Cells were treated with glutaraldehyde for 1 hour at room temperature with gentle shaking. Next, RBCs were pelleted at 500g for 5 mins at 4°C and washed twice with 25 mL 0.1M glycine in DPBS. Finally, the rabbit RBC pellet was resuspended in 5 mL Ca^{2+} Mg^{2+} free DPBS and stored at 4°C until use.

hrGal-12 was diluted in UAG buffer and RCA was diluted in PBS. 50 μL of lectin was mixed with 50 μL of 4% RBC suspension in a 96 well COSTAR® plate with U-bottoms (07-200-95) and left for 1 hour. Wells with dispersed RBCs across the whole well show hemagglutination from lectin, while cells with a dot of RBCs in the middle show no response. UAG and PBS controls were also performed.

2.12 Cell viability and proliferation assays

HL-60 cells were diluted in a 1:1 ratio with 0.4% sterile filtered Trypan Blue (Gibco). Trypan blue stains dead cells blue. 25 μL of diluted cell suspension was loaded onto a hemocytometer and observed under a 10x objective (100x magnification). The two chambers of hemocytometer were counted to calculate average number of cells per square. Cell concentration was calculated using the formula: Concentration of cells/mL = Hemocytometer Average x Dilution Factor (2) x 10,000. Dead cells were counted and used to calculate the live cell concentration and cell viability.

For cell proliferation, HL-60 cells were grown in T25 flasks with a starting concentration of 0.1×10^6 cells/mL. Samples were taken in a sterile manner twice a day for 6 days to construct growth curves. Control HL-60 cells along with hrGal-12 treated cells at 10, 1, and 0.1 $\mu\text{g}/\text{mL}$ were done along with separate growth curves for UAG buffer controls. Population doubling time (PDT) was calculated from two measurements taken during the exponential phase of growth and compared between treatments.

2.13 Statistical analysis

Experiments were performed in biological triplicates (n=3) with at least two technical replicates per assay, unless stated otherwise. The statistical analysis was carried out using One-Way ANOVA followed by Tukey's HSD. Unpaired Student's t-tests were used to compare treatments. GraphPad Prism V8.0 was used for all statistical analysis and data visualization. A significance threshold of $p < 0.05$ was applied and all data presented as mean +/- standard deviation (SD).

Chapter 3

3 Results

3.1 Cloning, expression, and purification of hrGal-12

3.1.1 *In silico* analysis of human galectin-12 sequence

My first objective was to clone, express, and purify hexahistidine tagged human recombinant galectin-12 (hrGal-12) in BL21(DE3) *E. coli* cells. First, sequence and hydropathy analysis was performed on human galectin-12, including the recombinant construct in this study. The full-length human galectin-12 sequence (336 amino acids) was aligned with hrGal-12 used in this study and galectin-12 of other mammals (**Figure 7**). hrGal-12 (342 amino acids) does not contain the first 22 residues from full length Human galectin-12 but has a hexahistidine tag for nickel affinity chromatography and a thrombin cut site (**Figure 7**). Solubility prediction for recombinant proteins in *E. coli* shows galectin-12 to be at 0.22, which is lower than the average protein at 0.45. In contrast, galectin-1 and -3, displayed above average solubility scores (**Figure 8A**). Hydropathy scoring per residue shows galectin-12 with highly hydrophobic residues scattered along the whole protein in contrast to galectin-1 and -3 which are hydrophilic (**Figure 8B**). Hydrophobic residues in galectin-12 are not limited to carbohydrate recognition domains, which is consistent with their localization to lipid droplets. hrGal-12 in this study is 342 amino acids with a predicted molecular weight of 38 kDa and pI of 10.3. mrGal-12 is known to appear as a lower 35 kDa band on an SDS-PAGE gel due to galectin-12 having a basic isoelectric point (Maller et al., 2020).

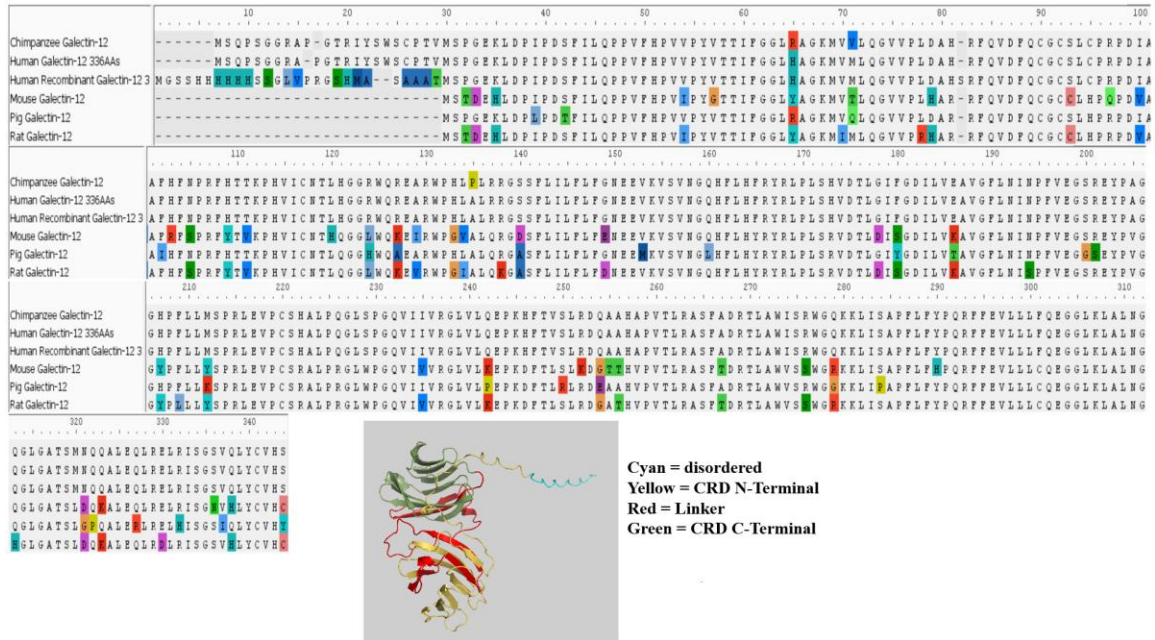


Figure 7. Sequence and structure of human galectin-12. Sequence alignments were generated in AliView with human, mouse, pig, rat, and chimpanzee galectin-12, and the human recombinant galectin-12 (hrGal-12) used in this study. Non-consensus residues in the alignment are highlighted. Structures rendered in AlphaFold were colored in PyMOL to highlight human galectin-12 domains as identified by previous sequence analysis (Yang et al., 2001). This alignment was done with the longest human galectin-12 isoform (336 residues), which is one of five major human galectin-12 isoforms. AlphaFold predicted local distance difference test (pLDDT) score = 90.44 (very high).

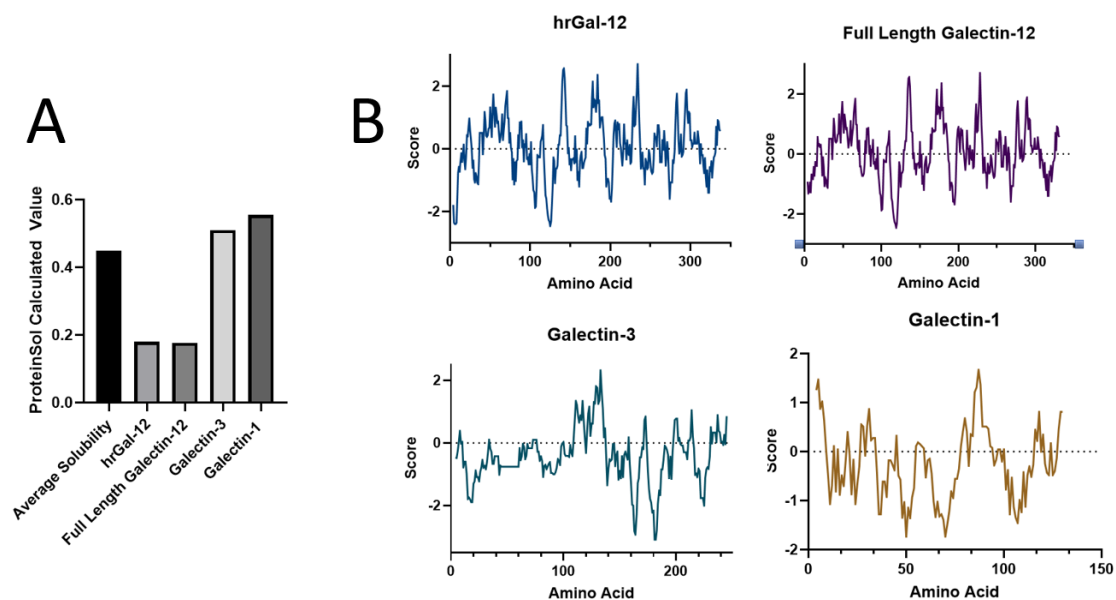


Figure 8. *In silico* prediction of human galectin-12 solubility and hydrophathy. A) Protein-Sol server prediction of recombinant protein solubility in *E. coli* for recombinant construct (hrGal-12), full length human galectin-12, galectin-3, and galectin-1. **B)** Hydrophathy plots (Kyte & Doolittle Scoring) for human galectin-12 displaying increased hydrophobic regions scattered throughout the sequence. Positive values indicate hydrophobic residues while negative values represent hydrophilic residues.

3.1.2 Cloning of *LGALS12* cDNA into pET-28a vector and expression in BL21(DE3) cells

LGALS12 cDNA insert was digested at NheI and XhoI cut sites (**Figure 9A**) along with pET-28a plasmid (**Figure 9B**). This pET28a-*LGALS12* plasmid was propagated in DH5 α cells and then transformed into BL21(DE3) cells. Colony PCR indicated that colonies appearing on LB-agar kanamycin plates (60 μ g/mL) were positive for the 1200 bp *LGALS12* insert (**Figure 9C**). Further, Sanger DNA sequencing of random colonies confirmed that the full sequence of hrGal-12 was present along with the His-Tag (**Figure 9B**).

Optimal induction of hrGal-12 was seen at 1 mM IPTG with an increased Coomassie staining at approximately 35 kDa and detection with α -6xHis antibody in BL21(DE3) lysates (**Figure 10A, B**). There was no hrGal-12 expression in BL21(DE3) lysates with no hrGal-12 plasmid or before induction with IPTG (**Figure 10B**).

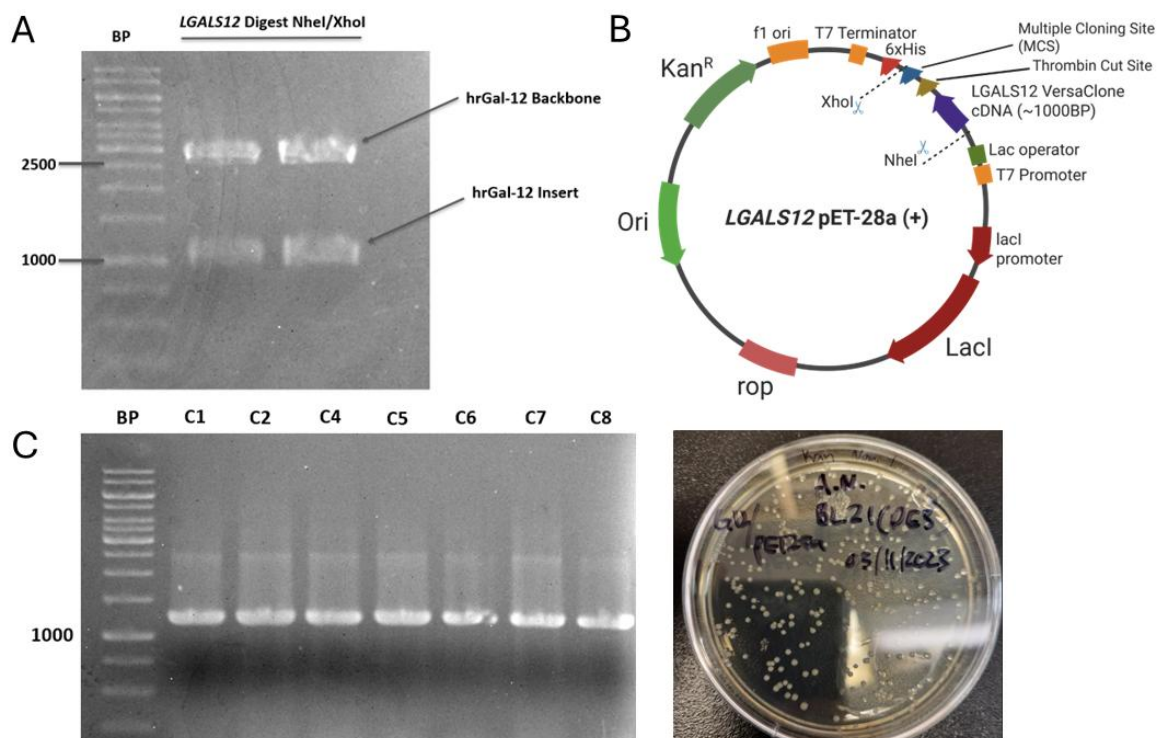


Figure 9. Digestion of *LGALS12* cDNA insert and ligation in pET-28a plasmid. **A)** Digestion of *LGALS12* insert and backbone from R&D BioTechne *LGALS12* VersaClone cDNA plasmid at NheI and XhoI sites. **B)** *LGALS12*-pET28a plasmid structure. The pET28a plasmid allows for IPTG inducible expression and selection of colonies with kanamycin resistance. Further there is a hexahistidine tag for IMAC. Figure made in BioRender. Sanger DNA sequencing was performed to confirm the hrGal-12 insert was cloned correctly into pET-28a plasmid **C)** Colony PCR screening of BL21(DE3) colonies with *LGALS12* pET-28a plasmid, along with BL21(DE3) colonies on LB-agar kanamycin plate. *LGALS12* insert is 342 amino acids or 1026 base pairs, with some additional residues before and after T7 forward/reverse primers binding site (~1200 BP amplicon). C1-C7 represents seven random colonies from kanamycin-agar plate.

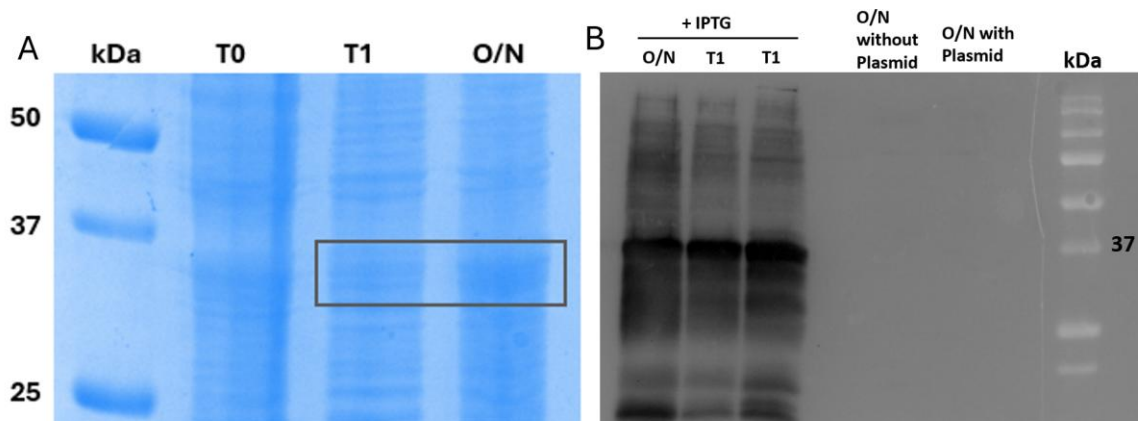


Figure 10. BL21(DE3) expression of hrGal-12 analyzed with SDS-PAGE and western blotting. **A)** SDS-PAGE of BL21(DE3) *E. coli* cell lysates at T0 (before IPTG) induction, 1 hour after IPTG induction (T1), and after overnight (O/N) expression 15 μ g of bacterial lysate loaded per lane. The 35 kDa region is highlighted with a box representing the size where hrGal-12 will be visible in BL21(DE3) lysates. hrGal-12 is basic (pI = 10.3) and runs lower on a denaturing gel. **B)** Western Blot with α -6xHis (HIS.H8) antibody at 1:2000 in BL21(DE3) lysates before and after induction with 1 mM IPTG. 500 ng of lysate loaded per lane. Both BL21(DE3) cells before induction with plasmid and BL21(DE3) cells without plasmid included as negative controls.

3.1.3 hrGal-12 purification with Ni-NTA and Size Exclusion Chromatography

BL21(DE3) pellets containing inclusion bodies were solubilized in lysis buffer containing 6M Gdn-HCl and 5 mM BME. Most hrGal-12 was recovered in the soluble fraction with a small amount remaining in the insoluble fraction at the lysis stage. Various detergents were tested to improve solubilization of hrGal-12 (e.g., 2-6% Triton-X100, 0.5-2% sodium deoxycholate, and RIPA buffer but were found to be ineffective (**Figure 11**). Sodium deoxycholate was key in the purification of mrGal-12 (Maller et al., 2020), but did not improve solubility of hrGal-12 in my experiments.

hrGal-12 was eluted from a 30 mL Ni-NTA column with 6 M guanidine and 400 mM imidazole over 21 mL in 7 x 3 mL fractions. Fractions 1-3 had the highest concentrations of hrGal-12 (**Figure 12**). Chloroform methanol precipitation of Gdn-HCl elution fractions prove hrGal-12 can be eluted from Ni-NTA beads with 6 M Gdn-HCl and 400 mM imidazole. Chloroform methanol precipitation was required observe elution fractions on an SDS-PAGE gel. Attempts to elute from the Ni-NTA beads using sodium acetate or urea were unsuccessful, as the protein remained bound (data not shown). Addition of PMSF or commercial bacterial protease inhibitor cocktail during lysis or dialysis did not improve the purity of hrGal-12 (data not shown).

After screening various buffers (**Table 4**) it was found that the urea, arginine, glutathione (UAG) buffer was able to successfully solubilize and refold hrGal-12 following Ni-NTA purification (**Figure 13**). hrGal-12 demonstrated a tendency to precipitate under all buffer conditions other than UAG. At the dialysis stage hrGal-12 precipitate formed overnight. Various styles of buffer exchange including refolding by dilution and ultrafiltration followed by concentration led to precipitation of hrGal-12 (not shown). High concentrations of urea, arginine, and glutathione were all required for solubility of hrGal-12. Eliminating or lowering even one of these components resulted in the precipitation of hrGal-12 (**Table 4**). The final refolding (UAG buffer) had a composition of 20 mM Na₂HPO₄, 0.18 mM EDTA, 0.5M L-Arginine, 2M Urea, 1.8 mM GSH (reduced glutathione), 0.9 mM GSSH (oxidized glutathione), with a pH of 7.5. SDS-PAGE analysis showed a major band at 35 kDa along with some smeared and degraded products

at 25 kDa and 10 kDa (**Figure 13**). These degraded products could be due to proteolytic cleavage at the linker region in bacterial cells. Galectin-12 is a basic protein with pI of 8.1, and therefore, runs at a lower apparent molecular weight on an SDS-PAGE denaturing gel.

Western blotting with human galectin-12 polyclonal antibody confirmed degraded products and the major band to be human recombinant galectin-12 (**Figure 14B**). hrGal-12 was also identified by anti-6xHis antibody but my blot quality was quite poor, and I could not optimize it (not shown). The hrGal-12 in bacterial lysates was identified clearly with the anti-6xHis antibody, as previously shown (**Figure 10B**). hrGal-12 was expressed overnight at 15 °C, 20 °C, and 23.5 °C, with expression at 23.5 °C yielding the highest protein recovery and the sharpest bands on SDS-PAGE following Ni-NTA purification. (**Figure 15C, D**). Other blots of hrGal-12 with human polyclonal galectin-12 antibodies were of lower quality but still identified the recombinant protein (**Figure 15A-F**).

1-5 mL of Ni-NTA hrGal-12 was injected into a S75 16/600 HiLoad Cytiva column with AKTA GO at 4°C equilibrated in UAG buffer. This SEC step allowed for further purification of the major band based on size (**Figure 14**). Alternative columns and buffer conditions were also tested but led to degradation or precipitation of hrGal-12 (data not shown). The 10 kDa degradation product and some smearing were removed with size exclusion, increasing the purity of the major band at 35 kDa. The final yield after SEC was ~3-5 mg/L of bacterial BL21(DE3) culture. SEC purified hrGal-12 was concentrated to 2 mg/mL and stored as small aliquots (50 µL/each) at -80°C. hrGal-12 was flash frozen at the Ni-NTA stages and again following SEC and concentration. Concentrating above 2 mg/mL caused hrGal-12 precipitation. ~20% of protein was lost at both size exclusion and concentration steps. This could be due to incomplete elution from SEC column and protein adsorbing to concentrator, consistent with galectin-12's hydrophobic properties. My attempt to purify the Ni-NTA hrGal-12 using a 30 kDa concentrator was ineffective with protein found both in the retentate and filtrate (data not shown). I attempted to purify hrGal-12 under native lysis conditions as described by Maller et al., 2020 and Cagnoni et al., 2024, but very low amounts of protein were detected in elution fractions (**Figure S1, S2**). In those studies, hrGal-12 was expressed in Rosetta (DE3) *E. coli*, whereas

BL21(DE3) cells were used in the present work, which may account for the failure of this protocol. Notably, hrGal-12 was reported to be soluble after native lysis in Rosetta (DE3) cells, whereas in BL21(DE3) it was largely insoluble, further suggesting that differences in the expression strain contributed to the observed outcome. Further, my western blotting with Invitrogen polyclonal human galectin-12 antibody showed some galectin-12 present in solution, but at an extremely low concentration and at incorrect apparent molecular weights (**Figure S2**). Native lysis of cells by sonication without denaturing hrGal-12 could not solubilize the protein, and various impurities bind to column with almost negligible amounts of the major band (**Figure S1**).

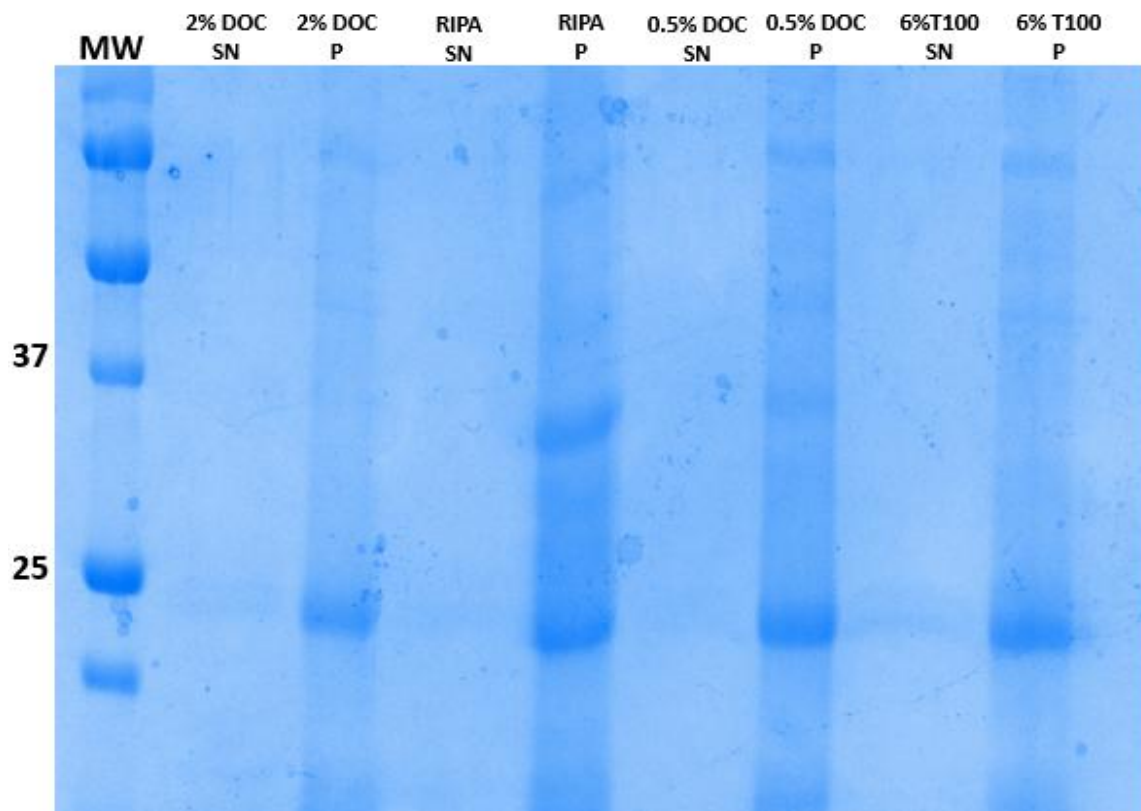


Figure 11. SDS-PAGE of pooled hrGal-12 fractions purified following lysis with detergents and subsequent Ni-NTA purification. BL21(DE3) lysates were solubilized in various detergents and purified by affinity chromatography. The gel shows Ni-NTA purified hrGal-12 remaining in the supernatant (soluble protein) and insoluble hrGal-12 precipitate following dialysis. These detergents did not improve the solubility or purity of hrGal-12. SN = hrGal-12 in solution. P = precipitated hrGal-12. MW = kDa with BlueElf ladder (ThermoFisher Scientific). DOC = sodium deoxycholate, T100 = Triton X-100. 2 μ g hrGal-12 precipitate loaded per lane. 15 μ L of supernatant without protein was loaded to show the lack of soluble protein.

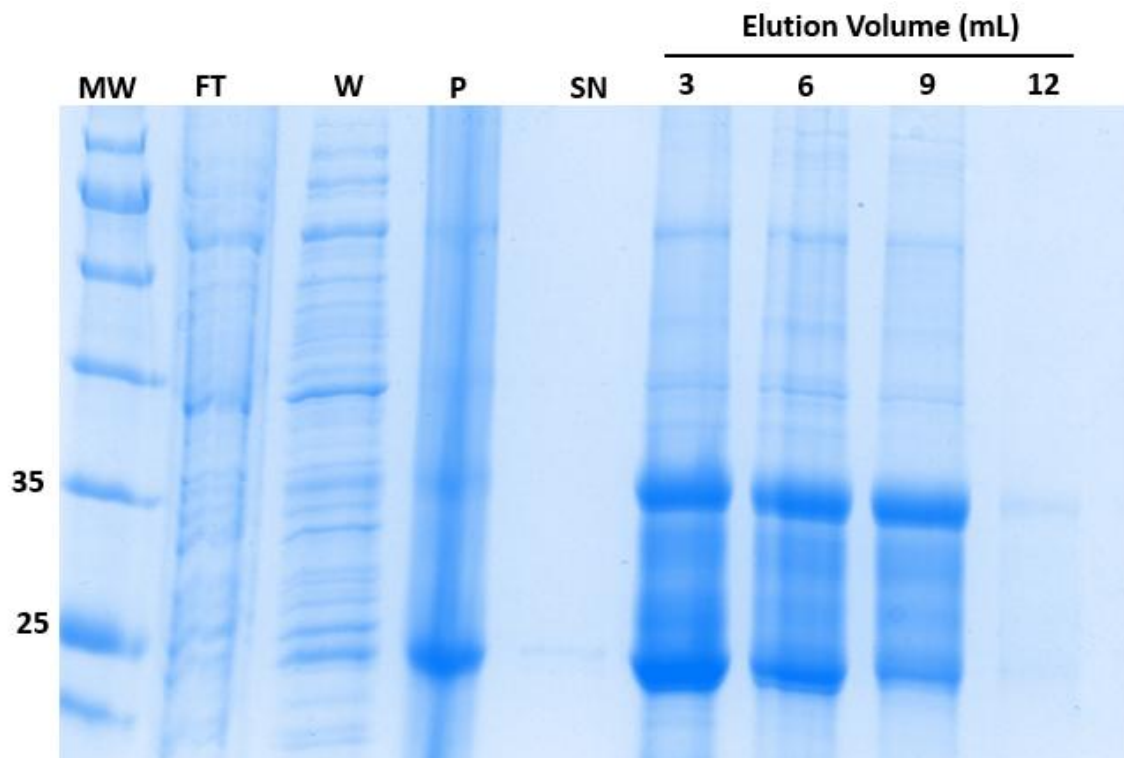


Figure 12. SDS-PAGE of recombinant hrGal-12 Ni-NTA purification. FT = Ni-NTA column flowthrough. W = wash with 6M Gdn-HCl, 5 mM BME, and Tris-HCl. P = precipitate following dialysis. SN = hrGal-12 in solution following dialysis with buffer 1. Lanes 6-9 represent fractions 1-4 of hrGal-12. The elution buffer was comprised of 6M Gdn-Hcl, 400 mM Imidazole, and 5 mM BME. Lanes show hrGal-12 elution fractions following chloroform methanol precipitation. 2 μ g hrGal-12 loaded per lane. SN lanes and 12 mL elution volume lane had minimal protein in solution.

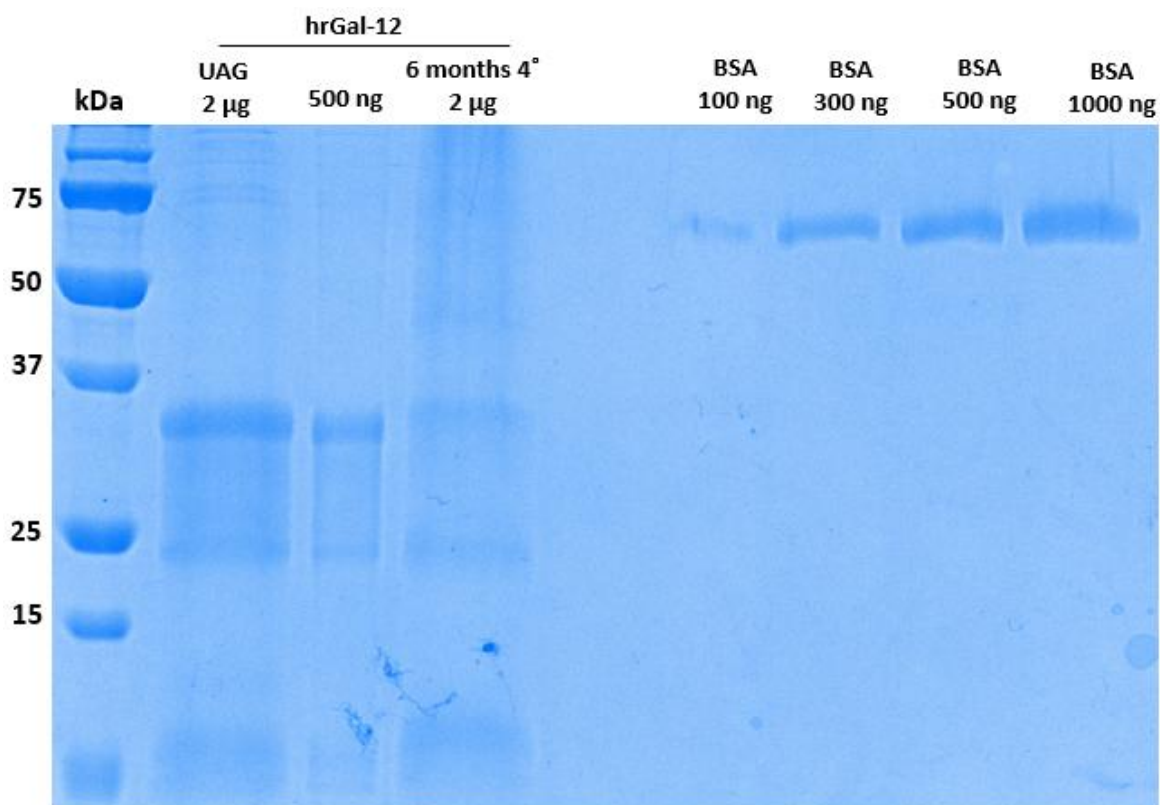


Figure 13. SDS-PAGE of hrGal-12 following dialysis and refolding in UAG buffer.

hrGal-12 lanes contain pooled elution fractions (21 mL total) collected after imidazole and guanidine hydrochloride (Gdn-HCl) elution. A prominent band corresponding to hrGal-12 is observed at approximately 35 kDa, along with lower-molecular-weight degradation products. Lanes 2 and 4 were loaded with 2 μg of hrGal-12. A BSA standard curve (100–1000 ng) is included to enable estimation of hrGal-12 concentration.

Table 4. Summary of refolding and dialysis buffers assessed with hrGal-12.

Buffer Name	Buffer Components¹	Precipitate Formed (Yes/No)
Buffer 1	20 mM Tris, 150 mM NaCl, 2 mM Dithiothreitol, pH 7.5	Y
Buffer 2	25 mM HEPES, 2 mM Dithiothreitol, 100 mM NaCl, 1 mM D-lactose, pH 7.5	Y
Buffer 3	0.5% sodium deoxycholate, 300 mM NaCl, 2 mM Dithiothreitol, 25 mM Imidazole, 25 mM HEPES, pH 7.5	Y
UAG Buffer	20 mM Na ₂ HPO ₄ , 0.5M L-arginine, 0.18 mM EDTA, 1.8 mM GSH, 0.9 mM GSSH, 2M Urea, pH 7.5	N
Modified UAG Buffer	20 mM Na ₂ HPO ₄ , 0.18 mM EDTA, 1.8 mM GSH, 0.9 mM GSSH, 2M Urea, pH 7.5	Y
UAG re-dialysis A	PBS, 5 mM BME, 1 mM EDTA, pH 7.5	Y
Buffer 4	200 mM NaCl, 2 mM Dithiothreitol, 35 mM HEPES, 10 mM Lactose, pH 7.5	Y
Buffer 5	PBS, 0.5% sodium deoxycholate, 5 mM BME, pH 7.5	Y
Buffer 6	PBS, 5 mM BME, 10 mM Lactose, 5 mM EDTA, pH 7.5	Y
Buffer 7	20 mM Na ₂ HPO ₄ , 55 mM L-arginine, 1.8 mM GSH, 0.9 mM GSSH, 0.5M Urea, pH 7.5	Y
Buffer 8	20 mM Na ₂ HPO ₄ , 0.5 M L-arginine, 0.18 mM EDTA, 1.8 mM GSH, 0.9 mM GSSH, 0.2M Urea, pH 7.5	Y
Buffer 9	150 mM NaCl, 2 mM KCl, 0.25M L-arginine, 0.05% polyethylene glycol 200, 50 mM MES, 1 mM EDTA, 0.1 mM GSH, 0.01 mM GSSH, pH 6	Y
Buffer 10	50 mM Tris, 150 mM ammonium persulfate, 1 mM EDTA, 0.25M L-arginine, 2 mM KCl, 0.1 mM GSH, 0.01 mM GSSH, pH 8.2	Y

¹ 21 mL of hrGal-12 elution fractions dialyzed in 1 L buffers 1 and 2. For all other buffers, 4 mL hrGal-12 elution fractions were dialyzed into 500 mL buffer overnight at 4°C.

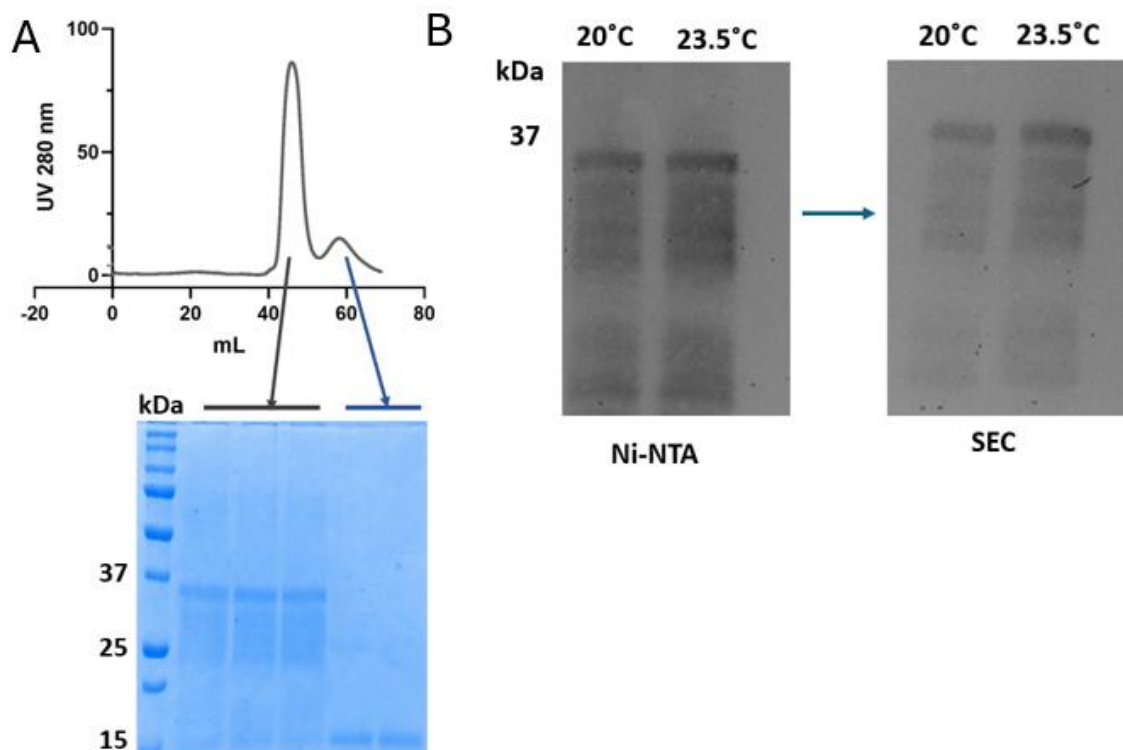


Figure 14. Size Exclusion Chromatography of hrGal-12 and immunodetection. A) Ni-NTA purified hrGal-12 was applied to an S75 16/600 HiLoad™ Cytiva column at a flow rate of 1 mL/minute. hrGal-12 eluted at ~40 mL from a total 140 mL column volume. Chromatogram shows UV280 over elution volume including major peak with hrGal-12. The SDS-PAGE gel of SEC fractions shows increase in major 35 kDa band (grey arrow) while removing 15 kDa degradation product (blue arrow). **B)** Western blots of Ni-NTA and SEC hrGal-12 Expressed at varying temperatures in BL21 (DE3) *E. coli*. The primary antibody used was a 1:500 dilution polyclonal galectin-12 (PA5-113236). The secondary antibody was a 1:5000 dilution of goat anti-rabbit HRP-linked. Immobilon classico HRP substrate was used, followed by chemiluminescent imaging. 500 ng hrGal-12 was loaded per lane.

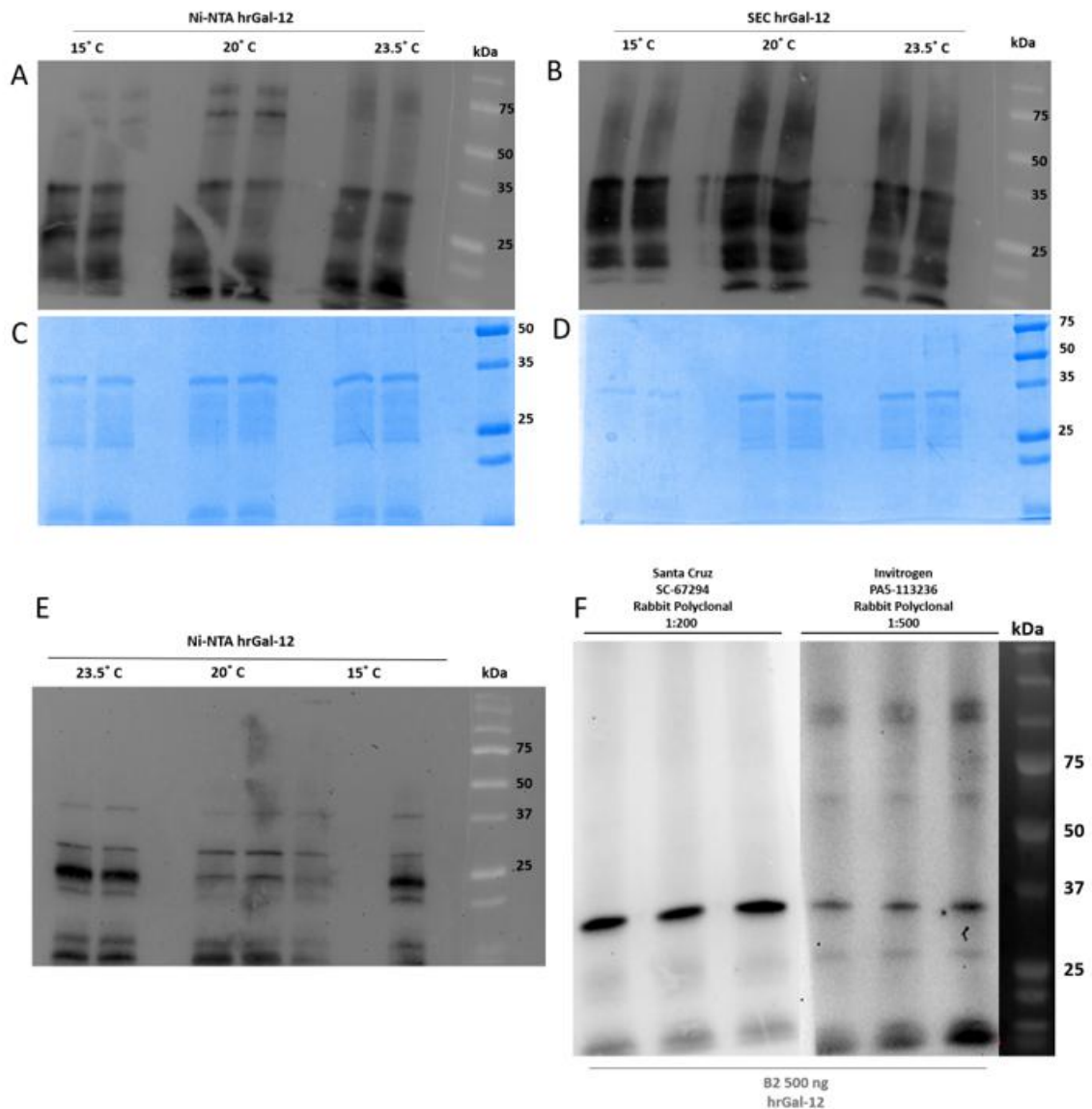


Figure 15. Additional western blots and SDS-PAGE of hrGal-12 expressed and purified at different temperatures **A)** Western blot of Ni-NTA-purified hrGal-12 probed with Invitrogen PA5-113236 polyclonal anti-galectin-12 antibody. **B)** Western blot of SEC-purified hrGal-12, probed with PA5-113236. For panels A and B, 500 ng hrGal-12 was loaded per lane (two technical replicates per temperature) **C)** SDS-PAGE gel of Ni-NTA purified hrGal-12. 2 μ g hrGal-12 loaded per lane. **D)** SDS-PAGE analysis of hrGal-12 following SEC purification. **E)** Western blot of hrGal-12 probed with the Santa Cruz SC-67294 polyclonal anti-galectin-12 antibody (1:1000 dilution, overnight). **F)** Comparison of primary galectin-12 antibody performance with 1 hour incubation.

3.1.4 Assessment of hrGal-12 stability, precipitation, and folding state

SDS-PAGE analysis showed that hrGal-12 remained stable when stored at 4°C for up to one week, with the room temperature sample having less intensity of the major band at 3- and 6-days. (**Figure 16**). For long-term storage, hrGal-12 was kept at -80°C. When mixed with PBS or water, hrGal-12 forms a flaky white precipitate within minutes (**Figure 17A**). The tendency of hrGal-12 to precipitate in simple buffers may limit this version of the recombinant protein from studies using cells in physiological conditions. hrGal-12 remained soluble in UAG buffer as shown by the single peak in hydrodynamic radius and a monodisperse autocorrelation function (**Figure 17C, D**). Further, the autocorrelation function remains the same when hrGal-12 is diluted in UAG but is delayed when hrGal-12 is diluted in PBS. Larger particles like protein aggregates move slowly leading to a delayed autocorrelation function. Further, the hrGal-12 aggregates in PBS increase in size over 5 minutes. Measurement of intrinsic fluorescence with increasing concentrations of Gdn-HCl shows an 8 nm red shift in the maximum emission wavelength (**Figure 18**). I was unable to perform circular dichroism spectroscopy due to the ability of arginine in UAG buffer to reflect polarized light. An excitation wavelength of 280 nm was used with emission captured from 290-450 nm. The right shift starts at 1M Gdn-HCl and increases up to 6M Gdn-HCl (**Figure 18**).

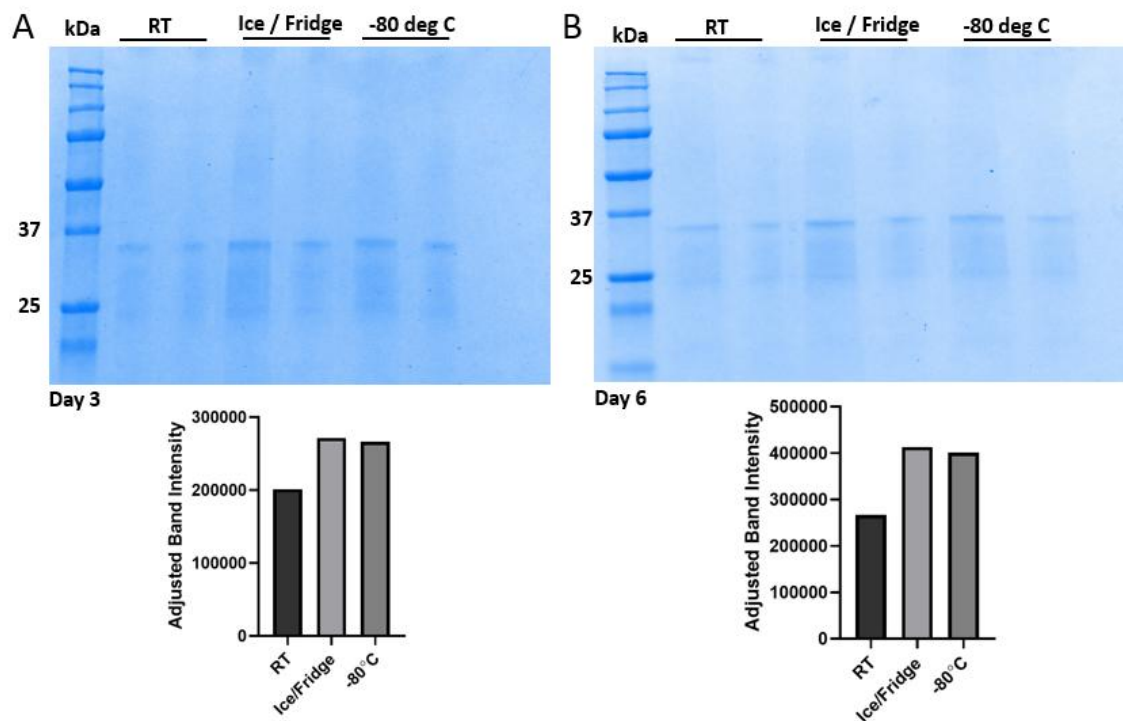


Figure 16. Stability of hrGal-12 at varying temperatures. hrGal-12 was stored at 22.5 °C (RT), 4 °C (fridge), and -80 °C, with samples taken at 3- and 6-days. **A)** hrGal-12 after 3 days **B)** hrGal-12 after 6 days. 1 µg hrGal-12 was loaded per lane. Densitometry of major hrGal-12 band performed in ImageLab software (BioRad).

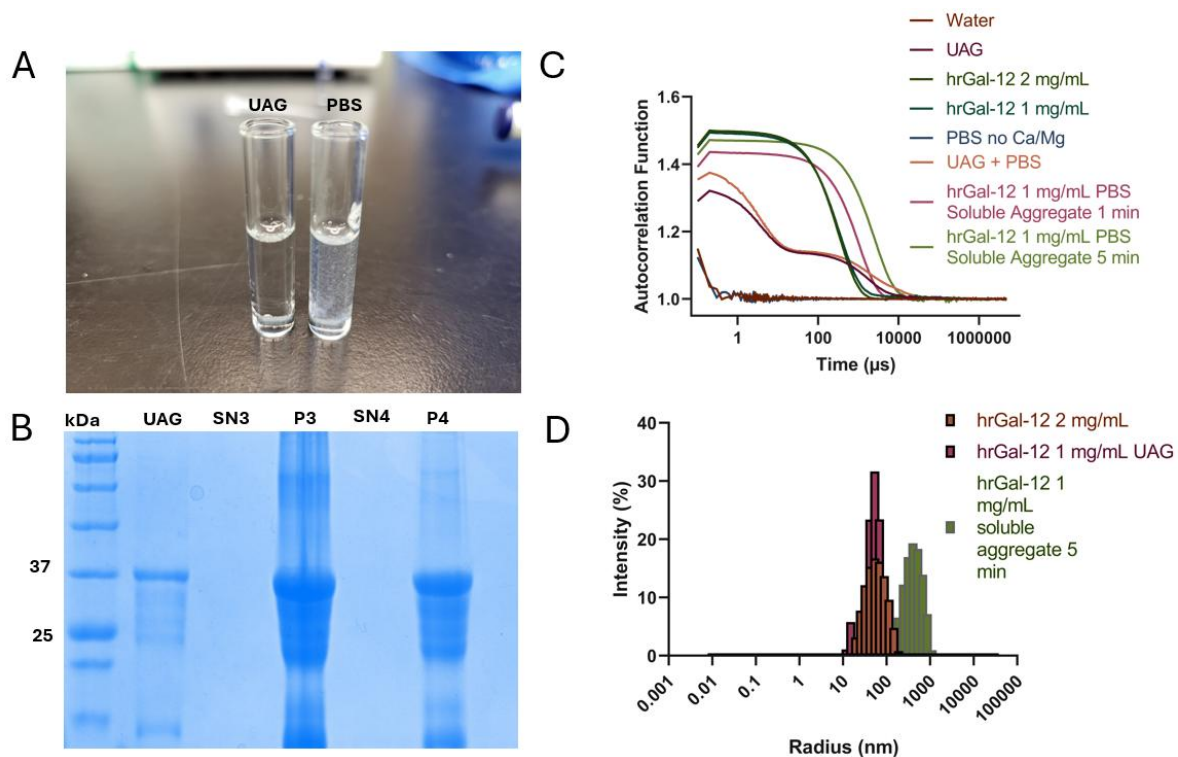


Figure 17. hrGal-12 precipitation and aggregation *in vitro*. **A)** hrGal-12 in solution with UAG buffer and resulting precipitate when diluted in PBS. **B)** SDS-PAGE showing hrGal-12 soluble in B2 (UAG buffer) lane. SN3/SN4 shows protein in solution following dialysis with buffer 3 and buffer 4, respectively. Lanes P3/P4 show hrGal-12 precipitate following dialysis in buffers 3 and 4, respectively. **C)** Autocorrelation function from DynaPro Wyatt DLS. hrGal-12 was diluted to 1 mg/mL from stock in both UAG and PBS. hrGal-12 in UAG at both 1 and 2 mg/mL shows one large galectin-12 oligomer in solution. **D)** Hydrodynamic radius of hrGal-12 in UAG and hrGal-12 soluble aggregates in PBS.

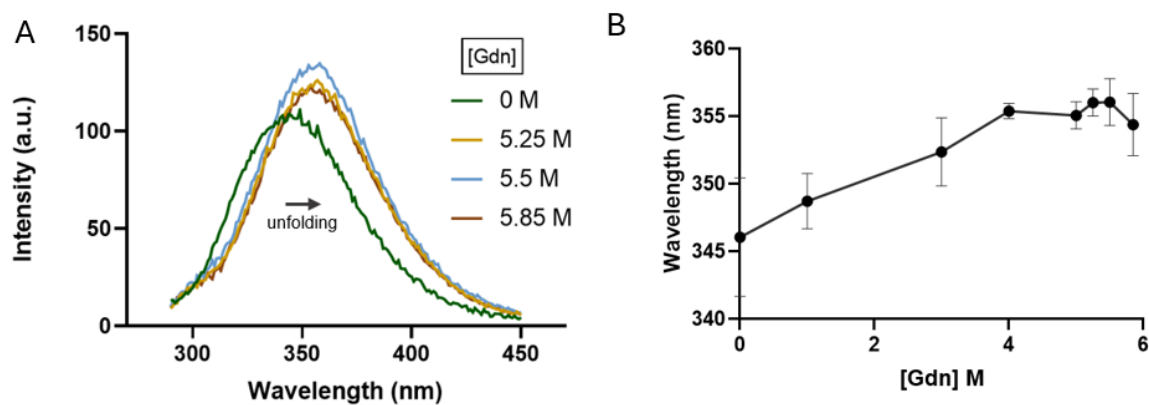


Figure 18. Chemical denaturation of hrGal-12 with Gdn-HCl. **A)** Intrinsic fluorescence emission of hrGal-12 measured with Varian Cary Eclipse fluorimeter. The excitation wavelength was 280 nm, and emission intensity was measured from 290-450 nm. Addition of Gdn-HCl causes a right shift in hrGal-12 maximum emission wavelength (λ -max) **B)** Shift in fluorescence emission maximum (λ -max) as a function of guanidine hydrochloride (Gdn-HCl) concentration (0-6 M). Approximately an 8 nm right shift in λ -max with increasing Gdn-HCl. Error bars represent +/- SD (n=3).

3.2 Biological activity of hexahistidine-tagged hrGal-12

3.2.1 hrGal-12 induced hemagglutination of rabbit RBCs

First, a hemagglutination assay was performed to test the lectin-like properties of hrGal-12. hrGal-12 induced hemagglutination of trypsinized rabbit RBCs at a concentration of 400 $\mu\text{g}/\text{mL}$ (**Figure 19A**). Rabbit RBCs were more sensitive to hemagglutination after glutaraldehyde fixation, with hrGal-12 demonstrating activity at a lower concentration of 25 $\mu\text{g}/\text{mL}$ (**Figure 19B**). Given that lactose is a standard inhibitor used to assess carbohydrate-dependent galectin activity, I examined whether it could block hrGal-12-induced agglutination. Lactose did not inhibit agglutination under the conditions tested. (**Figure 19B**). RCA has hemagglutination activity at a lower range from 1.25 $\mu\text{g}/\text{mL}$ in trypsinized rabbit RBCs, demonstrating the abundance of RCA ligands on cell surface in comparison with hrGal-12 ligands. RCA induced hemagglutination was inhibited by lactose, while hrGal-12 was not. The effect of citrus pectin on hrGal-12-mediated hemagglutination was examined to test whether complex glycans could inhibit galectin-12 activity. Citrus pectin was selected because it is enriched in fucosylated and galactose-containing polysaccharides that have been reported to interact with galectin-12. However, the addition of citrus pectin did not produce a consistent or dose-dependent inhibition of hrGal-12-induced hemagglutination (**Figure 19B**). PBS and UAG buffer alone showed no hemagglutination, confirming that aggregation was dependent on hrGal-12.

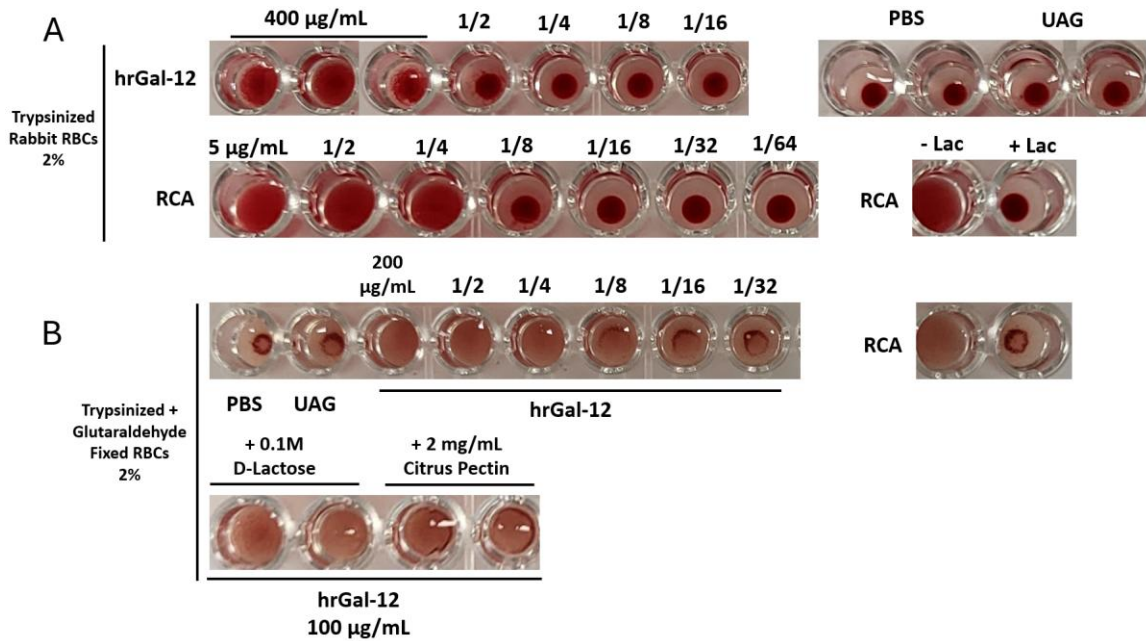


Figure 19. hrGal-12 induced hemagglutination of Rabbit Red Blood Cells (RBCs).

A) hrGal-12 induced hemagglutination of 2% solution of Trypsinized rabbit RBCs. 50 µL of RBCs were mixed with 50 µL of lectin solution and incubated for 2 hours at room temperature to measure hemagglutination. Controls with PBS and UAG buffer only are shown. Hemagglutination reactions were carried out in COSTAR™ U-bottom 96-well microplates. When the blood covers the well, this indicates lectin-crosslinking and hemagglutination. **B)** hrGal-12 induced hemagglutination following trypsinization and glutaraldehyde fixation.

3.2.2 hrGal-12 induced aggregation and adhesion of HL-60 cells

To test whether HL-60 cells have galectin-12 ligands on their cell surface, cell aggregation and adhesion assays were employed. hrGal-12 induced formation of small HL-60 aggregates which were detected with both microscopy and a platelet aggregometer. hrGal-12 induced HL-60 cell aggregation at a minimum concentration of 5 $\mu\text{g}/\text{mL}$ and reached a maximal aggregation response at 20 $\mu\text{g}/\text{mL}$ (**Figure 20A-C**). Dose–response analysis indicated half-maximal aggregation at approximately 9.7 $\mu\text{g}/\text{mL}$ hrGal-12. Despite the UAG buffer changing the light transmission properties of HL-60 cells, hrGal-12 induced aggregation at 20 $\mu\text{g}/\text{mL}$ was still significant ($p < 0.05$) (**Figure 20B-C**). At 6% (v/v) UAG buffer, the hrGal-12 aggregation rate was trending up but not significant ($p = 0.067$) (**Figure 20B**).

Microscopy revealed that hrGal-12 was only able to generate small HL-60 aggregates while the plant lectin, RCA, produced large cellular aggregates at a similar concentration (**Figure 21**). hrGal-12 induced HL-60 aggregation appeared to be inhibited by citrus pectin, suggesting galectin-12 has a complex glycan specificity (**Figure 21**). hrGal-12 and RCA induced aggregates appeared to stay intact under microscope following treatment with 1 mg/mL DNase, showing that HL-60 aggregates were not formed due to release of DNA from dead cells (data not shown).

HL-60 cells adhered to surfaces coated with hrGal-12 in a concentration-dependent manner. Plates coated with 350 $\mu\text{g}/\text{mL}$ hrGal-12 produced a significant increase in the crystal violet adhesion index measured at 570 nm ($p < 0.05$; **Figure 22A–B**). Detectable adhesion was observed at coating concentrations as low as 25 $\mu\text{g}/\text{mL}$, with progressively stronger adhesion up to 800 $\mu\text{g}/\text{mL}$ (**Figure 22C**). In comparison, RCA induced maximal HL-60 adhesion at a much lower coating concentration of 50 $\mu\text{g}/\text{mL}$, indicating that galectin-12 ligands are less abundant on the HL-60 cell surface than RCA-binding glycans.

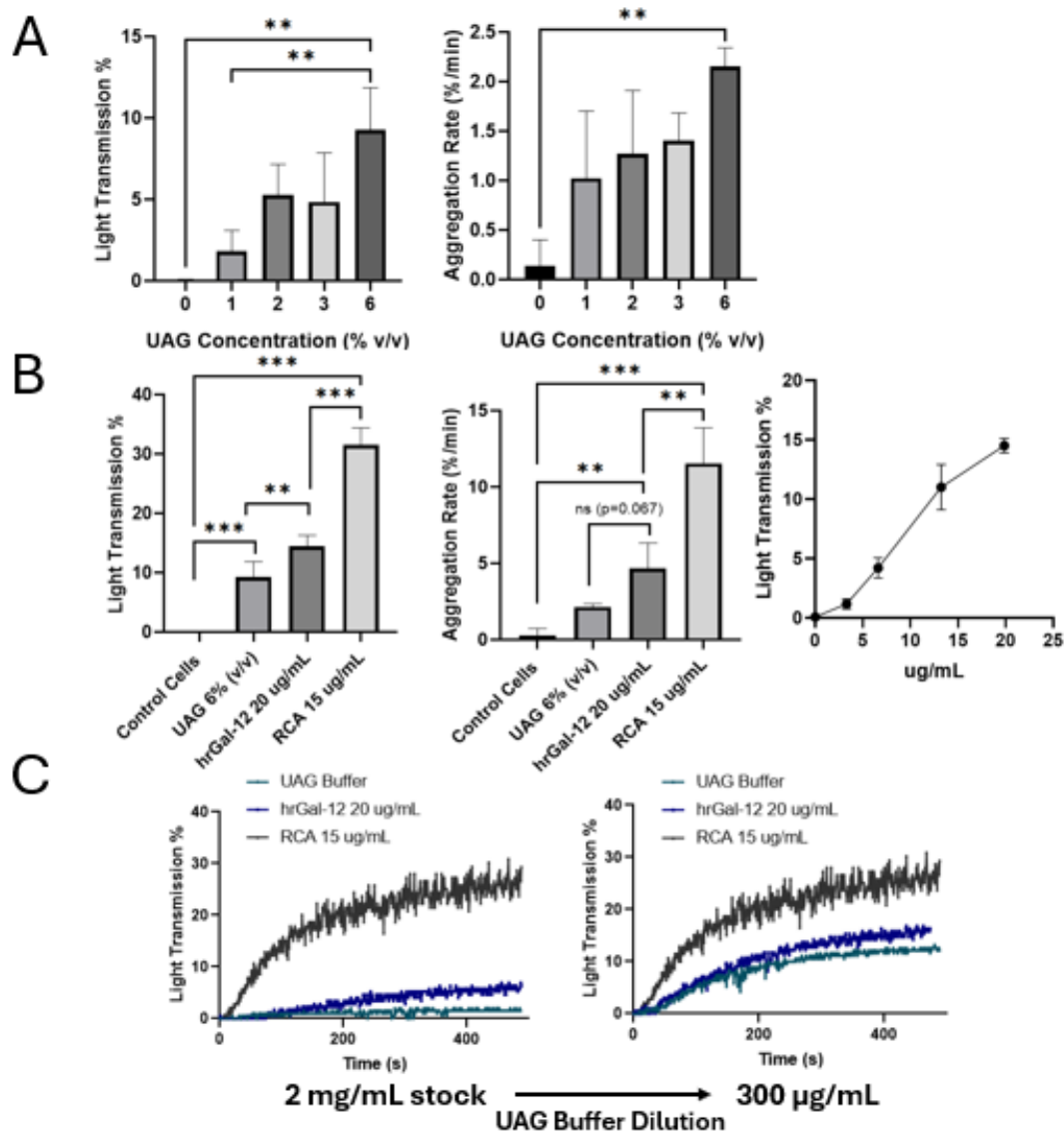


Figure 20. hrGal-12-induced aggregation of HL-60 cells. Aggregation was measured as a percent (%) light transmission, using a SOLAR AP2110 aggregometer following lectin addition. **A)** Effect of UAG buffer on light transmission and aggregation rate of HL-60 cells. **B)** hrGal-12 dose response including light transmission % and aggregation rate (%/min) including RCA response at 15 µg/mL. **C)** hrGal-12 aggregometer output for hrGal-12 at 20 µg/mL (blue) including RCA (grey) and UAG buffer (turquoise). Left panel: hrGal-12 added directly from a 2 mg/mL stock solution. Right panel: hrGal-12 pre-diluted in UAG buffer to 300 µg/mL prior to addition. One-way ANOVA with Tukey's HSD was used to assess significant differences, which are indicated by * ($p < 0.05$), ** ($p < 0.01$), and *** ($p < 0.001$). Error bars represent mean \pm SD ($n=3$).

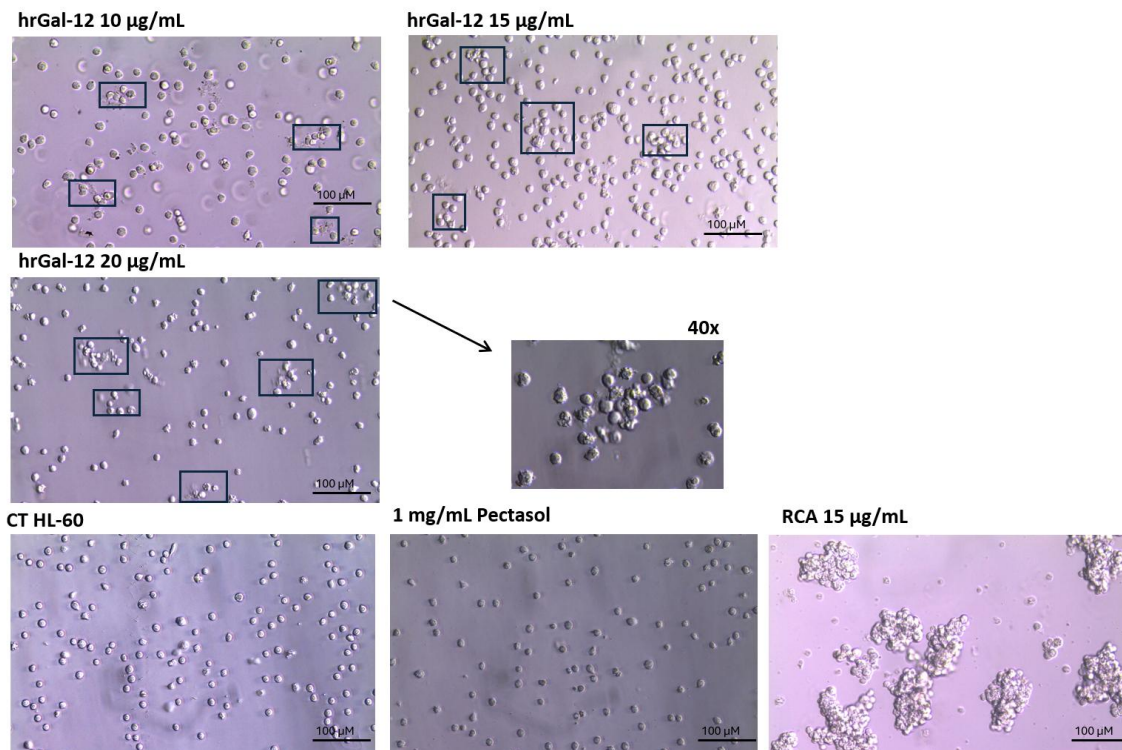


Figure 21. Visualization of hrGal-12 induced HL-60 aggregates. Treatment of HL-60 cells with hrGal-12 at 10, 15, and 20 µg/mL led to visible cellular aggregates (outlined by blue boxes). Live HL-60 cells were transferred from cuvette to 35 mm suspension dishes for imaging at 20x objective using an inverted Leica microscope. Bottom left: Untreated HL-60 cells. Bottom right: HL-60 cells treated with RCA (15 µg/mL) with characteristic aggregates. Bottom (middle): HL-60 cells with citrus pectin (Pectasol) addition before hrGal-12 treatment.

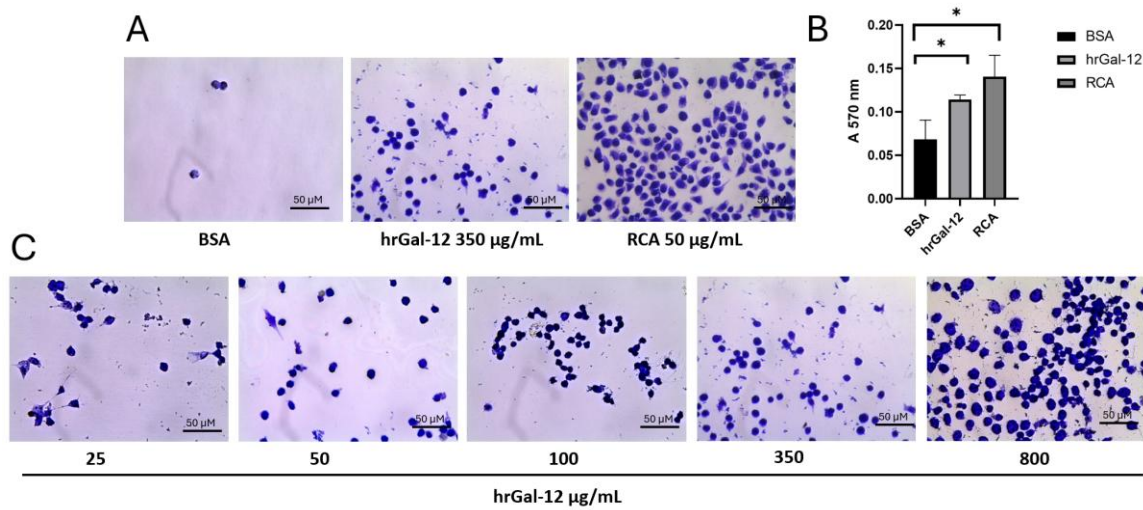


Figure 22. Adhesion of HL-60 cells to immobilized hrGal-12. **A)** Representative images of HL-60 cell adhesion to immobilized lectins visualized with Crystal Violet staining. **B)** Adhesion Index (570 nm absorbance) quantified with solubilized Crystal Violet stain. RCA was used as a positive control for adhesion. Error bars +/-SD (n=3). **C)** Dose-dependent HL-60 cell adhesion to hrGal-12. Images of fixed HL-60 cells taken at 100x magnification, using an inverted Leica microscope.

3.3 Effects of hrGal-12 on growth and differentiation of HL-60 cells

3.3.1 hrGal-12 lowers growth rate of HL-60 cells

hrGal-12 reduced HL-60 cell growth in a dose-dependent manner over 6-days, with a significant decrease observed at 10 $\mu\text{g/mL}$ (**Figure 23A**). hrGal-12 and UAG buffer treated cells maintained a viability over 90% throughout the 6-day period like the control cells. (**Figure 23A**). Cells treated with 10 $\mu\text{g/mL}$ hrGal-12 had a population doubling time (PDT) of 40.2 hours ($p < 0.05$) compared with control HL-60 cells with a PDT of 26.8 hours and UAG treated HL-60 cells with a PDT of 28.6 hours (**Figure 23B**). Treatment with 1 $\mu\text{g/mL}$ and 0.1 $\mu\text{g/mL}$ hrGal-12 also showed lower growth rates trends compared to the control (**Figure 23B**). Growth reduction was evident at 3 days from seeding concentration of 0.1×10^6 cells/mL.

3.3.2 hrGal-12 increases cell differentiation markers *NCF1* and *NCF2* in HL-60 cells

Treatment with hrGal-12 at a concentration of 10 $\mu\text{g/mL}$ resulted in approximately a two-fold increase in cell differentiation markers *NCF1* ($p < 0.05$) and *NCF2* ($p < 0.05$) (**Figure 24**). Furthermore, hrGal-12 induced a dose-dependent effect on *NCF1* levels across concentrations of 0.1, 1, and 10 $\mu\text{g/mL}$ (**Figure 24**). ATRA treatment produced a 2.5-fold increase in *NCF1* expression ($p < 0.001$), while DMSO treatment resulted in a 2.7-fold increase ($p < 0.001$). An increase in *NCF2* expression was also observed following treatment with hrGal-12 and DMSO.

ATRA and DMSO treatment led to clear changes in nuclear morphology with more lobulated nuclei, while hrGal-12 had minimal impact, which showed that this preparation of hrGal-12 is not inducing neutrophil-like differentiation of HL-60 cells (**Figure 25**).

Last, I looked at a key lipogenic gene to see if its expression changed as a first step in evaluating the ability of hrGal-12 to induce lipogenesis in HL-60 cells. Overall, hrGal-12 had no effect on *DGATI* expression (**Figure S3**). Further, *DGATI* levels appear lower in all samples compared to housekeeping *ACTB* gene.

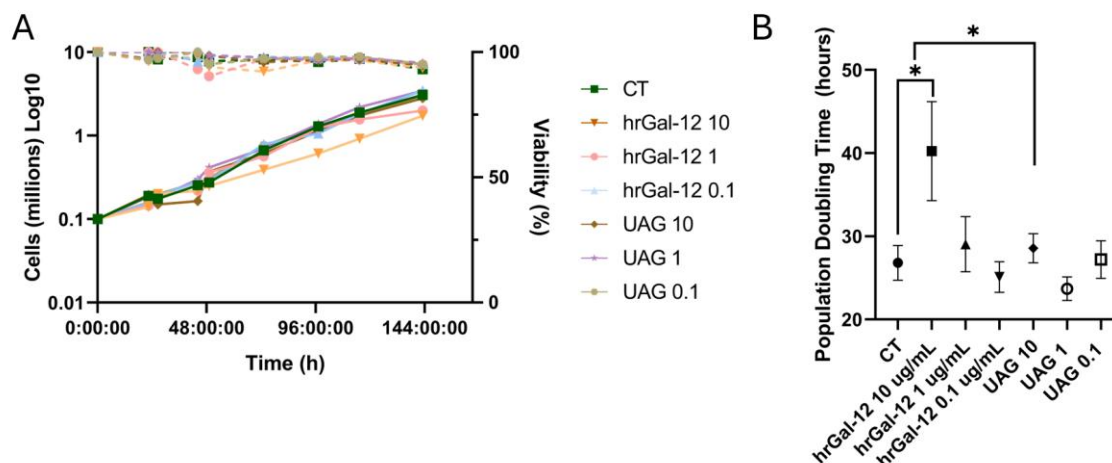


Figure 23. hrGal-12 reduces HL-60 cell growth at 10 µg/mL without affecting cell viability. **A)** HL-60 cell concentration (cells/mL) and viability (%) over 6 days. Cells were treated with hrGal-12 at 10, 1, and 0.1 µg/mL, along with corresponding UAG buffer controls. HL-60 cell viability over 6 days measured with Trypan Blue. Solid lines represent growth curves while dotted lines represent cell viability. **B)** Population doubling time (PDT) of HL-60 cells treated with hrGal-12 and UAG * $p < 0.05$. Error bars +/- SD (n=3). For all panels, CT = control HL-60 cells. G12 10, 1, and 0.1 = HL-60 cells treated with 10, 1, and 0.1 µg/mL hrGal-12, respectively. UAG 10, 1, and 0.1 = HL-60 cells treated with UAG buffers corresponding to the hrGal-12 treatment.

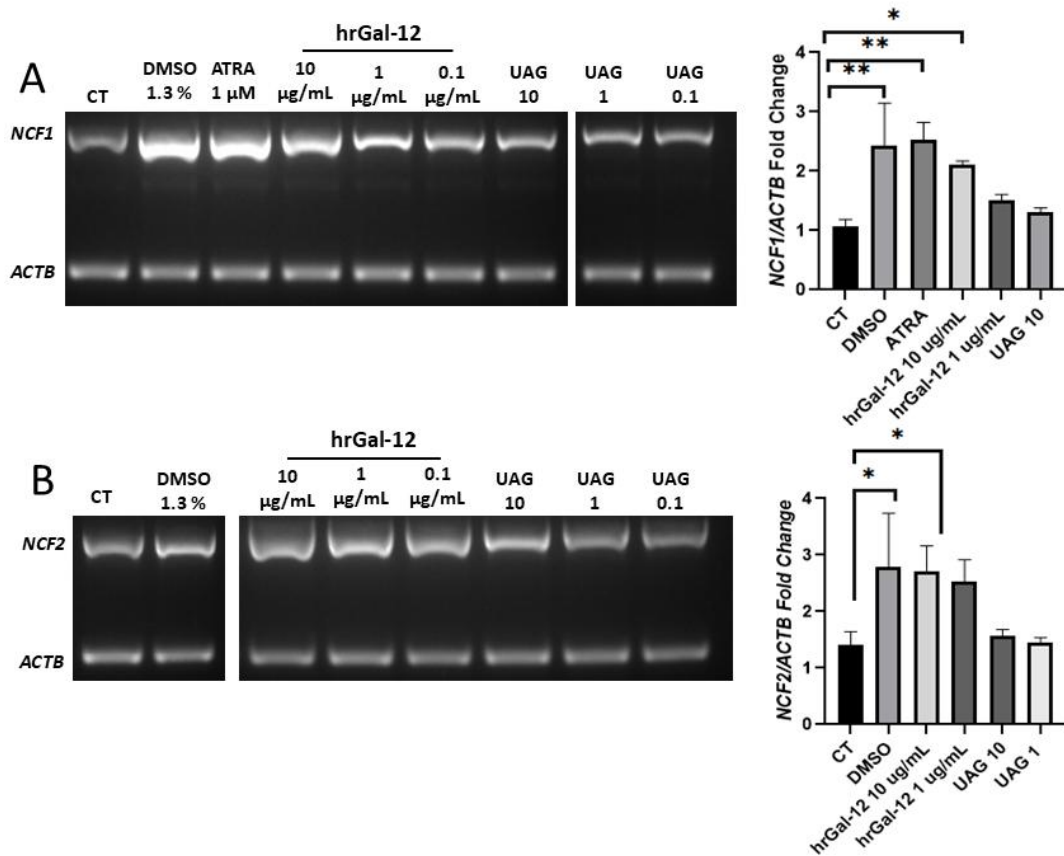


Figure 24. hrGal-12 increases cell differentiation markers *NCF1* and *NCF2*. HL-60 cells treated with hrGal-12, DMSO, and ATRA for 72 hours. RT-PCR performed on a 2% agarose gel. **A)** *NCF1* amplicon at 747 and **B)** *NCF2* amplicon at 767 bp. Both *NCF1* and *NCF2* were multiplexed with *ACTB* on agarose gel. Right panels show densitometrical analysis of gene expression performed in ImageJ. One-way ANOVA with Tukey's HSD were performed and significant differences are presented as *($p < 0.05$), **($p < 0.01$), and ***($p < 0.001$). Error bars represent mean \pm SD ($n=3$).

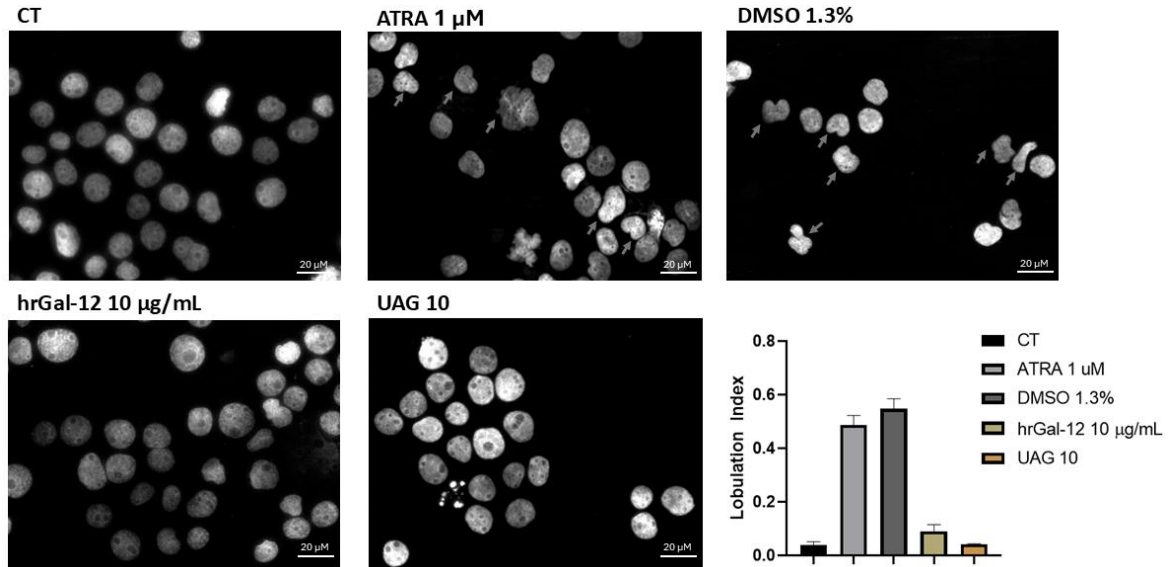


Figure 25. Nuclear morphology of HL-60 cells following treatment with hrGal-12, ATRA, and DMSO. DAPI stained nuclei following methanol fixation after 72-hour cell treatments. Representative images from three independent experiments are shown ($n = 3$). Grey arrows indicate nuclei exhibiting altered or lobulated morphology. The nuclear lobulation index was used to quantify changes in nuclear morphology following treatment.

Chapter 4

4 Discussion

The goal of my research was to produce recombinant full length human galectin-12, characterize its biochemical properties, and test its effects on the promyelocytic HL-60 cell line. Overall, I successfully cloned hexahistidine tagged *LGALS12* into pET-28a vector at the *NheI* and *XhoI* cut sites and expressed hrGal-12 in BL21(DE3) *E. coli* cells. hrGal-12 was purified under denaturing conditions using Ni-NTA and SEC, followed by solubilization and refolding in the specialized UAG buffer. hrGal-12 was concentrated to 2 mg/mL and remained stable at -80°C up to a year, and after thawing in a fridge for up to a week. hrGal-12 was recognized with commercially available human polyclonal galectin-12 and monoclonal anti-6xHis antibodies.

Next, I explored the biological properties of hrGal-12. hrGal-12 induced hemagglutination of rabbit red blood cells, implying its lectin-like activity. Further, trypsinized and glutaraldehyde fixed RBCs were more sensitive to hrGal-12 induced hemagglutination. Glutaraldehyde fixation alters cell surface sialylation, potentially increasing the availability of galectin-12-compatible ligands. hrGal-12 also induced weak aggregation of HL-60 cells, showing compatible galectin-12 ligands on the HL-60 cell surface. This was further demonstrated as HL-60 cells adhered to immobilized hrGal-12 in a dose-dependent manner. hrGal-12 induced HL-60 cell responses were not inhibited by lactose, and the glycan-specificity of my preparation remains unknown apart from a general inhibitory effect of citrus pectin.

Importantly, hrGal-12 lowered the growth rate of HL-60 cells without impacting cell viability. Finally, I tested whether hrGal-12 can induce differentiation of HL-60 cells. hrGal-12 upregulated key cell differentiation markers *NCF1* and *NCF2* but had no effect on relevant nuclear and cell morphology, which questioned a type of differentiation or interfering influence of refolding buffer. Overall, my findings demonstrate the challenging properties of this version of recombinant galectin-12, which can interact with HL-60 cells but precipitates under physiological conditions raising issues of its stability, folding state, optimization of purification methods, and biological activity.

4.1 Interpretation

4.1.1 Challenges and optimization of hrGal-12 production

Galectin-12 is a hydrophobic protein and its aggregation *in vitro* has been an ongoing obstacle in its purification (Yang et al., 2011; Maller et al., 2020; Tsao et al., 2025; Zhang et al., 2025). This was reconfirmed by my hydropathy analysis with Kyte & Doolittle based hydrophobic scoring, which showed hydrophobic residues scattered throughout the human galectin-12 sequence. After probing BL21(DE3) lysates with His tag antibody, I show hrGal-12 expression at the size of ~35 kDa along with degraded hrGal-12 products. After cell lysis in 6 M guanidine, most of the hrGal-12 was present in the soluble lysis fraction. Cell lysis by sonication or in the presence of various detergents was unable to solubilize hrGal-12, consistent with its hydrophobic nature. hrGal-12 was most likely expressed in inclusion bodies, necessitating the use of guanidine for solubilization, as this chaotropic reagent is standard and widely established for extracting proteins from inclusion bodies (Yamaguchi & Miyazaki, 2014). Although galectin-12 is not a membrane protein, it is associated with the lipid droplet membrane intracellularly, leading to similar challenges during purification. During purification, hrGal-12 bound successfully to the Ni-NTA column but required strong denaturants (Gdn-HCl) and 400 mM imidazole for elution. When eluted with sodium acetate or urea-based buffers, hrGal-12 remained bound to the Ni-NTA resin. hrGal-12 was fully dissolved in the 6 M guanidine elution buffer. Overall, I report a yield of ~ 3 mg/L bacterial culture with the major band and degraded products at 1:1 ratio. The degraded bands were confirmed to be hrGal-12 via western blotting (**Figure 14; Figure 15A-F**).

Following Ni-NTA purification, hrGal-12 was further purified using SEC, a common second step in recombinant protein production (Morimoto & Walinda, 2024). Although SEC and concentration of hrGal-12 were necessary to create a high-quality stock, both steps result in significant yield losses which display batch-to-batch variability. This is hard to mitigate with hydrophobic proteins, which are known to adsorb onto chromatographic columns and glassware (Lerro et al., 1993). Potentially, concentrating the hrGal-12 before SEC could allow for more protein loading onto the column and less yield loss at this stage. I loaded the Ni-NTA hrGal-12 without concentrating and loaded

protein in a 5 mL sample loop which resulted in ~20% hrGal-12 loss. At the concentration stage, equilibration with UAG buffer before concentration appeared to prevent hrGal-12 adsorption onto membrane. The use of ion exchange (IEX) or HIC columns required manipulation of the UAG buffer composition and either left hrGal-12 stuck on the column or degraded. For IEX, a carboxymethyl (CM) Sepharose Fast Flow weak cation-exchange column (Cytiva) was tested, among others (**Table 1**). With IEX, proteins are bound at low salt and eluted with high salt. The low salt buffer contained no arginine, and high salt variations with arginine and NaCl appeared to cause less degradation of hrGal-12 than use of NaCl for ionic strength alone (**Figure S4**). I identified the S75 SEC 16/6000 HiLoad Cytiva column to be effective for purification of hrGal-12 in UAG. Further optimization of IEX and HIC conditions and columns need to be tested in the context of hrGal-12 purification. Mouse and human recombinant galectin-12 were successfully isolated using Q-sepharose column, followed by a gradient elution with NaCl through a carboxymethyl Sepharose column and concentration with a Vivaspin 20 concentrator (Maller et al., 2020; Cagnoni et al., 2024). This same method was ineffective for purifying hrGal-12 in my study, but their studies used Rosetta (DE3) cells while I used BL21(DE3) cells for expression.

My attempt to purify hrGal-12 in BL21(DE3) cells using the protocol for hrGal-12 and mrGal-12 in Rosetta (DE3) cells was unsuccessful. Specifically, hrGal-12 was not solubilized during cell lysis with sonication. The lysis and dialysis with full length hrGal-12 by Cagnoni et al. (2024) was done in a simple buffer comprised of HEPES and NaCl buffer with 8 mM BME. They demonstrate glycan-binding of their preparation of hrGal-12, but no cell responses or hemagglutination results are presented. The protocol I have developed for hrGal-12 is simpler given that the protein binds to a his-tag and only requires a single straightforward size exclusion step. Further, my preparation does not use complex and expensive enzymes or protease inhibitors during cell lysis, allowing for feasible scale-up of hrGal-12 production in an academic lab. The downside is the complicated nature of the UAG buffer, which limits certain assays including circular dichroism and cell-based light transmission. Future work with this preparation will need to address the complexity of the UAG buffer or find better ways to solubilize hrGal-12.

At the dialysis stage, hrGal-12 precipitated under all buffers tested other than the UAG buffer, with 2M urea, 0.5M arginine, 1.8 mM GSH, and 0.9 mM GSSH. This solubility issue with hrGal-12 was expected given the number of hydrophobic residues along the entirety of the galectin-12 molecule (**Figure 8**). These residues have been suggested to underlie the intracellular lipid droplet localization of galectin-12 (Yang et al., 2011). The use of urea and arginine in refolding buffers is well documented in the literature, though the exact mechanisms by which they facilitate refolding remain a topic of debate (Ng & Konermann, 2024). Arginine can bind to acidic residues blocking salt bridge formation, interfering with hydrophobic contacts, and forms networks which prevent proteins aggregation (Ng & Konermann, 2024). Arginine may work similarly to guanidine or urea, which both promote protein refolding and stability at lower concentrations below 3 M (Yamaguchi & Miyazaki, 2014; Roufarshbaf & Akbari, 2023). Although I screened over 10 buffers using traditional dialysis membranes, large-scale buffer-screening approaches are commonly used for recombinant proteins because they allow rapid testing of many more conditions and increase the likelihood of identifying buffers compatible with the protein (Vincentelli et al., 2004).

The production of recombinant proteins creates an environment for the protein during expression and purification that is vastly different than the native protein in human cells, which is known to impact the solubility of hydrophobic proteins (Feller & Lewitzky, 2012). SDS-PAGE showed hrGal-12 at the size of 35 kDa, along with degradation products at 25 and 15 kDa. hrGal-12 had a predicted size of 38 kDa but tends to run lower on a denaturing gel due to its basic isoelectric point (Maller et al., 2020). The degradation product at 15 kDa was completely removed following SEC. Given the size of the two degraded products, they may indicate proteolytic degradation of hrGal-12 at the linker region. Native bacterial proteases can target linker regions in bacterial expression systems (Murby et al., 1996). The strain used in this study, BL21 (DE3), is deficient in common bacterial proteases like OmpT-protease but may have some proteases that were able to recognize the hrGal-12 linker region. The linker region and hydrophobic residues may be altered with site-directed mutagenesis to increase solubility and prevent proteolytic cleavage, which may reduce the degradation I observed with my preparation (Murby et al., 1996).

Another group has purified the N-terminal human gal-12 expressed in *E. coli* inclusion bodies with the addition of a 67 residue (P67) tag. The P67 tag is comprised of eight anti-parallel β -sheets arranged into a flat barrel structure. The N-terminal domain of human galectin-12 displays hemagglutination activity, providing an explanation for why full-length galectin-12 can agglutinate cells despite its atypical C-terminal domain. (Zhang et al., 2025). This P67 tag method was unable to produce full length active hrGal-12, and the authors claim this could be due to an interaction between the two CRDs during purification. This method is interesting as the dialysis stage is reduced to only a few hours, and the yield of proteins appears to be enhanced with the P67 tag. Full length active galectin-8 was also purified using the P67 tag, and addition of this tag paired with my purification protocol may enable full length hrGal-12 to be purified more efficiently.

Many recombinant proteins aggregate *in vitro*, and this aggregation poses a major challenge for purification of proteins for biological studies and the large-scale production of therapeutic recombinant proteins. I did not test endotoxin levels in my hrGal-12 sample as my project did not explore the therapeutic properties of hrGal-12 in an *in vivo* model. As Ni-NTA beads with plastic column chromatography can lead to aggregation in traditional buffers, a potential solution is to elute the protein off the Ni-NTA beads using a detergent concentration gradient with AKTA GO system (Royster et al., 2021). The AKTA system can be set up and fully automated from cell-lysis to multi-stage purification of proteins. Implementing this for hrGal-12 would be useful for improving purity and yield. Additionally, a periplasmic secretion tag can be added to the existing plasmid to force expression of hrGal-12 in the cytoplasm and not inclusion bodies (Yamaguchi & Miyazaki, 2014).

4.1.2 hrGal-12 induced aggregation and adhesion of HL-60 cells confirms compatible cell-surface galectin-12 ligands

hrGal-12 treatment induced aggregation of HL-60 cells, with maximal induction at 20 $\mu\text{g}/\text{mL}$, and an EC_{50} value of 9.7 $\mu\text{g}/\text{mL}$. This aggregation occurred within minutes of addition of hrGal-12. Despite the interference of UAG buffer in light transmission measurements with aggregometer, there was still a significant effect of hrGal-12. The HL-60 aggregates were much smaller than RCA induced aggregates, which could be due

to a lower amount of galectin-12 specific glycans on HL-60 cell surface in comparison to RCA compatible glycans. HL-60 cells also adhered to immobilized hrGal-12. Both the aggregation and adhesion effects of hrGal-12 were dose-dependent. As galectin-12 has two CRDs, each one may bind to one HL-60 cell leading to aggregates and further crosslinking to create larger cell aggregates.

It is unknown whether differentiated HL-60 cells have altered adhesion or aggregation with hrGal-12. Previous work has shown that HL-60 cells treated with CoCl₂ (hypoxia mimic) have increased adhesion responses to immobilized plant lectins like RCA (Timoshenko et al., 2016). The adhesion assay is interesting as I was able to remove all UAG buffers and hrGal-12 remained active. In AML cells, where there are lower galectin-12 levels, these cells may be less adhesive and more likely to move and promote tumor growth. Although this is unproven with galectin-12, many human galectins have been implicated in the epithelial to mesenchymal (EMT) transition, a hallmark of cancer (Ribatti et al., 2020; Perez-Moreno et al., 2024). EMT in fibrosis is also common, and galectin-12 is known to alter macrophage polarization and be involved in fibrosis in fatty liver disease (Lee et al., 2023). For example, galectin-1 is known to be pro-fibrotic and promote EMT in lung idiopathic pulmonary fibrosis (Kathiriya et al., 2017). Interestingly, galectin-1 and galectin-3 expression appears to be inversely correlated to galectin-12 expression, which may have biological implications in terms of cell adhesion and migration (Vinnai et al., 2017; McTague et al., 2022). Cancer cells have altered glycosylation and cell surface glycans compared to healthy cells, and this can alter the affinities of galectins to the cell surface in the tumor microenvironment (Perez-Moreno et al., 2024).

Interestingly, galectin-9, another tandem-repeat galectin, is able to induce cell aggregation and apoptosis of human melanoma cell lines when added exogenously (Kageshita et al., 2002). After addition of recombinant galectin-9, small aggregates were present near the 2-hour mark, and aggregate size increased up to 12 hours. In melanoma, higher galectin-9 levels are associated with better prognosis and lower galectin-9 levels are associated with greater tumor thickness. In MDA-MB-231 breast cancer cells, galectin-3 binding protein uses cell surface galectin-1 to create large cell aggregates,

which are predicted to improve cancer cell survival in the blood stream and promote metastasis (Lin et al., 2015). This Gal-3BP mediated MDA-MB-231 aggregation was carbohydrate dependent and inhibited by lactose but not sucrose. In comparison to human galectins, plant lectins are well characterized to induce cell aggregation and adhesion. The aggregates induced by castor bean *Ricinus communis* agglutinin (RCA) can be inhibited by lactose (Timoshenko et al., 2016). These findings with other galectins and lectins indicate that the cell aggregation observed with hrGal-12 is a common functional property of galectins, consistent with their ability to crosslink cell-surface glycans and promote cell–cell interactions.

My preparation of hrGal-12 induced aggregation of rabbit RBCs, known as hemagglutination, a common test for galectin activity (Gasson et al., 2024). Trypsinized and glutaraldehyde fixed RBCs were more prone to hrGal-12 induced hemagglutination than trypsinized RBCs alone. Neuraminidase treatment and trypsinization of red blood cells alters their sialic acid residues and cell surface charge, making them more prone to aggregation (Böhler & Linderkamp, 1993; Gasson et al., 2024). The observation that hrGal-12 interacts with both HL-60 cells and erythrocytes suggests that these cell types present cell-surface glycans that are recognized by human galectin-12. This is important as galectins are known to bind to glycans on cell surface of foreign pathogens to alert the immune system and target pathogens for destruction (Liu & Stowell, 2023; Thurston et al., 2012). For example, galectin-8 can remarkably identify glycans on vacuoles with *Salmonella*, and recruit an adaptor protein to signal those vacuoles for autophagy (Thurston et al., 2012).

hrGal-12 induced cell responses were not inhibited by lactose, which is consistent with murine rGal-12, and reports that lactosyl sepharose chromatography are ineffective with hrGal-12 (Maller et al., 2020; Nishi, 2020). Microscopic analysis of aggregates showed citrus pectin (Pectasol) as an inhibitor of hrGal-12 induced HL-60 aggregation. Pectin is a large and complex polysaccharide which has fucosylated glycans that galectin-12 could potentially bind to. Pectin is known to bind to galectin-3 and reduce its pro-tumorigenic effect on metastasis and cell adhesion (Zhang et al., 2016). Galectin-3 binding to pectin has been assessed with various biophysical techniques including surface

plasmon resonance, bio-layer interferometry, and hemagglutination assays. Similar studies should be performed with hrGal-12 and potential ligands including pectin. PectaSol-C, a modified version of citrus pectin, is currently being tested in clinical trials and is shown to have anti-cancer effects in cancer cell lines *in vitro* (Wdowiak et al., 2018).

As expected, lactose was unable to inhibit hrGal-12 cell responses. This has also been shown with mouse recombinant galectin-12, which interacts with more complex fucosylated structures (Maller et al., 2020). Cagnoni et al. (2024) show via solid-phase binding assays that hrGal-12 also preferentially binds 3'-fucosylated glycans such as 3'-fucosyllactose and Lewis X. hrGal-12 was able to bind these fucosylated structure with μM affinities, like those reported for mrGal-12. hrGal-12 cannot be purified using a lactosyl-sepharose matrix which works to purify many other galectins (Nishi, 2020).

hrGal-12 appears to have a low affinity for lactose and N-acetyllactosamine, which various other galectins interact with (Cagnoni et al., 2024). Interestingly, galectin-12 ligands like 3'-fucosyllactose are found in human breast milk, and certain groups of women have been found to have more production of 3'-fucosyllactose oligosaccharides (Samuel et al., 2019; Cagnoni et al., 2024). These human milk oligosaccharides may provide unique nutritional benefits compared to those found in breast milk replacements or cow's milk, leading countries like United States and Australia to give approval for addition of 3'-fucosyllactose and 2'-fucosyllactose (Amin et al., 2025). It should be noted that after adipocytes, galectin-12 expressed mostly in breast tissue, and breast adipose tissue. Further, galectin-1, -3, and -9 have been reported in breast milk in association with early development (Rio-Aige et al., 2022). Compared to healthy peripheral blood leukocytes, HL-60 cells are shown to have changes in cell surface fucosylated glycans, caused by an increase in sialic acid structures (Van Beek et al., 1975). Cancer cells tend to have larger surface oligosaccharides, like in human carcinomas, which are noted to have large fucosylated structures (Smets & Van Beek, 1984). Upon differentiation of embryonal carcinoma cells, the surface carbohydrate size decreases (Smets & Van Beek, 1984).

4.1.3 hrGal-12 lowers growth rate of HL-60 cells and upregulates cell differentiation markers

Galectins regulate neutrophil function, including activation, extravasation, and phagocytosis, through glycan binding both intra- and extracellularly (Robinson et al., 2019). Previous work from this laboratory has proposed that ATRA treatment of HL-60 cells is associated with increased *LGALS12* expression and features consistent with an N1-like, anti-tumor neutrophil phenotype, whereas DMSO treatment decreases *LGALS12* levels and is associated with a more pro-tumorigenic phenotype (Vinnai et al., 2017; Tazhitdinova et al., 2024). Both ATRA and DMSO induce lobulated nuclear morphology and increase expression of the NADPH oxidase subunits *NCF1* and *NCF2*, consistent with neutrophil differentiation.

In this study, treatment of HL-60 cells with recombinant human galectin-12 (hrGal-12) resulted in increased *NCF1* and *NCF2* expression, indicating activation of differentiation-associated components of the NADPH oxidase complex. Notably, hrGal-12 treatment reduced cell growth rate without affecting cell viability or inducing overt nuclear lobulation, suggesting that galectin-12 may be involved in aspects of myeloid differentiation through mechanisms distinct from those used by ATRA or DMSO. While these findings do not demonstrate hrGal-12 as an inducer of neutrophilic differentiation, they support a role for galectin-12 in modulating differentiation-associated pathways. This interpretation is consistent with prior reports demonstrating that other galectins, such as galectin-3, can directly activate neutrophil functional responses including NADPH oxidase-dependent respiratory burst signaling (Truong et al., 1994).

The classification of neutrophil phenotypes is important for understanding immune responses in cancer, yet there are currently few reliable molecular markers that distinguish N1 from N2 neutrophils (Wang et al., 2018). Tumor-associated neutrophils can be polarized toward either phenotype depending on intracellular signaling pathways and extracellular cues. N1 neutrophils exert anti-tumor activity through production of hydrogen peroxide (H₂O₂), nitric oxide, tumor necrosis factor- α , and enhanced T-cell activation, whereas N2 neutrophils promote tumor growth, metastasis, immune suppression, and angiogenesis via increased reactive oxygen species (ROS), reactive

nitrogen species, neutrophil extracellular traps (NETs), and vascular endothelial growth factor production (Wang et al., 2018).

Given that galectins are known regulators of neutrophil adhesion, activation, and turnover, these phenotypic distinctions provide a framework for interpreting the effects of recombinant galectin-12 (Robinson et al., 2019). The ability of hrGal-12 to induce HL-60 cell aggregation and alter differentiation-associated markers suggests that galectin-12 may participate in myeloid differentiation, potentially influencing pathways related to lipid metabolism, reactive oxygen species generation, and cell–cell interactions. While additional work is needed to establish whether galectin-12 biases cells toward N1- or N2-like phenotypes, these data implicate galectin-12 as a contributor to myeloid differentiation programs.

Lowering *LGALS12* levels in the NB4 acute promyelocytic leukemia (APL) cell line was previously shown to promote ATRA-induced differentiation while inhibiting lipid droplet formation (Xue et al., 2016), which contrasts with the proposed role of galectin-12 as a tumor suppressor in other leukemia contexts (Tazhitdinova & Timoshenko, 2020; Tazhitdinova et al., 2024). Notably, NB4 cells express higher baseline levels of galectin-12 than HL-60 cells, but the functional relevance of these differences for leukocyte differentiation remains unresolved. In the present study, treatment of HL-60 cells with hrGal-12 increased differentiation-associated markers but did not induce classical neutrophil differentiation, suggesting that hrGal-12 may promote an alternative or intermediate myeloid differentiation state. This interpretation is supported by the known plasticity of HL-60 cells, which can be driven toward distinct myeloid lineages depending on the differentiation stimulus. For example, dimethylformamide, phorbol 12-myristate 13-acetate (PMA), and calcium ionophore A23187 induce granulocytic differentiation through distinct signaling pathways (Manda-Handzlik et al., 2018). ATRA-treated HL-60 cells release neutrophil extracellular traps (NETs) only following PMA stimulation, whereas DMSO-treated HL-60 cells require CI treatment to induce NET formation; in contrast, dimethylformamide treated HL-60 cells release NETs in response to either PMA or calcium ionophore. PMA induces an artificial respiratory burst via protein kinase C mediated activation of the NADPH oxidase complex, resulting in

NET formation. Both ATRA- and DMSO-treated HL-60 cells produce H₂O₂ following PMA stimulation (Tazhitdinova et al., 2024), whereas N-formyl-L-methionyl-L-leucyl-L-phenylalanine (fMLP) induces H₂O₂ production only in DMSO-treated HL-60 cells. This difference has been attributed to expression of N-formyl peptide receptor 1 in DMSO-treated but not ATRA-treated cells. My findings indicate that while hrGal-12 influences differentiation-associated pathways in HL-60 cells, further functional assays, such as ROS production, NET formation, and receptor expression profiling, will be required to define the specific phenotype induced by hrGal-12.

As hrGal-12 reduced the growth rate of HL-60 cells without affecting viability, this suggests a shift away from proliferation that is consistent with differentiation-associated cellular reprogramming. Similar effects have been reported previously, where increased galectin-12 expression via transfection in Jurkat T cells suppressed cell growth, while galectin-9 overexpression had no effect (Yang et al., 2001). Preliminary observations reported by Yang et al. (2001) suggest that hrGal-12 treatment may be associated with reduced cyclin A levels and altered retinoblastoma protein phosphorylation; however, these findings remain correlative and require direct experimental validation. Together, these observations are consistent with a potential role for galectin-12 in cell-cycle regulation.

Supporting previous work, galectin-12 knockdown in human SZ95 sebocytes resulted in reduced expression of cyclin A1 and cyclin-dependent kinase 2 (CDK2), accompanied by decreased cell proliferation (Tsao et al., 2023, 2025). Whether hrGal-12 similarly modulates cyclins, CDKs, or cell-cycle regulators in HL-60 cells remains to be determined. Differentiation is frequently coupled to cell-cycle exit and coordinated changes in cyclins, CDKs, and lineage-specific transcription factors (Ruijtenberg & van den Heuvel, 2016). Given that HL-60 cells can be directed toward multiple myeloid lineages, including macrophages, monocytes, and dendritic cells, depending on the differentiation stimulus (Guo et al., 2012; Takahashi et al., 2014), the specific lineage and phenotype induced by hrGal-12 require further characterization.

Overall, increased galectin-12 levels in AML models appear to be associated with reduced proliferation and features consistent with relief of the differentiation block; however, the precise differentiation trajectory and functional phenotype induced by hrGal-12 remain unresolved. While galectin-12 may ultimately serve as a marker of myeloid differentiation states or neutrophil phenotypic polarization, additional mechanistic and functional studies are required to determine whether galectin-12 plays a causal role in lineage specification or can be leveraged therapeutically in differentiation-based cancer treatments.

4.1.4 Galectin-12 in lipid metabolism

Although I observed no changes in *DGAT1* expression following hrGal-12 treatment, this does not exclude the possibility that galectin-12 modulates other components of the lipogenic pathway. Both *DGAT1* and *DGAT2* catalyze the final step in triglyceride synthesis, with *DGAT2* more strongly associated with *de novo* lipogenesis (Yen et al., 2008). Cancer cells frequently exhibit altered lipid metabolism and preferential lipid synthesis from carbohydrates, which may involve differential regulation of lipogenic genes beyond *DGAT1* (Menendez & Lupu, 2007). Therefore, the absence of *DGAT1* changes in this study does not rule out broader effects of hrGal-12 on lipid metabolism.

Galectin-12 has been previously shown to be upregulated at the G1/S cell checkpoint and implicated in cell cycle arrest (Yang et al., 2001). Cell cycle arrest is associated with an increase in lipid-droplets (Lee et al., 2024). Changes in lipid metabolism are common in cancer and decreased galectin-12 can mean increased lipolytic signaling (Yang et al., 2011). This could mean a shift in energy sources to lipids in the lipid droplets as a fuel source in the tumor microenvironment. The increase in lipolytic signaling associated with reduced galectin-12 expression has been well documented in porcine models and may also be relevant to galectin-12 signaling in cancer cells (Wu et al., 2024). These findings raise the possibility that increasing galectin-12 levels could induce lipogenesis. In agricultural contexts, galectin-12 modulation could increase intramuscular fat deposition, an important determinant of pork quality, and recombinant galectin-12 administration may represent a more practical alternative to genetic modification for manipulating galectin-12 levels in specific tissues.

In the context of this study, however, I was not able to identify changes in lipid droplet content in hrGal-12–treated HL-60 cells using 4,4-difluoro-4-bora-3a,4a-diaza-s-indacene staining. Therefore, while existing literature supports a role for galectin-12 in lipid metabolism, whether recombinant galectin-12 can directly induce lipogenesis *in vitro* remains unknown and warrants further investigation.

I observed no detectable change in *DGAT1* expression following hrGal-12 treatment, suggesting that hrGal-12–induced differentiation may engage pathways distinct from those activated by DMSO- or ATRA-induced neutrophil differentiation. Supporting this point, differentiation of HL-60 cells with 2-3-dihydrogeranylgeranoic acid has been shown to induce lipid droplet formation without promoting neutrophilic differentiation (Kodaira et al., 2007). These findings raise the possibility that hrGal-12–associated lipid droplet changes may occur independently of classical neutrophil differentiation and could involve novel mechanisms. Consistent with this idea, increasing evidence indicates that lipid droplet content and lipid metabolism are altered in neutrophils and other myeloid cells in cancer (Menendez & Lupu, 2007; Melo & Weller, 2016; Grabner et al., 2021; Jiang et al., 2022). In cells with relatively low galectin-12 expression, such as HL-60 cells, enhanced lipolytic signaling has been reported, raising the possibility that re-introduction of hrGal-12 partially restores lipid metabolic balance during myeloid differentiation.

4.2 Conclusions and applications

To conclude, I have successfully developed a protocol for the solubilization and purification of full-length version of hexahistidine-tagged human galectin-12 in *E. coli* and explored its biological properties in HL-60 and rabbit RBCs. hrGal-12 was cloned using the NheI and XhoI cut sites into a pET28a vector and expressed in BL21(DE3) cells. hrGal-12 was isolated via its hexahistidine tag with Ni-NTA beads and further purified with SEC using FPLC. The protein was soluble in a complex buffer with copious amounts of arginine, urea, and glutathione (UAG), and was unstable in PBS or water. hrGal-12 was successfully immunodetected with human polyclonal galectin-12

antibodies and monoclonal 6xHis antibody. Next, I demonstrated hrGal-12 has lectin-like activity by its ability to induce hemagglutination of rabbit blood cells (**Figure 26**).

Further, my results suggest that HL-60 cells may have specific glycans on cell surface that galectin-12 can bind to, which may explain the hrGal-12 induced aggregation and adhesion. The exact glycan specificity of human galectin-12 is complex, but recent studies have showed recombinant mouse and human Gal-12 preferentially bind to 3'-fucosylated glycans (Maller et al., 2020; Cagnoni et al., 2024).

Importantly, I show that hrGal-12 lowers growth rate and increases differentiation-associated markers in HL-60 cells (**Figure 26**). This work builds on previous studies defining HL-60 neutrophil phenotypes induced by ATRA and DMSO and identifying *LGALS12* expression as a marker of neutrophil phenotypic state (Tazhitdinova, 2023; Tazhitdinova et al., 2024). ATRA and DMSO are known to induce neutrophil-like differentiation through distinct pathways, and hrGal-12 may also activate unique signaling programs associated with differentiation and lipid metabolism (Tazhitdinova et al., 2024). Although the exact neutrophil phenotype induced by hrGal-12 remains unresolved, I observed a reduction in HL-60 cell growth following hrGal-12 treatment, without a corresponding loss of viability, which is consistent with a shift from proliferation toward differentiation. Such growth arrest is a hallmark of differentiating cells and is often mediated by inhibition of CDKs through regulators such as Siamese-related 4 (Burda & Roeder, 2022). Understanding the hrGal-12-induced HL-60 phenotype will require further gene- and protein-level analyses to define the transcriptional and signaling networks engaged by hrGal-12, similar to previously established gene regulatory circuits for ATRA-induced differentiation (Tasseff et al., 2017).

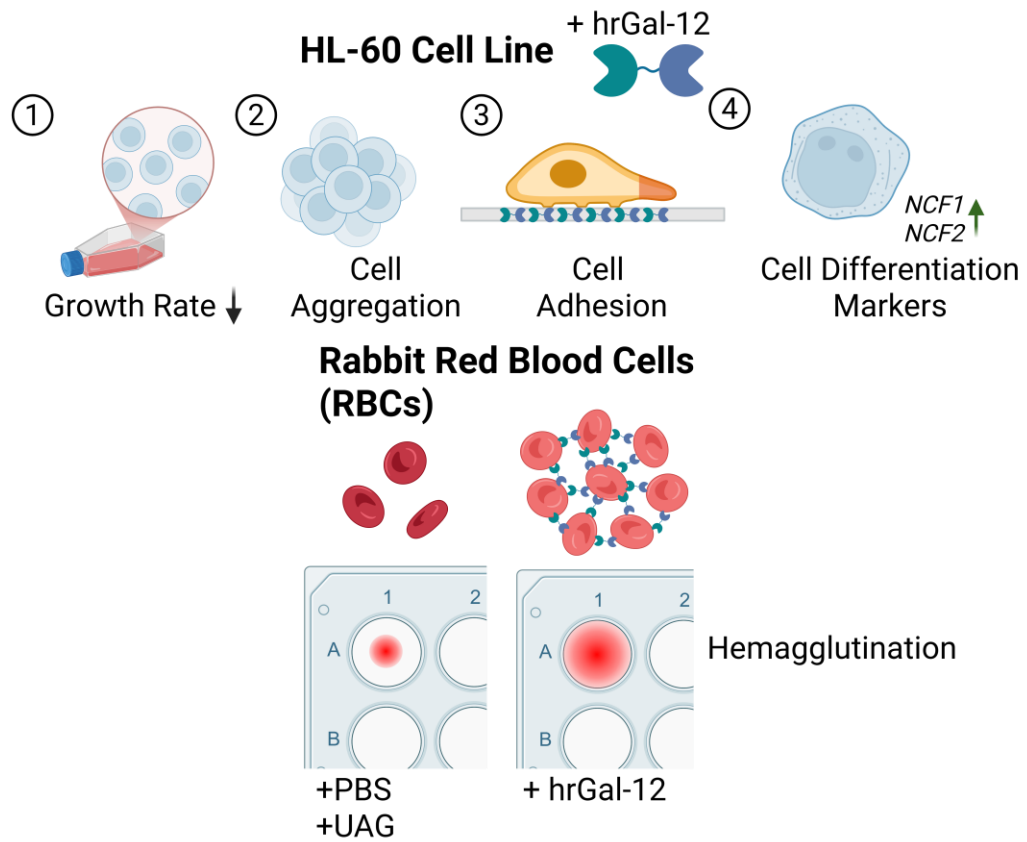


Figure 26. Biological effects of human recombinant galectin-12 on HL-60 cells and rabbit red blood cells. Figure was prepared in BioRender.

In this study, hrGal-12 was only soluble in buffers containing high concentrations of urea, arginine, and glutathione, whereas the P67-tagged N-terminal hrGal-12 was solubilized in phosphate-buffered saline (PBS). Most recombinant galectins can be solubilized using common dialysis and refolding buffers containing relatively low concentrations of reducing agents or detergents (Nishi, 2020; Prato et al., 2020). The hrGal-12 preparation generated in this work precipitated rapidly in PBS or water, likely due to exposure of hydrophobic surfaces that promote protein aggregation. These observations highlight the challenges associated with purifying full-length human galectin-12 and emphasize the importance of developing better strategies to stabilize aggregation-prone recombinant proteins during purification.

This study further suggests that extracellular hrGal-12 can bind to complex cell-surface glycans on both HL-60 cells and rabbit red blood cells. Currently, little is known about the biological role of extracellular or secreted galectin-12 (Popa et al., 2018). Although galectin-12 is primarily considered an intracellular protein, small amounts have been reported to be secreted via non-classical mechanisms, and this secretion is inhibited following neutrophilic differentiation of HL-60 cells (Tazhitdinova et al., 2024). The ability of exogenously added hrGal-12 to induce cell aggregation and hemagglutination in this study supports the possibility that extracellular galectin-12 may participate in cell–cell interactions under specific conditions.

Overall, this study reports a novel and reproducible method for the expression, purification, and refolding of active full-length human recombinant galectin-12. In addition, I demonstrate that exogenously added hrGal-12 can influence cellular differentiation-associated markers in HL-60 cells. Together, these findings establish recombinant human galectin-12 as a useful tool for studying galectin-12 biology and support a role for this protein in regulating cell proliferation, differentiation, and adhesion in myeloid cells.

4.3 Study limitations and future directions

My work provides an optimized purification approach for the purification of hrGal-12 and demonstrates its biological activity *in vitro*, including effects consistent with the induction of differentiation-associated markers in HL-60 cells. While galectin-12 has been proposed as a tumor suppressor gene, further studies using this preparation and more soluble formulations of hrGal-12 will be required to define its role in regulating cell proliferation and differentiation.

Although my preparation of hrGal-12 is active, the major hrGal-12 band was accompanied by degraded products, and further optimization may improve purity. Testing more columns and purification methods along with changing the plasmid itself are promising avenues to increase hrGal-12 purity, apart from the improvement I saw with SEC. Protease inhibitors in the lysis buffer and refolding buffer did not improve the purity or activity of hrGal-12 in this study. Expressing in alternate strains of *E. coli* like the Rosetta (DE3) and the use of terrific broth may further increase the yield and purity of hrGal-12.

Galectin-12 displays non-canonical glycan specificity, with a known preference for fucosylated glycans (Maller et al., 2020; Cagnoni et al., 2024). Based on this specificity, future work will be required to determine whether the hrGal-12-induced hemagglutination, aggregation, and adhesion observed in this study can be inhibited by previously identified for galectin-12, including 3'-fucosyllactose and 2'-fucosyllactose (Maller et al., 2020). Attempts to characterize hrGal-12 glycan binding using a glycan array were inconclusive, which may reflect instability of this hrGal-12 preparation under the assay conditions rather than an absence of glycan binding. Alternative approaches, including solid-phase carbohydrate binding assays previously used to characterize both mrGal-12 and hrGal-12, should therefore be applied to this preparation (Maller et al., 2020; Cagnoni et al., 2024). Notably, hrGal-12 immobilized on COSTAR plates retained the ability to induce cell adhesion, suggesting that the protein remains functionally active even without UAG buffer. This observation supports the feasibility of immobilized-protein assays for future galectin-12 glycan-binding studies. Quantitative approaches such as isothermal titration calorimetry, along with the hemagglutination and adhesion

assays used in this study, will be important next steps to test whether this preparation of hrGal-12 demonstrates specific glycan binding activity.

One limitation of the hrGal-12 preparation used in this study is that the composition of the UAG refolding buffer interferes with several light transmission–based assays. For example, treatment of HL-60 cells with UAG buffer alone altered light transmission in the SOLAR aggregometer, complicating interpretation of aggregation measurements. In addition, the high arginine concentration in UAG buffer introduces substantial noise in circular dichroism spectroscopy, preventing reliable secondary structure determination using this method. This is why I opted to use intrinsic fluorescence spectroscopy and chemical denaturation assays to assess hrGal-12 folding, although the precise structural state of the protein remains unknown.

While I tested many refolding buffers, a systematic large-scale solubility screen was not performed and may identify alternative buffer compositions that improve hrGal-12 stability and purity. Additional biophysical approaches could also be applied to further assess protein folding. Notably, *VPS13C* has been shown to be critical for galectin-12 stability in cells, raising the possibility that co-expression with *VPS13C* or molecular chaperones may enhance hrGal-12 solubility and stability during recombinant expression (Yang et al., 2016).

Another remaining question is whether hrGal-12 enters HL-60 cells following addition to the culture medium or functions exclusively through interactions with cell surface glycans. The mechanism by which galectin-12 is internalized or secreted by HL-60 cells has not yet been experimentally resolved. Fluorescent labeling approaches, such as fluorescein isothiocyanate conjugation, would enable quantitative measurement of intracellular hrGal-12.

To further characterize the HL-60 phenotype induced by hrGal-12, flow cytometric analysis with annexin V and 4,4-difluoro-4-bora-3a,4a-diaza-s-indacene staining should be performed following differentiation, as previously established for ATRA- and DMSO-treated HL-60 cells (Tazhitdinova et al., 2024). In addition, prior studies of neutrophil-like differentiation in HL-60 cells have measured hydrogen peroxide production to

confirm activation of the respiratory burst. Applying similar assays following PMA or fMLP stimulation of hrGal-12–treated HL-60 cells would provide functional insight into ROS generation. Finally, expanded qPCR analysis of lipogenic, lipolytic, cell-cycle, and immune receptor genes will be essential to define the molecular identity of the hrGal-12–induced differentiated phenotype.

Additionally, assessing my preparation of hrGal-12 in other human adipocyte, sebocyte, and cancer cell lines is of considerable interest. Based on prior studies implicating galectin-12 in lipid metabolism and differentiation in these cell types, hrGal-12 may, in theory, promote lipogenesis and differentiation in adipocytes and sebocytes. There is also a need for a high-resolution structure of galectin-12, which may be achievable through crystallography or solution NMR using the hrGal-12 preparation generated in this study. Another outstanding question is the full scope of galectin-12 protein–protein interactions and their biological significance. To date, perilipin-1 and VPS13C are among the best-characterized galectin-12 interacting proteins.

Overall, I show that full-length hexahistidine-tagged hrGal-12 can be purified from BL21(DE3) cells and remain active following refolding. This preparation is suitable for use in future cell biology studies. I demonstrate that hrGal-12 increases key differentiation-associated markers in HL-60 cells, suggesting that galectin-12 may contribute to myeloid differentiation.

References

- Abedin, M. J., Kashio, Y., Seki, M., Nakamura, K., & Hirashima, M. (2003). Potential roles of galectins in myeloid differentiation into three different lineages. *J Leukoc Biol*, *73*(5), 650–656.
- Almkvist, J., & Karlsson, A. (2002). Galectins as inflammatory mediators. *Glycoconj J*, *19*(7–9), 575–581.
- Amin, T., Amin, M. M., Adikari, A. A. D. I., Zheng, X., Ning, Y., & Wang, B. (2025). Clinical evidence and mechanistic pathways of human milk oligosaccharide supplementation for health benefits: An updated review. *Front Nutr*, *12*, 1599678.
- Assem, M., El-Araby, R. E., Al-Karmalawy, A. A., Nabil, R., Kamal, M. A. M., Belal, A., Ghamry, H. I., Abourehab, M. A. S., Ghoneim, M. M., Alshahrani, M. Y., & El Leithy, A. A. (2023). Promoter methylation might shift the balance of Galectin-3 & 12 expression in de novo adult acute myeloid leukemia patients. *Front Genet*, *14*, 1122864.
- Basit, H., Tan, M. L., & Webster, D. R. (2025). Histology, Kupffer cell. In *StatPearls*. StatPearls Publishing.
- Baum, L. G. (2011). Burn control, an adipocyte-specific function for galectin-12. *Proc Natl Acad Sci USA*, *108*(46), 18575–18576.
- Baxter, S. S., Carlson, L. A., Mayer, A. M. S., Hall, M. L., & Fay, M. J. (2009). Granulocytic differentiation of HL-60 promyelocytic leukemia cells is associated with increased expression of Cul5. *In Vitro Cell Dev Biol Anim*, *45*(5–6), 264–274.
- Benvenuto, E., Broer, I., D'Aoust, M.-A., Hitzeroth, I., Hundleby, P., Menassa, R., Oksman-Caldentey, K.-M., Peyret, H., Salgueiro, S., Saxena, P., Stander, J., Warzecha, H., & Ma, J. (2023). Plant molecular farming in the wake of the closure of Medicago Inc. *Nat Biotechnol*, *41*(7), 893–894.

- Bhakta, S. B., Lundgren, S. M., Sesti, B. N., Flores, B. A., Akdogan, E., Collins, S. R., & Mercer, F. (2024). Neutrophil-like cells derived from the HL-60 cell-line as a genetically-tractable model for neutrophil degranulation. *PLoS One*, *19*(2), e0297758.
- Böhler, T., & Linderkamp, O. (1993). Effects of neuraminidase and trypsin on surface charge and aggregation of red blood cells. *Clin Hemorheol Microcirc*, *13*(6), 775–778.
- Buchanan, S. K. (1999). β -Barrel proteins from bacterial outer membranes: Structure, function and refolding. *Curr Opin Struct Biol*, *9*(4), 455–461.
- Burda, I., & Roeder, A. H. K. (2022). Stepping on the molecular brake: Slowing down proliferation to allow differentiation. *Dev Cell*, *57*(5), 561–563.
- Burnett, M. J. B., & Burnett, A. C. (2020). Therapeutic recombinant protein production in plants: Challenges and opportunities. *Plants, People, Planet*, *2*(2), 121–132.
- Buscajoni, L., Martinetz, M. C., Berkemeyer, M., & Brocard, C. (2022). Refolding in the modern biopharmaceutical industry. *Biotechnol Adv*, *61*, 108050.
- Cagnoni, A. J., Massaro, M., Cutine, A. M., Gimeno, A., Pérez-Sáez, J. M., Manselle Cocco, M. N., Maller, S. M., Di Lella, S., Jiménez-Barbero, J., Ardá, A., Rabinovich, G. A., & Mariño, K. V. (2024). Exploring galectin interactions with human milk oligosaccharides and blood group antigens identifies BGA6 as a functional galectin-4 ligand. *J Biol Chem*, *300*(8), 107573.
- Cao, Z.-Q., & Guo, X.-L. (2016). The role of galectin-4 in physiology and diseases. *Protein Cell*, *7*(5), 314–324.
- Celie, P. H., Parret, A. H., & Perrakis, A. (2016). Recombinant cloning strategies for protein expression. *Curr Opin Struct Biol*, *38*, 145–154.
- Collins, S. (1987). The HL-60 promyelocytic leukemia cell line: Proliferation, differentiation, and cellular oncogene expression. *Blood*, *70*(5), 1233–1244.

- El Leithy, A. A., Helwa, R., Assem, M. M., & Hassan, N. H. A. (2015). Expression profiling of cancer-related galectins in acute myeloid leukemia. *Tumour Biol*, *36*(10), 7929–7939.
- Farhad, M., Rolig, A. S., & Redmond, W. L. (2018). The role of Galectin-3 in modulating tumor growth and immunosuppression within the tumor microenvironment. *Oncoimmunology*, *7*(6), e1434467.
- Fasshauer, M., Klein, J., Lossner, U., & Paschke, R. (2002). Negative regulation of adipose-expressed galectin-12 by isoproterenol, tumor necrosis factor alpha, insulin and dexamethasone. *Eur J Endocrinol*, *147*(4), 553–559.
- Faust, K., Freitag, N., Barrientos, G., Hartel, C., & Blois, S. M. (2021). Galectin-levels are elevated in infants born preterm due to amniotic infection and rapidly decline in the neonatal period. *Front Immunol*, *11*, 599104.
- Fekete, S., Beck, A., Veuthey, J.-L., & Guillaume, D. (2014). Theory and practice of size exclusion chromatography for the analysis of protein aggregates. *J Pharm Biomed Anal*, *101*, 161–173.
- Feller, S. M., & Lewitzky, M. (2012). Very “sticky” proteins—not too sticky after all? *Cell Commun Signal*, *10*(1), 15.
- Fryk, E., Silva, V. R. R., & Jansson, P.-A. (2022). Galectin-1 in obesity and type 2 diabetes. *Metabolites*, *12*(10), 930.
- Gasson, R., Roper, J. A., & Slack, R. J. (2024). A quantitative human red blood cell agglutination assay for characterization of galectin inhibitors. *Int J Mol Sci*, *25*(12), 6756.
- Gopalan, V., Saremi, N., Sullivan, E., Kabir, S., Lu, C.-T., Salajegheh, A., Leung, M., Smith, R. A., & Lam, A. K. (2016). The expression profiles of the galectin gene family in colorectal adenocarcinomas. *Hum Pathol*, *53*, 105–113.

- Gorudko, I. V., Buko, I. V., Cherenkevich, S. N., Polonetsky, L. Z., & Timoshenko, A. V. (2008). Lectin-induced aggregates of blood cells from patients with acute coronary syndromes. *Arch Med Res*, *39*(7), 674–681.
- Grabner, G. F., Xie, H., Schweiger, M., & Zechner, R. (2021). Lipolysis: Cellular mechanisms for lipid mobilization from fat stores. *Nat Metab*, *3*(11), 1445–1465.
- Günther, J., & Galuska, S. P. (2023). A brief history of galectin evolution. *Front Immunol*, *14*, 1147356.
- Harrison, W. J., Bull, J. J., Seltmann, H., Zouboulis, C. C., & Philpott, M. P. (2007). Expression of lipogenic factors galectin-12, resistin, SREBP-1, and SCD in human sebaceous glands and cultured sebocytes. *J Invest Dermatol*, *127*(6), 1309–1317.
- Hermenean, A., Oatis, D., Herman, H., Ciceu, A., D'Amico, G., & Trotta, M. C. (2022). Galectin-1 a key player between tissue repair and fibrosis. *Int J Mol Sci*, *23*(10), 5548.
- Hotta, K., Funahashi, T., Matsukawa, Y., Takahashi, M., Nishizawa, H., Kishida, K., Matsuda, M., Kuriyama, H., Kihara, S., Nakamura, T., Tochino, Y., Bodkin, N. L., Hansen, B. C., & Matsuzawa, Y. (2001). Galectin-12, an adipose-expressed galectin-like molecule possessing apoptosis-inducing activity. *J Biol Chem*, *276*(36), 34089–34097.
- Hsu, Y.-A., Kuo, Y.-H., Chen, C.-S., Chen, Y.-C., Huang, C.-C., Chang, C.-Y., Lin, C.-J., Lin, C.-W., Lin, H.-J., Liu, F.-T., & Wan, L. (2018). Galectin-12 is involved in corn silk-induced anti-adipogenesis and anti-obesity effects. *Am J Chin Med*, *46*(5), 1045–1063.
- Huang, Y., Wang, H.-C., Zhao, J., Wu, M.-H., & Shih, T.-C. (2021). Immunosuppressive roles of galectin-1 in the tumor microenvironment. *Biomolecules*, *11*(10), 1398.
- Jacob, R., & Gorek, L.-S. (2024). Intracellular galectin interactions in health and disease. *Semin Immunopathol*, *46*(1), 4.
- Jiang, J., Tu, H., & Li, P. (2022). Lipid metabolism and neutrophil function. *Cell Immunol*, *377*, 104546.

- Johnson, I. S. (1983). Human insulin from recombinant dna technology. *Science*, *219*(4585), 632–637.
- Kageshita, T., Kashio, Y., Yamauchi, A., Seki, M., Abedin, M. J., Nishi, N., Shoji, H., Nakamura, T., Ono, T., & Hirashima, M. (2002). Possible role of galectin-9 in cell aggregation and apoptosis of human melanoma cell lines and its clinical significance. *Int J Cancer*, *99*(6), 809–816.
- Kamili, N. A., & Stowell, S. R. (2016). Editorial: Feel the burn: blocking galectin-12 helps leukemic cells differentiate while staying lean. *J Leukoc Biol*, *100*(4), 640–642.
- Kathiriya, J. J., Nakra, N., Nixon, J., Patel, P. S., Vaghasiya, V., Alhassani, A., Tian, Z., Allen-Gipson, D., & Davé, V. (2017). Galectin-1 inhibition attenuates profibrotic signaling in hypoxia-induced pulmonary fibrosis. *Cell Death Discov*, *3*(1), 17010.
- Katzenmaier, E.-M., André, S., Kopitz, J., & Gabius, H.-J. (2014). Impact of sodium butyrate on the network of adhesion/growth-regulatory galectins in human colon cancer in vitro. *Anticancer Res*, *34*(10), 5429–5438.
- Katzenmaier, E.-M., Kloor, M., Gabius, H.-J., Gebert, J., & Kopitz, J. (2017). Analyzing epigenetic control of galectin expression indicates silencing of galectin-12 by promoter methylation in colorectal cancer. *IUBMB Life*, *69*(12), 962–970.
- Katzenmaier, E.-M., Fuchs, V., Warnken, U., Schnölzer, M., Gebert, J., & Kopitz, J. (2019). Deciphering the galectin-12 protein interactome reveals a major impact of galectin-12 on glutamine anaplerosis in colon cancer cells. *Exp Cell Res*, *379*(2), 129–139.
- Kodaira, Y., Kusumoto, T., Takahashi, T., Matsumura, Y., Miyagi, Y., Okamoto, K., Shidoji, Y., & Sagami, H. (2007). Formation of lipid droplets induced by 2,3-dihydrogeranylgeranoic acid distinct from geranylgeranoic acid. *Acta Biochim Pol*, *54*(4), 777–782.
- Kwiatkowska, J., Stein, E., Romanenko, A., Plens-Gałąska, M., Podsiadła-Białoskórska, M., Szołajska, E., Kühn, U., & Kamieniarz-Gdula, K. (2025). A beginners guide to Sf9 and Sf21 insect cell line culture and troubleshooting. *Sci Rep*, *15*(1), 19907.

- Kyte, J., & Doolittle, R. F. (1982). A simple method for displaying the hydropathic character of a protein. *J Mol Biol*, *157*(1), 105–132.
- Labrou, N. E. (2021). Protein purification technologies. In N. E. Labrou (Ed.), *Protein Downstream Processing: Design, Development, and Application of High and Low-Resolution Methods* (pp. 3–10). Springer US.
- Lee, H., Horbath, A., Kondiparthi, L., Meena, J. K., Lei, G., Dasgupta, S., Liu, X., Zhuang, L., Koppula, P., Li, M., Mahmud, I., Wei, B., Lorenzi, P. L., Keyomarsi, K., Poyurovsky, M. V., Olszewski, K., & Gan, B. (2024). Cell cycle arrest induces lipid droplet formation and confers ferroptosis resistance. *Nat Commun*, *15*(1), 79.
- Lee, J.-L., Wang, Y.-C., Hsu, Y.-A., Chen, C.-S., Weng, R.-C., Lu, Y.-P., Chuang, C.-Y., & Wan, L. (2023). Galectin-12 modulates Kupffer cell polarization to alter the progression of nonalcoholic fatty liver disease. *Glycobiology*, *33*(8), 673–682.
- Lee, Y.-R., Shim, H.-J., Yu, H.-N., Song, E.-K., Park, J., Kwon, K.-B., Park, J.-W., Rho, H.-W., Park, B.-H., Han, M.-K., & Kim, J.-S. (2005). Dimethylsulfoxide induces upregulation of tumor suppressor protein PTEN through nuclear factor- κ B activation in HL-60 cells. *Leuk Res*, *29*(4), 401–405.
- Leffler, H. (2018). Galectin history, some stories, and some outstanding questions. *Trends Glycosci Glycotechnol*, *30*(172), SE129–SE135.
- Lerro, K. A., Orlando, R., Zhang, H. Z., Usherwood, P. N. R., & Nakanishi, K. (1993). Separation of the sticky peptides from membrane proteins by high-performance liquid chromatography in a normal-phase system. *Anal Biochem*, *215*(1), 38–44.
- Lin, E.-S., Hsu, Y.-A., Chang, C.-Y., Lin, H.-J., Chen, C. S., & Wan, L. (2020). Ablation of galectin-12 inhibits atherosclerosis through enhancement of m2 macrophage polarization. *Int J Mol Sci*, *21*(15), Article 15.
- Lin, T.-W., Chang, H.-T., Chen, C.-H., Chen, C.-H., Lin, S.-W., Hsu, T.-L., & Wong, C.-H. (2015). Galectin-3 binding protein and galectin-1 interaction in breast cancer cell aggregation and metastasis. *J Am Chem Soc*, *137*(30), 9685–9693.

- Lin, F.-J., Huang, Y.-H., Tsao, C.-H., Hsieh, W.-C., Lo, Y.-H., Zouboulis, C. C., Chen, H.-L., & Liu, F.-T. (2023). Galectin-12 regulates immune responses in the skin through sebaceous glands. *J Invest Dermatol*, *143*(11), 2120-2131.e7.
- Liu, F.-T., & Rabinovich, G. A. (2005). Galectins as modulators of tumour progression. *Nat Rev Cancer*, *5*(1), 29–41.
- Liu, F.-T., & Stowell, S. R. (2023). The role of galectins in immunity and infection. *Nat Rev Immunol*, *23*(8), 505–517.
- Mahalingaiah, P. K., Palenski, T., & Van Vleet, T. R. (2018). An *in vitro* model of hematotoxicity: Differentiation of bone marrow–derived stem/progenitor cells into hematopoietic lineages and evaluation of lineage-specific hematotoxicity. *Curr Protoc Toxicol*, *76*(1), e45.
- Majka, S. M., Fox, K. E., Psilas, J. C., Helm, K. M., Childs, C. R., Acosta, A. S., Janssen, R. C., Friedman, J. E., Woessner, B. T., Shade, T. R., Varella-Garcia, M., & Klemm, D. J. (2010). De novo generation of white adipocytes from the myeloid lineage via mesenchymal intermediates is age, adipose depot, and gender specific. *Proc Natl Acad Sci USA*, *107*(33), 14781–14786.
- Maller, S. M., Cagnoni, A. J., Bannoud, N., Sigaut, L., Pérez Sáez, J. M., Pietrasanta, L. I., Yang, R., Liu, F., Croci, D. O., Di Lella, S., Sundblad, V., Rabinovich, G. A., & Mariño, K. V. (2020). An adipose tissue galectin controls endothelial cell function via preferential recognition of 3-fucosylated glycans. *FASEB J*, *34*(1), 735–753.
- McCue, J. T. (2009). Chapter 25 Theory and use of hydrophobic interaction chromatography in protein purification applications. In *Methods Enzymol* (Vol. 463, pp. 405–414). Elsevier.
- McTague, A., Tazhitdinova, R., and Timoshenko, A. V. (2022). O-GlcNAc-mediated regulation of galectin expression and secretion in human promyelocytic HL-60 cells undergoing neutrophilic differentiation. *Biomolecules*, *12*, 1763.
- Melo, R. C. N., & Weller, P. F. (2016). Lipid droplets in leukocytes: Organelles linked to inflammatory responses. *Exp Cell Res*, *340*(2), 193–197.

- Menendez, J. A., & Lupu, R. (2007). Fatty acid synthase and the lipogenic phenotype in cancer pathogenesis. *Nat Rev Cancer*, 7(10), 763–777.
- Modenutti, C. P., Capurro, J. I. B., Di Lella, S., & Martí, M. A. (2019). The structural biology of galectin-ligand recognition: Current advances in modeling tools, protein engineering, and inhibitor design. *Front Chem*, 7, 823.
- Morimoto, D., & Walinda, E. (2024). A fast and simple automated multi-step protein purification method for ÄKTA go systems. *Protein Expr Purif*, 223, 106560.
- Mukherjee, R., Kim, S. W., Park, T., Choi, M. S., & Yun, J. W. (2015). Targeted inhibition of galectin 1 by thiodigalactoside dramatically reduces body weight gain in diet-induced obese rats. *Int J Obes (Lond)*, 39(9), 1349–1358.
- Murby, M., Uhlén, M., & Ståhl, S. (1996). Upstream strategies to minimize proteolytic degradation upon recombinant production in *Escherichia coli*. *Protein Expr Purif*, 7(2), 129–136.
- Nagae, M., Nishi, N., Nakamura-Tsuruta, S., Hirabayashi, J., Wakatsuki, S., & Kato, R. (2008). Structural analysis of the human galectin-9 n-terminal carbohydrate recognition domain reveals unexpected properties that differ from the mouse orthologue. *J Mol Biol*, 375(1), 119–135.
- Nehmé, R., & St-Pierre, Y. (2023). Targeting intracellular galectins for cancer treatment. *Front Immunol*, 14, 1269391.
- Ng, Y. K., & Konermann, L. (2024). Mechanism of protein aggregation inhibition by arginine: Blockage of anionic side chains favors unproductive encounter complexes. *J Am Chem Soc*, 146(12), 8394–8406.
- Nishi, N., Shoji, H., Seki, M., Itoh, A., Miyanaka, H., Yuube, K., Hirashima, M., & Nakamura, T. (2003). Galectin-8 modulates neutrophil function via interaction with integrin M. *Glycobiology*, 13(11), 755–763.

- Nishi, N. (2020). A note on expression and purification of recombinant galectins. *Glycoforum*, 23, A15.
- Nose, F., Yamaguchi, T., Kato, R., Aiuchi, T., Obama, T., Hara, S., Yamamoto, M., & Itabe, H. (2013). Crucial role of perilipin-3 (TIP47) in formation of lipid droplets and PGE2 production in HL-60-derived neutrophils. *PLoS One*, 8(8), e71542.
- Olins, A. L., & Olins, D. E. (2004). Cytoskeletal influences on nuclear shape in granulocytic HL-60 cells. *BMC Cell Biol*, 5, 30.
- Pace, K. E., Hahn, H. P., & Baum, L. G. (2003). Preparation of recombinant human galectin-1 and use in t-cell death assays. In *Methods Enzymol* (Vol. 363, pp. 499–518). Elsevier.
- Perez-Moreno, E., Oyanadel, C., de la Peña, A., Hernández, R., Pérez-Molina, F., Metz, C., González, A., & Soza, A. (2024). Galectins in epithelial-mesenchymal transition: Roles and mechanisms contributing to tissue repair, fibrosis, and cancer metastasis. *Biol Res*, 57, 14.
- Perillo, N. L., Pace, K. E., Seilhamer, J. J., & Baum, L. G. (1995). Apoptosis of T cells mediated by galectin-1. *Nature*, 378(6558), 736–739.
- Popa, S. J., Stewart, S. E., & Moreau, K. (2018). Unconventional secretion of annexins and galectins. *Semin Cell Dev Biol*, 83, 42–50.
- Popot, J.-L. (2014). Folding membrane proteins in vitro: A table and some comments. *Arch Biochem Biophys*, 564, 314–326.
- Prato, C. A., Carabelli, J., Cattaneo, V., Campetella, O., & Tribulatti, M. V. (2020). Purification of recombinant galectins expressed in bacteria. *STAR Protoc*, 1(3), 100204.
- Ribatti, D., Tamma, R., & Annesse, T. (2020). Epithelial-mesenchymal transition in cancer: A historical overview. *Transl Oncol*, 13(6), 100773.
- Riggs, P. D. (2018). Overview of protein expression vectors for *E. coli*. *Curr Protoc Essential Lab Tech*, 17(1), e23.

- Rio-Aige, K., Girbal, M., Selma-Royo, M., Parra-Llorca, A., González, S., Martínez-Costa, C., Castell, M., Collado, M. C., Pérez-Cano, F. J., & Rodríguez-Lagunas, M. J. (2022). Galectins-1, -3 and -9 are present in breast milk and have a role in early life development. *Nutrients*, *14*(20), 4338.
- Robinson, B. S., Arthur, C. M., Evavold, B., Roback, E., Kamili, N. A., Stowell, C. S., Vallecillo-Zúniga, M. L., Van Ry, P. M., Dias-Baruffi, M., Cummings, R. D., & Stowell, S. R. (2019). The sweet-side of leukocytes: Galectins as master regulators of neutrophil function. *Front Immunol*, *10*, 1763.
- Rosano, G. L., & Ceccarelli, E. A. (2014). Recombinant protein expression in *Escherichia coli*: Advances and challenges. *Front Microbiol*, *5*, 172.
- Roufarshbaf, M., & Akbari, V. (2023). Development of Solubilization and Refolding Buffers. In J. Kopp & O. Spadiut (Eds.), *Inclusion Bodies* (Vol. 2617, pp. 155–164). Springer US.
- Royster, A., Mir, S., & Mir, M. A. (2021). A novel approach for the purification of aggregation prone proteins. *PLoS ONE*, *16*(11), e0260143.
- Ryan, B. J., & Henahan, G. T. (2017). Avoiding proteolysis during protein purification. In D. Walls & S. T. Loughran (Eds.), *Protein Chromatography: Methods and Protocols* (pp. 53–69). Springer.
- Samuel, T. M., Binia, A., de Castro, C. A., Thakkar, S. K., Billeaud, C., Agosti, M., Al-Jashi, I., Costeira, M. J., Marchini, G., Martínez-Costa, C., Picaud, J.-C., Stiris, T., Stoicescu, S.-M., Vanpeé, M., Domellöf, M., Austin, S., & Sprenger, N. (2019). Impact of maternal characteristics on human milk oligosaccharide composition over the first 4 months of lactation in a cohort of healthy European mothers. *Sci Rep*, *9*(1), 11767.
- Shamova, E. V., Gorudko, I. V., Drozd, E. S., Chizhik, S. A., Martinovich, G. G., Cherenkevich, S. N., & Timoshenko, A. V. (2011). Redox regulation of morphology, cell stiffness, and lectin-induced aggregation of human platelets. *Eur Biophys J*, *40*(2), 195–208.
- Sharma, R., Anupa, A., Kateja, N., & Rathore, A. S. (2022). Optimization of the in-vitro refolding of biotherapeutic Fab Ranibizumab. *Biochem Eng J*, *187*, 108601.

- Sherazi, A. A., Jariwala, K. A., Cybulski, A. N., Lewis, J. W., Karagiannis, J., Cumming, R. C., & Timoshenko, A. V. (2018). Effects of global O-GlcNAcylation on galectin gene-expression profiles in human cancer cell lines. *Anticancer Res*, *38*(12), 6691–6697.
- Smets, L. A., & Van Beek, W. P. (1984). Carbohydrates of the tumor cell surface. *Biochim Biophys Acta*, *738*(4), 237–249.
- Tallman, M. S., Andersen, J. W., Schiffer, C. A., Appelbaum, F. R., Feusner, J. H., Ogden, A., Shepherd, L., Willman, C., Bloomfield, C. D., Rowe, J. M., & Wiernik, P. H. (1997). All-trans-retinoic acid in acute promyelocytic leukemia. *N Engl J Med*, *337*(15), 1021–1028.
- Tasseff, R., Jensen, H. A., Congleton, J., Dai, D., Rogers, K. V., Sagar, A., Bunaciu, R. P., Yen, A., & Varner, J. D. (2017). An effective model of the retinoic acid induced HL-60 differentiation program. *Sci Rep*, *7*(1), 14327.
- Tazhitdinova, R., & Timoshenko, A. V. (2020). The emerging role of galectins and O-GlcNAc homeostasis in processes of cellular differentiation. *Cells*, *9*(8), 1792.
- Tazhitdinova, R. (2023). Role and regulation of galectin-12 in the context of cellular differentiation (Master's thesis, Western University). Western University Electronic Thesis and Dissertation Repository.
- Tazhitdinova, R., Cristiano, S., Yi, J., Zhurov, V., DeKoter, R. P., & Timoshenko, A. V. (2024). Expression and secretion of galectin-12 in the context of neutrophilic differentiation of human promyeloblastic HL-60 cells. *J Cell Physiol*, *239*(6), e31288.
- Teichberg, V. I., Silman, I., Beitsch, D. D., & Resheff, G. (1975). A beta-D-galactoside binding protein from electric organ tissue of *Electrophorus electricus*. *Proc Natl Acad Sci USA*, *72*(4), 1383–1387.
- Thijssen, V. L. J. L., Postel, R., Brandwijk, R. J. M. G. E., Dings, R. P. M., Nesmelova, I., Satijn, S., Verhofstad, N., Nakabeppu, Y., Baum, L. G., Bakkers, J., Mayo, K. H., Poirier, F., & Griffioen, A. W. (2006). Galectin-1 is essential in tumor angiogenesis and is a target for antiangiogenesis therapy. *Proc Natl Acad Sci USA*, *103*(43), 15975–15980.

- Thurston, T. L. M., Wandel, M. P., von Muhlinen, N., Foeglein, Á., & Randow, F. (2012). Galectin-8 targets damaged vesicles for autophagy to defend cells against bacterial invasion. *Nature*, *482*(7385), 414–418.
- Tihanyi, B., & Nyitray, L. (2020). Recent advances in CHO cell line development for recombinant protein production. *Drug Discov Today Technol*, *38*, 25–34.
- Timoshenko, A. V., Lanteigne, J., & Kozak, K. (2016). Extracellular stress stimuli alter galectin expression profiles and adhesion characteristics of HL-60 cells. *Mol Cell Biochem*, *413*(1), 137–143.
- Tindall, B., Demircioglu, D., & Uhlig, T. (2021). Recombinant bacterial endotoxin testing: A proven solution. *BioTechniques*, *70*(5), 290–300.
- Tsao, C.-H., Hsieh, W.-C., Yang, R.-Y., Lo, Y.-H., Tu, T.-J., Ke, L.-Y., Zouboulis, C. C., & Liu, F.-T. (2022). Galectin-12 modulates sebocyte proliferation and cell cycle progression by regulating cyclin A1 and CDK2. *Glycobiology*, *32*(1), 73–82.
- Tsao, C.-H., Hsieh, W.-C., Lin, F.-J., Yang, R.-Y., Chang, M.-T., Apaya, M. K., Shyur, L.-F., Ke, L.-Y., Zouboulis, C. C., & Liu, F.-T. (2023). The critical role of galectin-12 in modulating lipid metabolism in sebaceous glands. *J Invest Dermatol*, *143*(6), 913-924.e4.
- Tsao, C.-H., Hsieh, W.-C., Lin, F.-J., Liu, F.-T., & Yang, R.-Y. (2025). Galectin-12 in the regulation of sebocyte proliferation, lipid metabolism, and immune responses. *Biomolecules*, *15*(6), 837.
- Van Beek, W. P., Smets, L. A., & Emmelot, P. (1975). Changed surface glycoprotein as a marker of malignancy in human leukaemic cells. *Nature*, *253*(5491), 457–460.
- Vincentelli, R., Canaan, S., Campanacci, V., Valencia, C., Maurin, D., Frassinetti, F., Scappucini-Calvo, L., Bourne, Y., Cambillau, C., & Bignon, C. (2004). High-throughput automated refolding screening of inclusion bodies. *Protein Sci*, *13*(10), 2782–2792.

- Vinnai, J. R., Cumming, R. C., Thompson, G. J., & Timoshenko, A. V. (2017). The association between oxidative stress-induced galectins and differentiation of human promyelocytic HL-60 cells. *Exp Cell Res*, *355*(2), 113–123.
- Wan, L., Lin, H.-J., Huang, C.-C., Chen, Y.-C., Hsu, Y.-A., Lin, C.-H., Lin, H.-C., Chang, C.-Y., Huang, S.-H., Lin, J.-M., & Liu, F.-T. (2016). Galectin-12 enhances inflammation by promoting M1 polarization of macrophages and reduces insulin sensitivity in adipocytes. *Glycobiology*, *26*(7), 732–744.
- Wan, L., Yang, R.-Y., & Liu, F.-T. (2018). Galectin-12 in cellular differentiation, apoptosis and polarization. *Int J Mol Sci*, *19*(1), 176.
- Wang, Q. M., Jones, J. B., & Studzinski, G. P. (1996). Cyclin-dependent kinase inhibitor p27 as a mediator of the G1-S phase block induced by 1,25-dihydroxyvitamin D3 in HL-60 cells. *Cancer Res*, *56*(2), 264–267.
- Wang, X., Qiu, L., Li, Z., Wang, X.-Y., & Yi, H. (2018). Understanding the multifaceted role of neutrophils in cancer and autoimmune diseases. *Front Immunol*, *9*, 2456.
- Wdowiak, K., Francuz, T., Gallego-Colon, E., Ruiz-Agamez, N., Kubeczko, M., Grochoła, I., & Wojnar, J. (2018). Galectin targeted therapy in oncology: Current knowledge and perspectives. *Int J Mol Sci*, *19*(1), 210.
- Weller, P. F., Ackerman, S. J., Nicholson-Weller, A., & Dvorak, A. M. (1989). Cytoplasmic lipid bodies of human neutrophilic leukocytes. *Am J Pathol*, *135*(5), 947–959.
- Wingfield, P. T. (2015). Overview of the purification of recombinant proteins. *Curr Protoc Protein Sci*, *80*(1), 6.1.1-6.1.35.
- Wu, W., Yin, Y., Huang, J., Yang, R., Li, Q., Pan, J., & Zhang, J. (2024). CRISPR/Cas9-mediated gene knockout in pigs proves that *LGALS12* deficiency suppresses the proliferation and differentiation of porcine adipocytes. *Biochim Biophys Acta Mol Cell Biol Lipids*, *1869*(3), 159424.

- Xue, H., Yang, R.-Y., Tai, G., & Liu, F.-T. (2016). Galectin-12 inhibits granulocytic differentiation of human NB4 promyelocytic leukemia cells while promoting lipogenesis. *J Leukoc Biol*, *100*(4), 657–664.
- Yamaguchi, H., & Miyazaki, M. (2014). Refolding techniques for recovering biologically active recombinant proteins from inclusion bodies. *Biomolecules*, *4*(1), 235–251.
- Yang, R. Y., Hsu, D. K., & Liu, F. T. (1996). Expression of galectin-3 modulates T-cell growth and apoptosis. *Proc Natl Acad Sci USA*, *93*(13), 6737–6742.
- Yang, R.-Y., Hsu, D. K., Yu, L., Ni, J., & Liu, F.-T. (2001). Cell cycle regulation by galectin-12, a new member of the galectin superfamily. *J Biol Chem*, *276*(23), 20252–20260.
- Yang, R.-Y., Hsu, D. K., Yu, L., Chen, H.-Y., & Liu, F.-T. (2004). Galectin-12 is required for adipogenic signaling and adipocyte differentiation. *J Biol Chem*, *279*(28), 29761–29766.
- Yang, R.-Y., Hsu, D., & Liu, F.-T. (2005). *Reducing galectin-12 activity to reduce formation of adipocytes* (United States Patent No. US20050250123A1).
- Yang, R.-Y., Yu, L., Graham, J. L., Hsu, D. K., Lloyd, K. C. K., Havel, P. J., & Liu, F.-T. (2011). Ablation of a galectin preferentially expressed in adipocytes increases lipolysis, reduces adiposity, and improves insulin sensitivity in mice. *Proc Natl Acad Sci USA*, *108*(46), 18696–18701.
- Yang, R.-Y., Havel, P. J., & Liu, F.-T. (2012). Galectin-12: A protein associated with lipid droplets that regulates lipid metabolism and energy balance. *Adipocyte*, *1*(2), 96–100.
- Yang, R.-Y., Xue, H., Yu, L., Velayos-Baeza, A., Monaco, A. P., & Liu, F.-T. (2016). Identification of VPS13C as a galectin-12-binding protein that regulates galectin-12 protein stability and adipogenesis. *PLoS ONE*, *11*(4), e0153534.
- Yang, R., Sun, L., Li, C.-F., Wang, Y.-H., Yao, J., Li, H., Yan, M., Chang, W.-C., Hsu, J.-M., Cha, J.-H., Hsu, J. L., Chou, C.-W., Sun, X., Deng, Y., Chou, C.-K., Yu, D., & Hung, M.-C. (2021). Galectin-9 interacts with PD-1 and TIM-3 to regulate T cell death and is a target for cancer immunotherapy. *Nat Commun*, *12*(1), 832.

- Yen, C.-L. E., Stone, S. J., Koliwad, S., Harris, C., & Farese, R. V. (2008). DGAT enzymes and triacylglycerol biosynthesis. *J Lipid Res*, *49*(11), 2283–2301.
- Yoo, H. C., Yu, Y. C., Sung, Y., & Han, J. M. (2020). Glutamine reliance in cell metabolism. *Exp Mol Med*, *52*(9), 1496–1516.
- Yunna, C., Mengru, H., Lei, W., & Weidong, C. (2020). Macrophage M1/M2 polarization. *Eur J Pharmacol*, *877*, 173090.
- Zeng, M. Y., Miralda, I., Armstrong, C. L., Uriarte, S. M., & Bagaitkar, J. (2019). The roles of NADPH oxidase in modulating neutrophil effector responses. *Mol Oral Microbiol*, *34*(2), 27–38.
- Zhang, B., Wang, T., Ni, S., Zong, Y., Wang, N., Si, Y., & Li, Y. (2025). A refolding tag for purifying bioactive recombinant proteins from *E. coli* inclusion bodies. *Int J Biol Macromol*, *322*, 146981.
- Zhang, D., Shen, L., Wu, W., Liu, K., & Zhang, J. (2022). Cloning and functional verification of a porcine adipose tissue-specific promoter. *BMC Genomics*, *23*(1), 394.
- Zhang, T., Zheng, Y., Zhao, D., Yan, J., Sun, C., Zhou, Y., & Tai, G. (2016). Multiple approaches to assess pectin binding to galectin-3. *Int J Biol Macromol*, *91*, 994–1001.
- Zick, Y., Eisenstein, M., Goren, R. A., Hadari, Y. R., Levy, Y., & Ronen, D. (2002). Role of galectin-8 as a modulator of cell adhesion and cell growth. *Glycoconj J*, *19*(7), 517–526.

Appendices

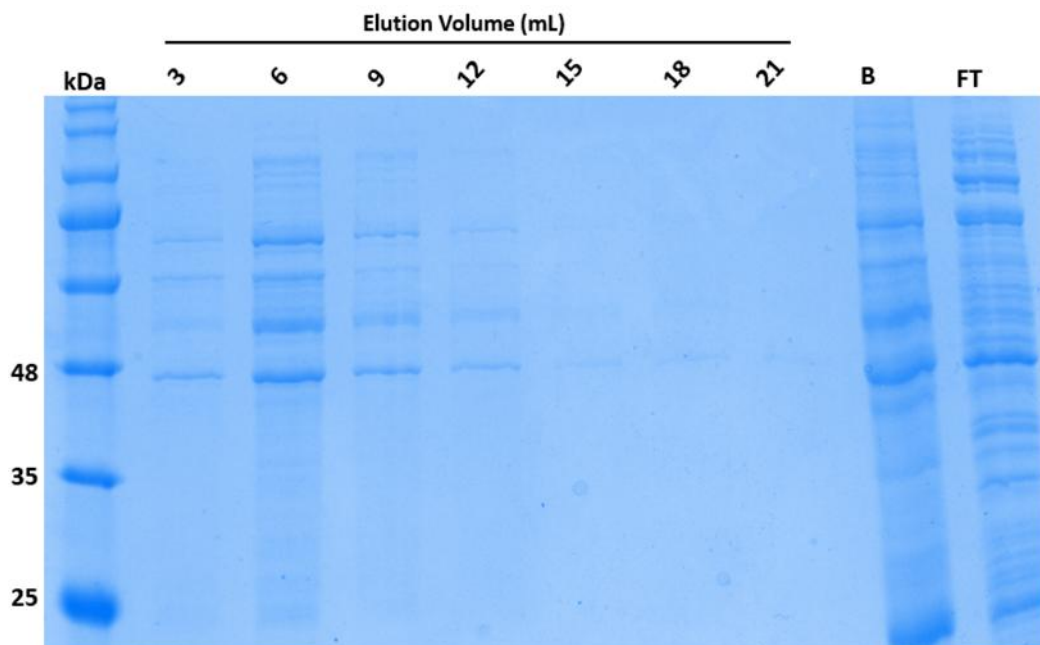


Figure S1. SDS-PAGE of hrGal-12 BL21(DE3) lysates purified under non-denaturing conditions with Ni-NTA beads. Elution fractions show no hrGal-12 at expected size of 35 kDa. Beads (B) and flowthrough (FT) also included. hrGal-12 is soluble in a specialized urea, arginine, glutathione, and disodium phosphate (UAG) buffer. 15 μ L of fractions, beads, and flowthrough loaded per lane.

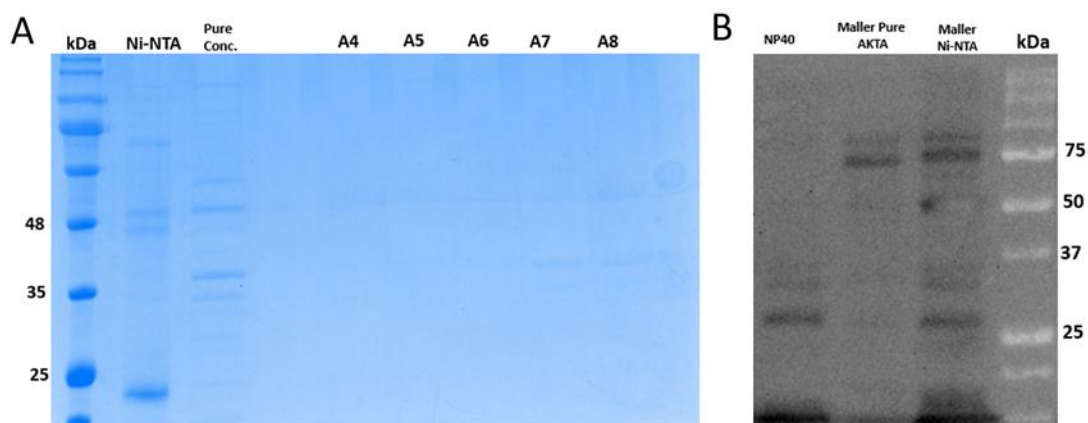


Figure S2. hrGal-12 purification attempt using protocol from Maller et al., 2020 developed for mrGal-12 and Cagnoni et al., 2024 for hrGal-12 in Rosetta DE3 *E. coli*. **A)** SDS-PAGE of elution fractions following AKTA PURE™ Q-Sepharose and Carboxymethyl-Sepharose chromatography. The Ni-NTA Lane shows pooled Ni-NTA fractions, while Pure Conc. Lane shows 16x concentrated AKTA elution fractions A4-A8. BL21(DE3) were lysed via sonication. 15 μ L of each fraction loaded per lane. **B)** Western blot of hrGal-12 following mrGal-12 style purification with Invitrogen PA5-113236 human galectin-12 polyclonal antibody 1:500. NP-40 lane is hrGal-12 purified with NP-40 detergent in lysis buffer. 500 ng protein loaded per lane.

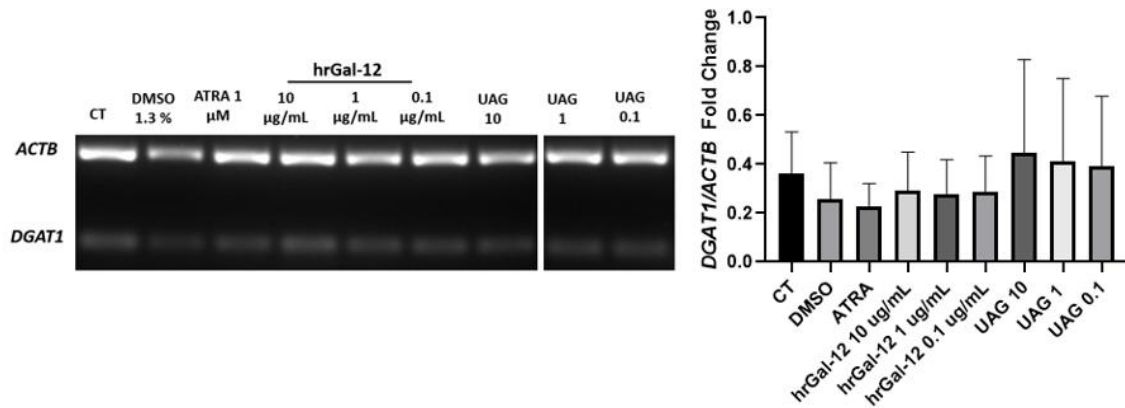


Figure S3. hrGal-12 has no effect on *DGAT1* expression. HL-60 cells treated with hrGal-12, DMSO, and ATRA for 72 hours. RT-PCR performed on a 2% agarose gel. Left panel shows PCR amplicons for *DGAT1* (60 BP) and *ACTB* (265 BP) multiplexed. Right panel shows densitometrical analysis of gene expression performed in ImageJ. One-way ANOVA with Tukey's HSD were performed and significant differences are presented as *($p < 0.05$), **($p < 0.01$), and ***($p < 0.001$). Error bars represent mean +/-SD (n=3).

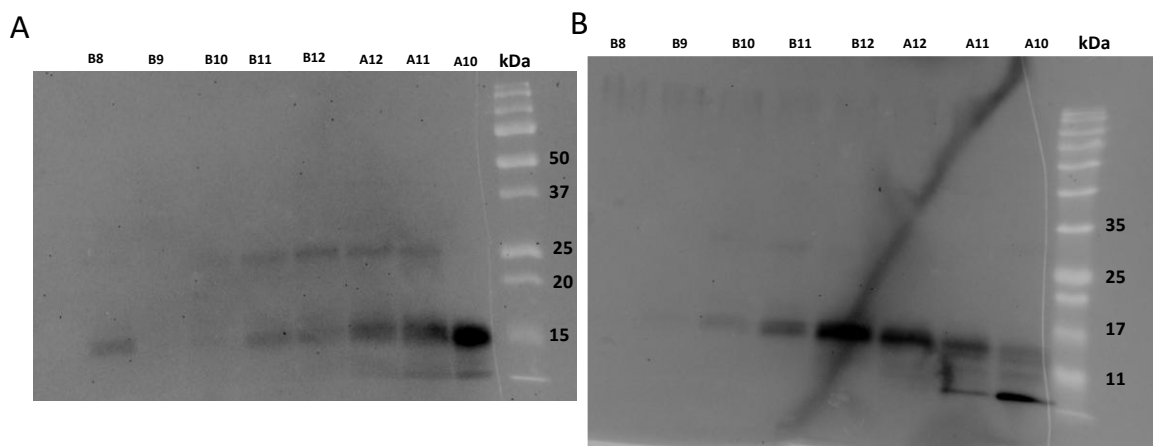


Figure S4. Western blots of hrGal-12 purified using various buffers on carboxymethyl fast flow IEX Cytiva column on AKTA GO chromatography system.

A) low salt = UAG no arginine. High salt = UAG with 250 mM arginine and 1M NaCl. The presence of some arginine leads to less degradation, but the IEX column is too harsh for hrGal-12. **B)** Low salt = UAG no arginine. High salt = UAG with no arginine + 1M NaCl. This buffer led to complete degradation of hrGal-12 into ~15 kDa fragments. Degraded hrGal-12 remains soluble in the buffer. SC-67294 galectin-12 polyclonal antibody used at 1:1000 dilution in both blots. 15 μ L of each AKTA fraction was mixed with SDS-loading buffer containing BME. Transfer onto PVDF membrane for 1 hour at room temperature with ice. Blocking with 1% milk and 5% BSA for 30 minutes at room temperature.

Curriculum Vitae

Name:	Aranya Nagar
Post-secondary Education and Degrees:	The University of Western Ontario London, Ontario, Canada 2023-2026 M.Sc. in Cell & Molecular Biology 2018-2023 B.Sc. Honours Specialization in Biology
Honours and Awards:	Western Graduate Research Scholarship (WGRS) 2023-2025 Selected Student Representative – Biology MSc Program Video Interview & Testimonial 2024 Dean’s Honours List The University of Western Ontario 2021 Entry Scholarship The University of Western Ontario 2018
Related Work Experience:	Teaching Assistant The University of Western Ontario 2023-2025 Intellectual Property Bootcamp Western Law & World Discoveries 2024 Vaccine Manufacturing Technology Co-Op Sanofi Pasteur 2021-2022
Volunteer Experience:	Society of Biology Graduate Students (SOBGS) Graduate Education committee member The University of Western Ontario 2024-2025 Western Graduate Research Forum (WGRF) 2025 Organizer The University of Western Ontario 2024-2025

Western Student Research Conference (WSRC) - Judge
The University of Western Ontario
2025

Society of Graduate Students Academic Committee member
The University of Western Ontario
2024-2025

Society of Biology Graduate Students Seminar Committee member
The University of Western Ontario
2023-2025

Publications:

Nagar, A (2024). Production and Characterization of Human Recombinant galectin-12. Inspiring Minds – A Digital Collection of Western’s Graduate Research, Scholarship and Creative Activity. 575.

Abstracts and Posters:

Nagar A., Stathopoulos P.B., Timoshenko A.V. (2025) Development, production, and characterization of human recombinant galectin-12 Biology Graduate Research Forum, Western University, London, Ontario, October 23-24th.

Nagar A., Stathopoulos P.B., Timoshenko A.V. (2025) Biological activity of human recombinant galectin-12. Ontario Cell Biology Symposium, Brock University, Niagara, Ontario, August 6th-7th.

Nagar A., Laus K., Timoshenko A.V. (2025) Cancer cell line models to study tissue-specific galectins. London Health Research Day, Western University, London, Ontario, May 13th.

Nagar A., Stathopoulos P.B., Timoshenko A.V. (2024) Human recombinant galectin-12: production and biological activity. Ontario Cell Biology Symposium, Guelph University, Guelph, Ontario, August 12th-13th.

Nagar A., Stathopoulos P.B., Timoshenko A.V. (2024) Investigating the aggregation and adhesion of acute myeloid leukemia HL-60 cells induced by human recombinant galectin-12. Immuno-Oncology Symposium, Western University, London, Ontario, May 30th.

Nagar A., Stathopoulos P.B., Timoshenko A.V. (2023) Production and biological activity of human recombinant galectin-12. Biology Graduate Research Forum, Western University, London, Ontario, October 26th-27th.